Synthesis, Radiolabelling and Pharmacological Evaluation of CO-Releasing Molecules

Dylan Giffard

University of Cape Town

February 2018

Synthesis, Radiolabelling and Pharmacological Evaluation of CO-Releasing Molecules

By

Dylan Giffard

Dissertation presented for the degree of

Master of Science

University of Cape Town

Supervisor: Associate Professor Gregory Smith

Plagiarism Declaration

I know the meaning of plagiarism and declare that all of the work in the document, **"Synthesis, Radiolabelling and Pharmacological Evaluation of CO-Releasing Molecules"**, is my own work and to the best of my knowledge has never been submitted for examination for any degree at any university. All sources of information are cited and fully referenced.

SIGNATURE: Signed by candidate

Dylan Giffard

DATE: 16 / 02 / 2018

Acknowledgements

Firstly, I would like to express my deepest gratitude and appreciation to Associate Professor Gregory Smith, my supervisor, for his invaluable advice, encouragement and criticism. This project would not have been possible without your guidance. I sincerely hope that many more pub lunches are on the cards.

I would also like to acknowledge Pete Roberts, for recording many, many NMR spectra for the duration of the project, and Eva Fischer-Fodor, for hosting me in Cluj-Napoca and teaching me all I know about cell cultures and antiproliferative evaluations.

My sincerest gratitude must be extended to Tameryn Stringer and Preshendren Govender, two postdoctoral fellows upon who I relied heavily. Tam, thank you so much for your help; the discussions about purification, synthetic strategies and general day-to-day stuff in the lab kept me going. And, of course, thank you for running the antiplasmodial assays for me. Preshen, your guidance with regard to the dendrimer functionalisation and characterisation was priceless. Thank you two so much.

I would like to thank each and every member of the Organometallic Research Group. The laughs make it all worthwhile.

Special thanks must be extended to Deirdre Brooks for all of the administrative help, but mostly for the long chats.

I must thank my mother, father and sister for their continued, unconditional support throughout my studies, whether it be financial or emotional. I am where I am now and I am who I am because of you. I love you.

Lastly, to my partner in crime, my brother from another mother, the caramel to my vanilla, and the other half to my bromance, Cody Williams, these past two years have been two of the best I've had, and I can only say that because of you. I will sorely miss the 12 o'clock lunches with you and Preshen. Knoppies Labuschagne, my son. We've made it.

Greg, Preshen and Cody, remember to always ask yourselves, are you asking the right questions?

Table of Contents

Conference Contributions

1. **Poster Presentation**: Dylan Giffard, Emmanuelle Jestin and Gregory S. Smith, *Group 7 Tricarbonyl Metallodendrimers for Therapeutic and Diagnostic Use*, presented at the 18th Biennual SACI Inorganic Chemistry Conference, Cape Town, South Africa, **2017**.

2. **Poster Presentation**: Dylan Giffard, Emmanuelle Jestin, Tameryn Stringer and Gregory S. Smith, *Group 7 Tricarbonyl Metallodendrimers: Synthesis and Applications*, presented at the University of Cape Town 10th Annual Science Postgraduate Symposium, Cape Town, South Africa, **2017**.

3. **Poster Presentation**: Dylan Giffard, Tameryn Stringer, Emmanuelle Jestin and Gregory S. Smith, *Mn(I) and Re(I) Tricarbonyl Metallodendrimers: Synthesis and Applications*, presented at the 1st Annual Modern Trends in Dendrimer Chemistry and Applications, Moscow, Russia, **2017**.

Abstract

The combatting of drug-resistant cancerous cell lines and strains of *P. falciparum* remain major global health problems to date, with hundreds of thousands of related deaths per annum. Early identification of solid tumours and infections, as well as the discovery of drugs with new mechanisms of action, are paramount in the fight against drug resistance. This study investigates the synthesis, characterisation and biological evaluation of new Mn(I) and Re(I) tricarbonyl metallodendrimers, in addition to the formation of a new ^{99m}Tc complex for use in diagnostic imaging.

Two series of mono- and multimeric picolylamine ligands, based on polyamine scaffolds, were prepared. One series of ligands was functionalised with Re(I)- and Mn(I)-tricarbonyl moieties, following the [2 + 1] approach, to form a series of cationic complexes. Additionally, a second series of neutral bidentate (*N,N*)-Mn(I) complexes were prepared. The ligands and complexes were characterised using a range of spectroscopic and analytical techniques, including ^{1}H, ^{13}C{^{1}H}, and ^{31}P{^{1}H} NMR spectroscopy, infrared spectroscopy, and mass spectrometry.

The stability and CO-release properties of the Mn(I) complexes were investigated using UV/Vis absorption spectroscopy. A decrease in the MLCT absorption band suggests the release of CO. CO-release was confirmed using a monomeric Mn(I) complex as a model with the myoglobin assay.

The *in vitro* antiproliferative activity of the Re(I) complexes was investigated against three cancerous cell lines (A431, DLD-1 and A2780) and one non-tumourigenic cell line (BJ). The complexes displayed moderate to good activity, with all IC_{50} values in the low micromolar range. The tetranuclear complex displayed the highest efficacy against the tested cell lines (IC_{50} = 6 – 14 µM). Selectivity towards the cancerous cell lines was observed for the tri- and tetranuclear complexes, with higher IC_{50} values against the BJ cell line. The *in vitro* antiproliferative activity of the Mn(I) complexes was evaluated against two cancerous cell lines (A431 and A375). The tetranuclear [2 + 1] Mn(I) complex displayed the best activity against both of the tested cell lines. The [2 + 1] complexes displayed higher *in vitro* activity than their bidentate counterparts.

The complexes were evaluated as *in vitro* antiplasmodial agents against chloroquine-sensitive (NF54) and chloroquine-resistant (K1) strains of *P. falciparum.* The [2 + 1] Mn(I) complexes

displayed enhanced activity over their Re(I) analogues and their bidentate counterparts. The tetranuclear [2 + 1] Mn(I) complex displayed the best activity against the K1 strain (IC_{50} = 0.99 µM) and the best resistance index (RI = 0.263) of all the tested complexes. Irradiation of selected Mn(I) complexes during incubation with the K1 strain resulted in an almost two-fold increase in activity of the [2 + 1] Mn(I) complexes, but a decrease in activity of the bidentate Mn(I) complexes.

Formation of the monomeric radiolabelled product was achieved by reacting $^{99m}Tc(bpy)(CO)_3$ with a monomeric ligand. The product was isolated using preparative HPLC, but the retention time did not match that of the Re(I) analogue, likely due to the difference in counterion. Radiolabelling of the multimeric ligands was unsuccessful.

Abbreviations, Symbols and Units

°	degrees
°C	degrees Celsius
Å	angstrom(s)
µ	micro
µM	micromolar
ACT	artemisinin combination therapy
ATR	attenuated total reflectance
br	broad
bpy	2,2’-bipyridyl
$^{13}C\{^{1}H\}$	proton decoupled carbon-13
calc	calculated
CO-Mb	carboxy-myoglobin
CORM	carbon monoxide releasing molecule
COSY	correlation spectroscopy
d	doublet
dd	doublet of doublets
ddd	doublet of doublet of doublets
dddd	doublet of doublet of doublet of doublets
DAB	1,4-diaminobutane
DCM	dichloromethane
Deoxy-Mb	deoxy-myoglobin
DMSO	dimethylsulfoxide
EA	elemental analysis

EI	electron ionisation
EPR	enhanced permeability and retention
Eqn.	equation
ESI	electrospray ionisation
EtOH	ethanol
Et_2O	diethyl ether
MS	mass spectrometry
FTIR	fourier transformed infrared spectroscopy
g	grams(s)
h	hour(s)
Hb	haemoglobin
Hb-CO	carboxy-haemoglobin
HO	haem oxygenase
HPLC	high-performance liquid chromatography
HR	high resolution
HSQC	heteronuclear single quantum correlation
Hz	hertz
IC_{50}	50 % inhibitory concentration
IR	infrared
J	coupling constant
LED	light-emitting diode
lit.	literature
m	multiplet
Mb	myoglobin

MeOH	methanol
min	minute(s)
mL	millilitre(s)
MLCT	metal to ligand charge transfer
mol	mole(s)
mmol	millimole(s)
MP	melting point
MS	mass spectrometry
m/z	mass to charge ratio
NMR	nuclear magnetic resonance
$^{31}P\{^{1}H\}$	proton decoupled phosphorus-31
PBS	phosphate buffer saline
photoCORM	photo-activated CORM
ppm	parts per million
q	quartet
qn	quintet
ROS	reactive oxygen species
RT	room temperature
s	singlet (NMR); strong intensity (IR)
t	triplet
TPPTS	triphenylphosphine trisulfonate
UV/Vis	ultraviolet-visible
w	weak intensity (IR)

Chapter 1 Introduction and Literature Review

1.1 Carbon Monoxide

Carbon monoxide (CO) is an odourless, colourless, chemically inert, diatomic gas.[1] It is a product of combustion of organic material, and is well known for its lethal effect when present in high concentrations.[1] In 1949 Sjostrand discovered that CO is produced endogenously in small quantities in the human body.[2] It is now known that small molecules, such as CO, NO and H_2S, play roles as chemical signalling molecules in mammalian organisms.[3-5]

The toxicity of CO to mammals is attributed to the high affinity between the CO molecule and haemoglobin (Hb), the iron-containing oxygen-transport protein found in mammals.[1, 6] The affinity between CO and haemoglobin is approximately 220 times stronger than the affinity between molecular oxygen and haemoglobin.[6] Under normal atmospheric conditions, the concentration of oxygen is much higher than that of CO, so oxygen is preferentially bound to haemoglobin. However, when the concentration of CO increases, haemoglobin binds the CO, forming carboxy-haemoglobin (Hb-CO). Due to the high affinity between CO and haemoglobin, CO dissociation from Hb-CO takes a relatively long time, and the haemoglobin is not available to transport oxygen in the blood. This can lead to tissue hypoxia and, at high levels of Hb-CO, death.[1, 6]

CO is produced endogenously from the oxidation of the haem cofactor,[7] which releases CO, iron and biliverdin (**Scheme 1.1**). Biliverdin is subsequently reduced to bilirubin by biliverdin reductase. This transformation can be seen visually in a bruise, where the initial injury liberates the O_2-haem complex, giving the skin a red-purple colour.[8] As O_2 is dissociated, the bruise turns blue, and eventually yellow as haem is converted to bilirubin.[8] The yellow of bilirubin is also observed in jaundice and in urine.[8]

The catabolism of haem is catalysed by the protein haem oxygenase,[6] which is present in two isoforms, a constitutive isoform, haem oxygenase-1 (HO-1) and an induced isoform, haem oxygenase-2 (HO-2). These enzymes are ubiquitous in the human body, with high concentrations in the brain, spleen, liver, smooth muscle tissues and vascular endothelial cells, and are involved in a number of physiological processes mostly related to stress response.[6, 9] The two isoforms of haem oxygenase help control the concentration of haem within the body.[7]

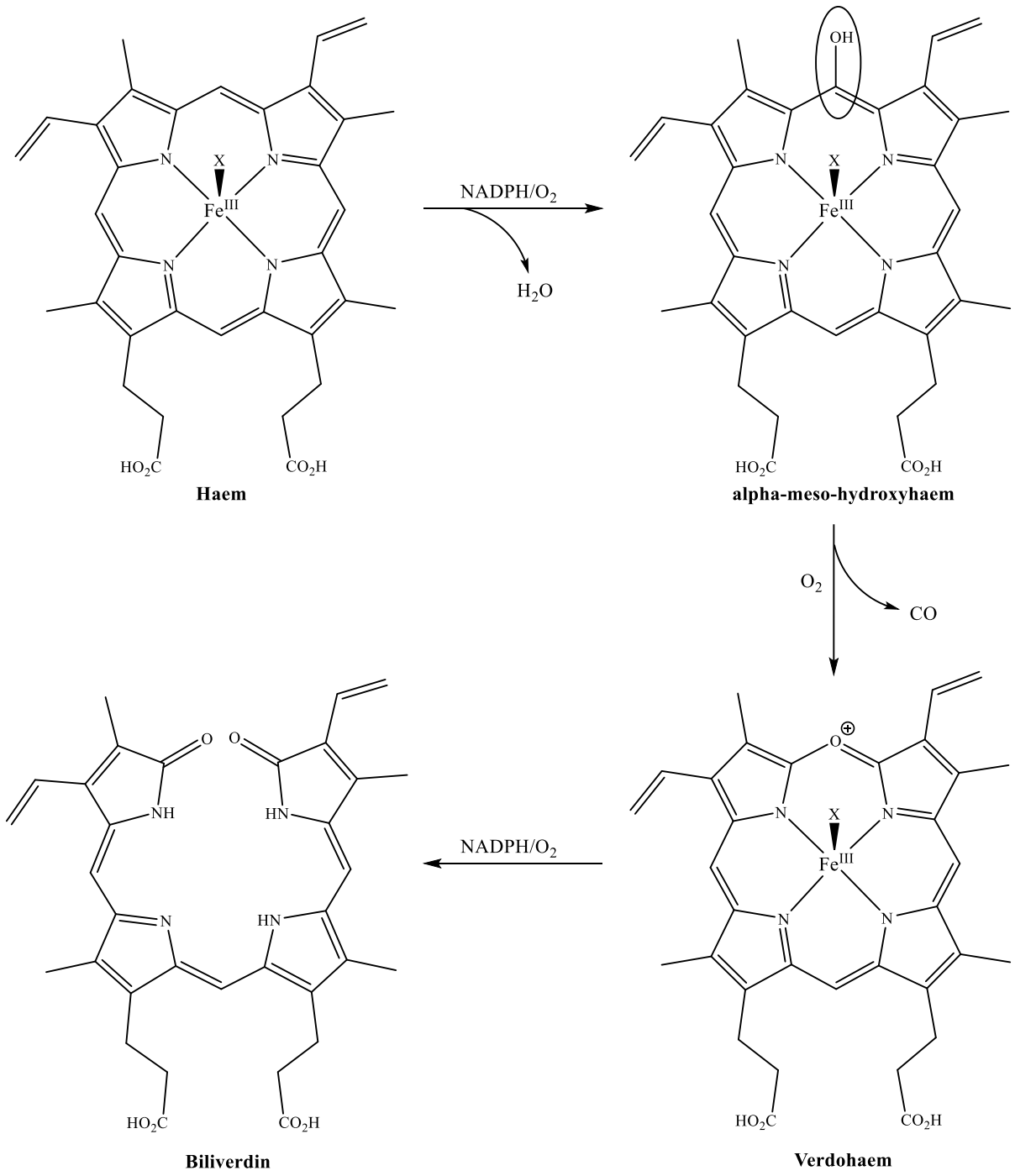

Scheme 1.1: Breakdown of haem by haem oxygenase, where **X** = O_2, NO, CO or H_2S, depending on the conditions (CO origination circled)[3]

86% of CO produced in humans is from the oxidation of haem. The remaining 14% of CO found in human bodies is generated from lipid peroxidation, photo-oxidation, bacteria and xenobiotics.[3]

CO interacts with several proteins, most containing the haem moiety, such as cytochrome c oxidase, guanylate cyclase, BK potassium channels and NADPH oxidase.[10]

The knowledge that endogenously produced CO contributes to important intracellular functions has changed the way the molecule is viewed. It has since been found to display a variety of protective effects across a range of pathologies. As a result, the use of CO has emerged as a new therapeutic strategy in medicine.

1.2 CO as a Therapeutic Agent

Since the discovery that CO not only plays a role in signalling within the cell, but also displays protective effects, new areas of investigation have opened up regarding the biological properties of the gas.[11]

Gaseous CO has been shown to have a wide range of effects, including vasodilatory, antiinflammatory, antiproliferative, antiapoptotic, and antihypoxia effects, and also protects from tissue reperfusion injury (restoring blood flow to a tissue or organ).[8] CO provides protection from organ graft rejection in mouse to rat transplantation experiments, in which the group exposed to 400 ppm CO for two days after the operation survived up to ten times longer than the group that breathed only air.[12] It has also been shown to improve cardiac energetics and safeguard the heart during reperfusion after cardiopulmonary bypass surgery in pigs.[13] In three rodent models, CO reversed already established pulmonary hypertension, a type of high blood pressure that affects the arteries both in the lungs and in the right side of the heart.[14]

Due to the antiinflammatory effects displayed by CO, it was suggested by Lee that CO could be used as a treatment for sepsis (systemic inflammation in response to an infection).[15] Sepsis remains a primary cause of death from infection, resulting from multiple organ dysfunction and eventually failure.[15]

It is thought that some of the biological effects displayed by CO are mediated through the binding of CO to metal centres.[10] For example, the copper centres in mitochondrial cytochrome c oxidase are targeted by CO, resulting in a decrease in consumption of molecular oxygen and an increase in production of reactive oxygen species (ROS).[10]

The use of CO gas as a therapeutic agent is limited owing to its toxicity at high concentrations and complete lack of specificity.[16] To circumvent this problem, Green and co-workers suggested using molecules that release CO to deliver the gas molecule in a controlled manner.[17]

These molecules display an expansive range of effects, including antiproliferative and antiplasmodial.

1.3 Malaria

Malaria is one of the most prevalent parasitic diseases worldwide.[18, 19] In 2015 alone, there were a reported 212 million new cases of malaria, which amounted to approximately 429 000 deaths.[20] The disease is caused by the *Plasmodium* parasite, which is spread to humans by the female *Anopheles* mosquito. Five species of *Plasmodium* cause malaria in humans: *P. falciparum, P. vivax, P. ovale, P. malariae* and *P. knowlesi*.[21] *P. falciparum* causes the most severe malaria cases, and most malaria-related deaths are attributed to *P. falciparum.*[18, 21]

P. falciparum has proven to be the deadliest and most difficult species to combat due to the rate at which it develops resistance towards antimalarial drugs. Chloroquine (**Figure 1.1A**), a common antimalarial drug, has been rendered drastically less effective due to the rise in chloroquine resistant strains of *P. falciparum.*[22]

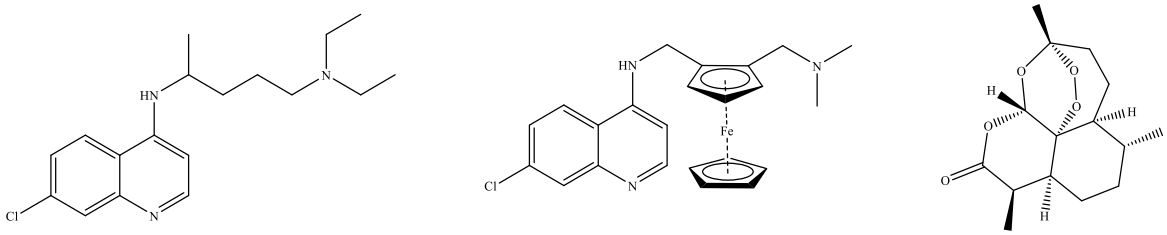

A **B** **C**

Figure 1.1: Chemical structures of chloroquine (A), ferroquine (B) and artemisinin (C)

The current recommended treatment for malaria is artemisinin-based combination therapy (ACT), which consists of an artemisinin derivative, and a partner drug. Combination therapy is employed to combat the rise in resistance. With that being said, artemisinin (**Figure 1.1C**) resistance is on the rise, and resistance of *P. falciparum* is rife across mainland Southeast Asia.[23] The increased resistance to current treatments calls for research into drugs that are not susceptible to current drug resistant strains.

Ferroquine (**Figure 1.1B**), a ferrocenyl-derivative of chloroquine, has managed to overcome the resistance gained against its parent compound. It exhibits potent *in vitro* and *in vivo* efficacy

against numerous chloroquine-resistant and chloroquine-sensitive strains of *Plasmodium*.[24, 25] Ferroquine is currently in phase 2 clinical trials.[26]

Due to the success of ferroquine, other biologically important organic and organometallic molecules have been modified to include the ferrocenyl moiety in order to improve activity. For example, benzimidazole, a bicyclic benzo-fused imidazole compound, whose derivatives have displayed potent antitumour, antiparasitic and antimicrobial activity,[27] were functionalised with one or two ferrocene moieties, which increased the efficacy against chloroquine-resistant and chloroquine-sensitive strains of *P. falciparum*.[28]

Furthermore, it has been shown by numerous groups that CO contributes immensely to the protective effects of HO-1 against cerebral malaria.[29-31] This is thought to be *via* CO binding to prosthetic haem groups of cell-free haemoglobin, forming carboxyhaemoglobin, which is not easily oxidised.[31] This restrains the molecule, not allowing it to contribute towards the pathogenic effects of cell-free haemoglobin,[32] and prevents the proinflammatory[33] and cytotoxic[34, 35] effects associated with haem release from haemoglobin.

Despite this, not much research has been performed into CO-releasing molecules for the treatment of malaria infections.

1.4 CORMs and other metal carbonyls

CO-releasing molecules (CORMs) are an attempt to exploit the beneficial properties of CO, while minimizing the toxic properties of the gas.[36] Many CORMs have now been synthesised with a range of functions in mind, including specificity and targeting.[36]

CORMs exhibit antiapoptotic properties, antiinflammatory effects, antimicrobial activity, applications in organ preservation, and therapeutic potential in vascular disease.[37] A partial explanation for the activity displayed by CORMs could be the accumulation of metal-carbonyl complexes inside the target cells, leading to high concentrations of CO within the cell, in addition to the metal-co-ligand fragment.[38] The vacant coordination site of the metal-co-ligand fragment could then become occupied by solvent molecules or could allow the binding of biomolecules.[9] These adducts may possess biological activity of their own, which could result in desirable or undesirable effects.[16]

Properties of CORMs, such as CO-release rates and solubility in aqueous media, need to be fine-tuned. This is most easily achieved by using metal-carbonyl compounds as CO releasing

molecules, which can be modified by altering the co-ligands bulk, basicity/acidity and charge.[39] Most CORMs are organometallic carbonyl complexes with a metal centre in a low oxidation state.[16] Since the development of the first CORMs, it has been reported that a number of different molecules release CO under physiological conditions. These include complexes with a wide variety of metal centres, including ruthenium, iron, manganese, vanadium, cobalt, iridium, chromium, rhenium, molybdenum and tungsten.[16]

Although organometallic carbonyl complexes represent the simplest way to form CORMs, not all CORMs are metal-based.

1.4.1 Non-metal-based CORMs

Several purely organic CO releasing molecules have been established. Haloalkanes, such as CH_2Cl_2, CHI_3 and $CHBr_3$ are metabolised to release CO.[8] These haloalkanes have the ability to protect the vasculature against oxidative stress and injury, inhibit the proliferation of vascular smooth muscle cells, modulate the activity of various immune system cells, and enhance the production of antiinflammatory cytokines, among other effects.[8]

Sodium boranocarbonate, named CORM-A1, is the only known non-metal-based CORM capable of releasing CO under aqueous conditions.[40]

1.4.2 Metal-based CORMs and Other Metal Carbonyls

Organometallic complexes present structural and stereochemical variety, with the possibility of rational ligand design and display a variety of mechanisms of action.[41]

As previously mentioned, CORMs based on metal-carbonyls can have a variety of metal centres, some of which will be discussed below.

1.4.2.1 Ruthenium carbonyls

The original patent regarding metal-based CORMs as therapeutic agents filed in 2002 contained two Ru-based complexes for biological work, CORM-2 and CORM-3 (**Figure 1.2**).[8, 42]

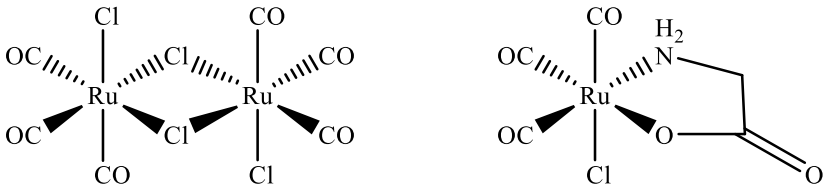

CORM-2 CORM-3

Figure 1.2: Structures of CORM-2 and CORM-3[8]

Owing to the commercial availability of CORM-2, as well as it being one of the first reported CORMs, it has received a considerable amount of attention.[8, 42] Many papers have been published documenting the biological use of CORM-2. They cover a wide range of applications, including, but not limited to, inducing vasorelaxation,[43] inhibiting cytokine-induced inflammatory response[44] and exhibiting antiproliferative effects on human T-cells.[45]

CORM-3 was the first water-soluble CORM to be tested in biological systems.[8] It displays bactericidal properties against a range of microorganisms, including Staphylococcus aureus, Pseudomonas aeruginosa and Escherichia coli.[9, 36] CORM-3 was able to decrease the bacterial count in the spleens of immunosuppressed mice in a similar manner as observed in immunocompetent mice, suggesting a direct antibacterial effect, rather than a host-mediated effect of the CORM.[11] It exhibits bactericidal properties against both normal and antibiotic resistant strans of *P. aeruginosa*, a common human pathogen, both *in vivo* and *in vitro*, which is mediated by the inhibition of bacterial respiration.[11] This microbe displays higher sensitivity towards CORM-3 than to host macrophages, and it was suggested that this is due to a greater accessibility of CO to the respiratory chain enzymes in the bacterium.[11] It was demonstrated unambiguously that CORM-3 is a powerful inhibitor of microbial respiration, and that the interference of respiratory metabolism correlates temporally with a rapid loss of bacterial viability.[46]

The mechanism of CO-release is unknown, and the rate of release is slow in pure water, but very rapid in the presence of myoglobin.[8] This is a common observation for CORMs, which often display faster CO-release in the presence of myoglobin.[47] When CORM-3 is dissolved in phosphate buffer for 24 hours, the complex is deactivated and does not release CO.[8] The slow dissociation of CO in water coupled with the fast dissociation of CO in the presence of myoglobin, along with the simple deactivation of the complex, makes CORM-3 ideal for use as a therapeutic CORM.[8] Solutions can be prepared and delivered without notable loss of CO,

which will be released after administration. The deactivated complex provides a reference sample that does not release CO, and thus the effects of the released CO can be investigated.[8] Yabluchanskiy and co-workers showed that CORM-3 can display neuroprotective or neurotoxic effects after intracerebral haemorrhage depending on the time of administration.[48]

It was suggested by Desmard and co-workers that the bactericidal effects displayed by CORM-2 and CORM-3 are amplified due to direct transfer of CO from the CORM to its potential target.[10]

1.4.2.2 Iron carbonyls

A number of [(η^4-2-pyrone)Fe(CO)$_3$] have been reported and tested for CO-release and toxicity. Some of these complexes are shown in **Figure 1.3**, along with two other iron-carbonyl complexes.

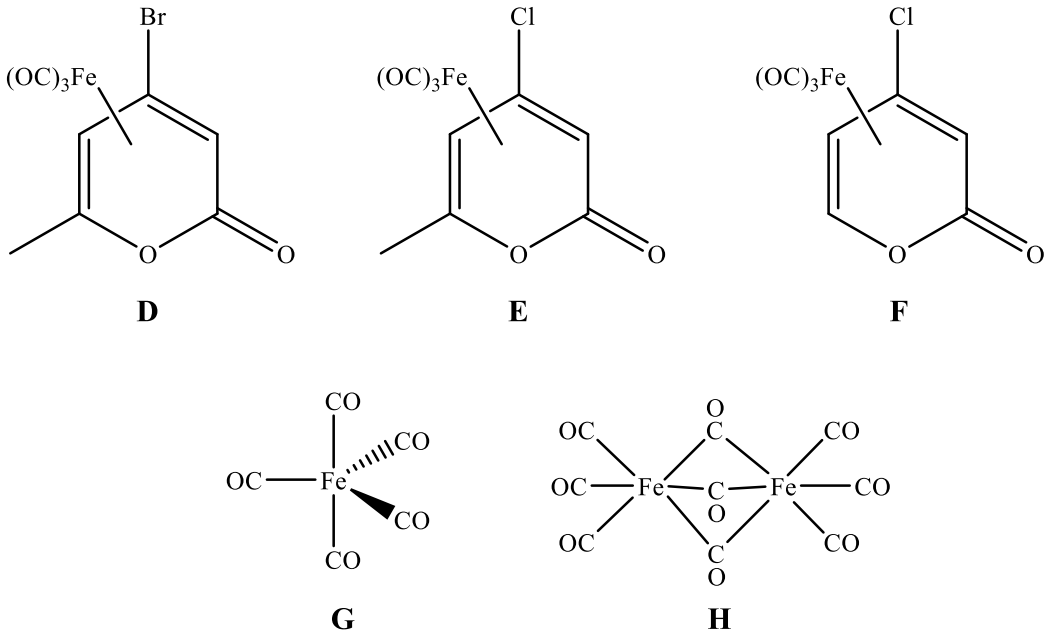

Figure 1.3: Three [(η^4-2-pyrone)Fe(CO)$_3$] CORMs (**D** – **F**) and two other Fe-based CORMS

Complexes **D** – **H** all release CO. Complex **D** exhibits vasodilatory effects of aortic rings pre-contracted with phenylephrine.[49] [CpFe(CO)$_3$]$^+$ was found to release CO at a rapid rate.[42] Subsequently, similar complexes with substituted Cp rings and dicarbonyl-halide complexes were studied.[50, 51]

1.4.2.3 Manganese carbonyls

There has been much interest in manganese complexes in recent years because the complexes often display antibacterial,[52] anticancer[53, 54] and antifungal properties.[55] $[Mn_2(CO)_{10}]$ (**Figure 1.4**) was first described as a CORM in the initial publications on the subject, and Mn(I) carbonyl complexes are known to release CO.[17, 42] It induces vasodilation upon CO-release, which occurs upon irradiation with light.[17] $[Mn_2(CO)_{10}]$ reportedly attenuates the inflammatory response in the lungs of thermally injured mice,[56] and activates K_{Ca} channels in arteriole smooth muscle cells.[57]

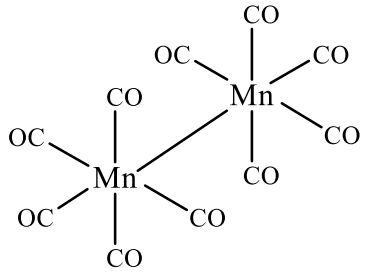

I

Figure 1.4: Photoactivatable CORM, $[Mn_2(CO)_{10}]$

$[Mn(CO)_5X]$ (where X = Cl, Br, I) all release CO in the presence of myoglobin at half-lives of $t_{1/2}$ = 970, 245, 384 minutes, respectively.[50] $[Mn(CO)_5Br]$ greatly reduces the viability of Escherichia coli and Staphylococcus aureus, but the bactericidal activity is nulled in the presence of myoglobin.[58]

Other manganese complexes, such as $[Mn(CO)_4X_2]^-$ (where X = Br, I, MeC(O)S) release CO relatively rapidly to myoglobin with half-lives of $t_{1/2}$ = <2, 12, 32 minutes, respectively.[59] $[Mn(CO)_4Br_2]^-$ displays no cytotoxicity at 100 µM.[59] $[Mn(CO)_4(SC(O)Me_2)]^-$ does not suppress the formation of $[NO_2]^-$ in murine RAW264.7 macrophages at 100 µM concentration, but does induce vasodilation.[59]

Ligand-functionalised polymers were demonstrated as carrier systems for manganese tricarbonyl-based CORMs.[60] Non-toxic carrier systems must be chosen carefully because the metal-polymer adduct may display toxicity even if neither the metal nor the polymer display toxicity on their own.[60]

It was demonstrated that Mn(III)-salen complexes affect cell viability by inducing apoptosis in MCF-7 (human breast cancer) and CCL228 (colon cancer) cells.[61]

Mn(I) tricarbonyl complexes developed by Schatzschneider *et al*., based on the [2 + 1] approach, with a functionalised 2,2'bipyridyl and a known antifungal azole derivative (**Figure 1.5**), displayed potent antifungal activity towards *L. major* and *T. brucei*, with IC_{50} values ranging from 2 – 5 µM.[62]

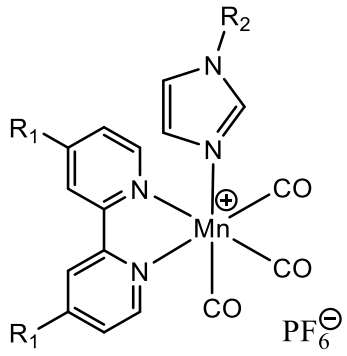

Figure 1.5: General structure of Mn(I) tricarbonyl complex synthesised by Schatzschneider *et al*., where R_1 = H or $COOCH_3$ and R_2 = known antifungal agent, clotrimazole, ketoconazole or miconazole.[62]

1.4.2.4 Rhenium carbonyls

Rhenium carbonyl complexes have been shown to display anti-cancer,[39, 63-67] anti-malarial[28] and anti-trypanosomal activity.[68] There is a review by Gasser *et al.* titled the Underestimated Potential of Organometallic Rhenium Complexes as Anticancer Agents,[69] which includes many Re(I) carbonyl complexes. Their potential is unmistakeable, and more research into their biological activity is necessary.

A rhenium CORM was synthesised by Zobi and co-workers using the biocompatible scaffold cyanocobalamin, and was named B_{12}-ReCORM-2.[70] In this heterodinuclear complex, the rhenium(II) moiety is coordinated to the axial cyano group of the cyanocobalamin (**Figure 1.6**). B_{12}-ReCORM-2 exhibits cytoprotective effects against ischemia-reperfusion injury in the rat model, but displays poor cellular uptake.[70]

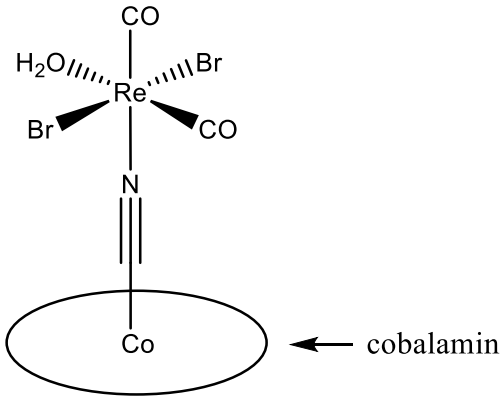

Figure 1.6: Structure of B_{12}-ReCORM-2[70]

Rhenium(I) tricarbonyl complexes have been shown to exhibit potent antiproliferative activity against a range of different cancer cell lines. A series Re(I) tricarbonyl complexes displayed IC_{50} values ranging from 1 – 5 µM against HeLa cells (cervical cancer).[63, 64] Furthermore, a series of selenium rhenium(I) tricarbonyl complexes displayed excellent activity (5 µM IC_{50}) against breast cancer MCF-7 cell line, while Re(I) tricarbonyls based on the [2 + 1] approach displayed potent activity (IC_{50} = 2 – 4 µM) against the breast cancer MDA-MB-468 cell line.[65, 66]

Additionally, it was shown by Illan-Cabeza and co-workers that rhenium tetracarbonyl complexes display strong cytotoxicity towards breast cancer MCF-7 tumour cells.[71]

Rhenium(I) tricarbonyl indolato complexes **J**, **K** and **L** (**Figure 1.7**) incite a strong light-induced antiproliferative effect in HeLa cells.[39]

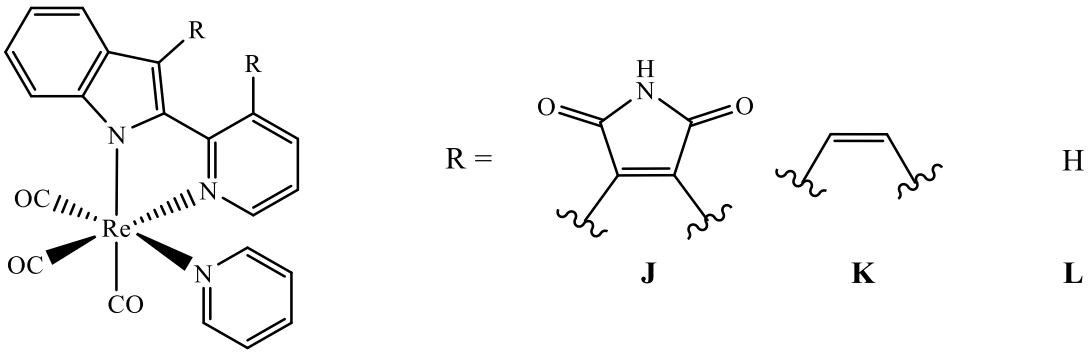

Figure 1.7: Rhenium indolato complexes[39]

The cyrhetrenyl benzimidazole displayed in **Figure 1.8M** was synthesised by Arancibia *et al*., and its antimalarial activity evaluated against chloroquine-sensitive and chloroquine-resistant strains of *P. falciparum*. The complex displayed better activity than its ferrocenyl analogue.[28]

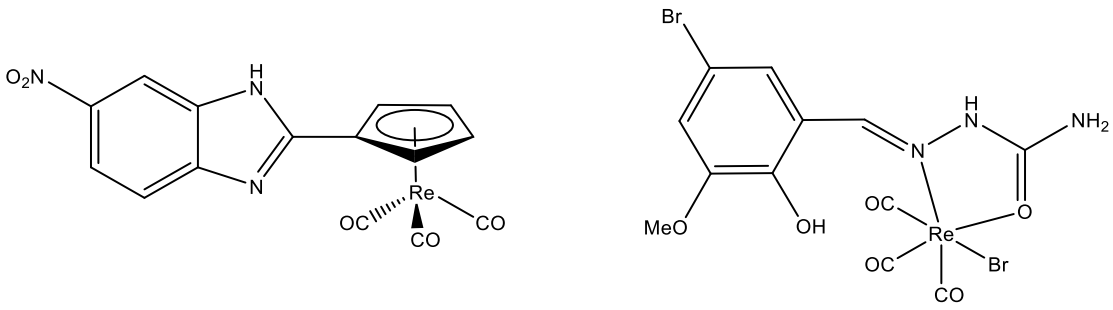

M **N**

Figure 1.8: Structures of Re(I) tricarbonyl complexes

Gambino *et al*. reported a series of salicylaldehyde semicarbazone Re(I) complexes, one of which is shown in **Figure 1.8N**, which displayed reasonable antitrypanosomal activity against *T. cruzi*.[68] Gambino *et al*. synthesised a similar series of Re(I) tricarbonyl complexes using thiosemicarbazone ligands, which displayed good *in vitro* activity and decent selectivity indexes against *T. cruzi* (with endothelial cells as a reference).

1.4.2.5 Chromium carbonyls

Chromium complexes **O** (where X = Cl, Br, I) and **P** release CO in the presence of myoglobin with $t_{1/2} \approx 200$ minutes for both complexes.[72] **Q** releases CO upon photolysis.[47] Structures are shown in **Figure 1.9**.

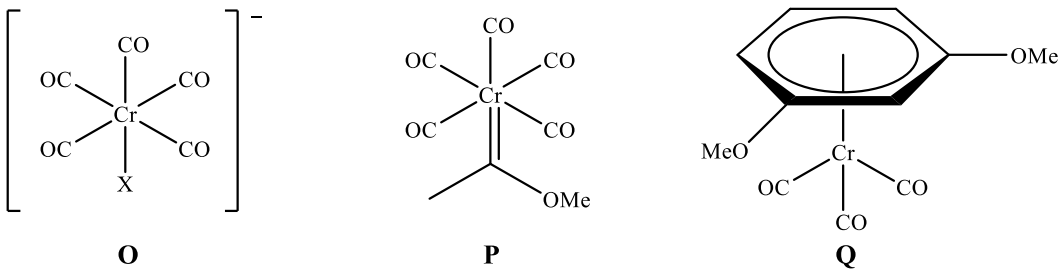

O **P** **Q**

Figure 1.9: Selected Cr-based CORMs

Nordlander *et al*. synthesised new organometallic analogues of chloroquine, shown in **Figure 1.10**, to overcome the extensive chloroquine resistance developed by *Plasmodium*.[73] These complexes displayed potent *in vitro* activity against chloroquine-resistant and chloroquine-sensitive strains of *Plasmodium*. In this case, complex **R** displayed activity twice as high as for the organic ligand against the chloroquine-resistant strain.

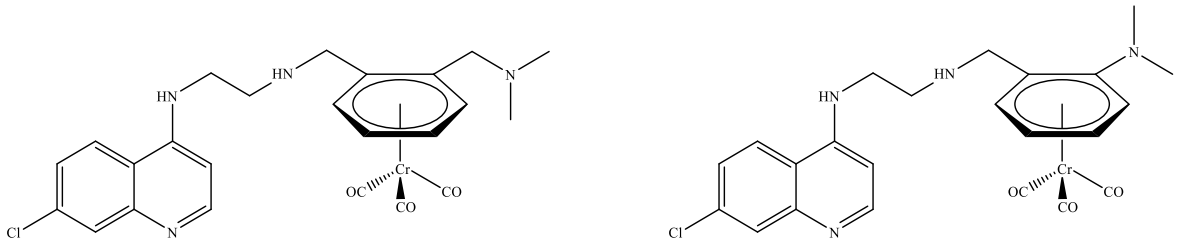

R **S**

Figure 1.10: Half sandwich Cr(I) tricarbonyl complexes synthesised by Nordlander *et al*.[73]

1.4.2.6 Molybdenum carbonyls

$[Mo(CO)_5X]^-$ (**Figure 1.11T**), where X = Cl, Br, I, release CO in the presence of myoglobin with $t_{1/2}$ = 718 – 2440 minutes.[72] $[Mo(CO)_5Br]^-$ greatly reduces the viability of Escherichia coli and Staphylococcus aureus, but the bactericidal effect is eliminated in the presence of myoglobin.[1, 58] In the rat model, symptoms of arthritis are diminished when treated with **T** (X = Br).[74]

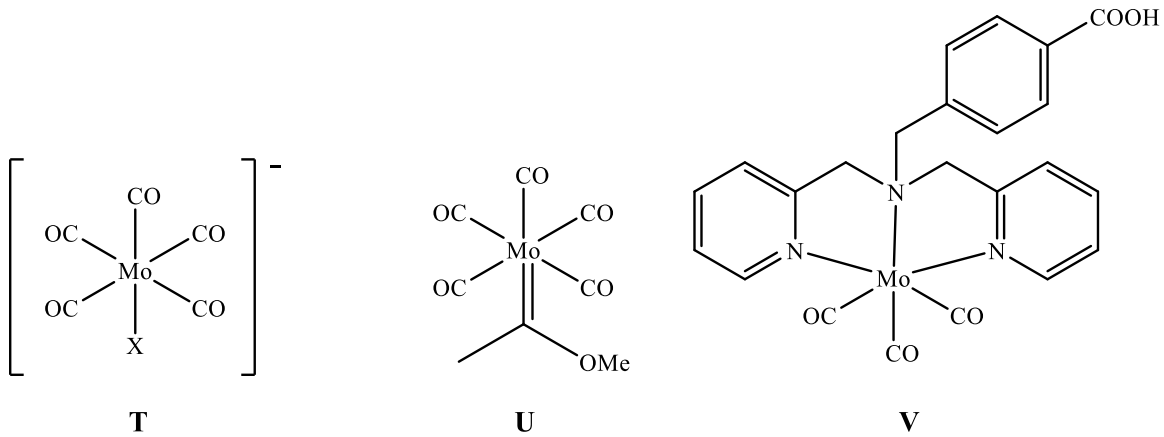

T **U** **V**

Figure 1.11: Selected Mo-based CORMs

Molybdenum tricarbonyls with tridentate N-donor ligands similar to that of complex **V** exhibit antibacterial activity against *Helicobacter pylori*.[75]

Salicylaldimine Mo(II) dicarbonyl complexes synthesised by Aziz *et al*. displayed decent antibacterial (against *S. aureus* and *E. coli*) and antifungal (against *A. flavus* and *A. niger*) properties.[76]

Known antituberculosis drug, isoniazid, was coordinated to an Mo tricarbonyl core by Jesudurai and Vancheesan, although the biological effects were never evaluated.[77]

1.4.2.7 Tungsten carbonyls

Along with tungsten complexes similar to complexes **O**, **P**, **T** and **U**, (**Figure 1.9**, **Figure 1.11**) are a six-coordinate tungsten-carbonyl complex with a TPPTS ligand (**Figure 1.12W**) and a seven-coordinate tungsten-carbonyl complex with two bidentate acac ligands (**Figure 1.2X**). CO dissociates from **W** upon irradiation with light.[78] Complex **X** releases CO with $t_{1/2}$ = 76 minutes.[72]

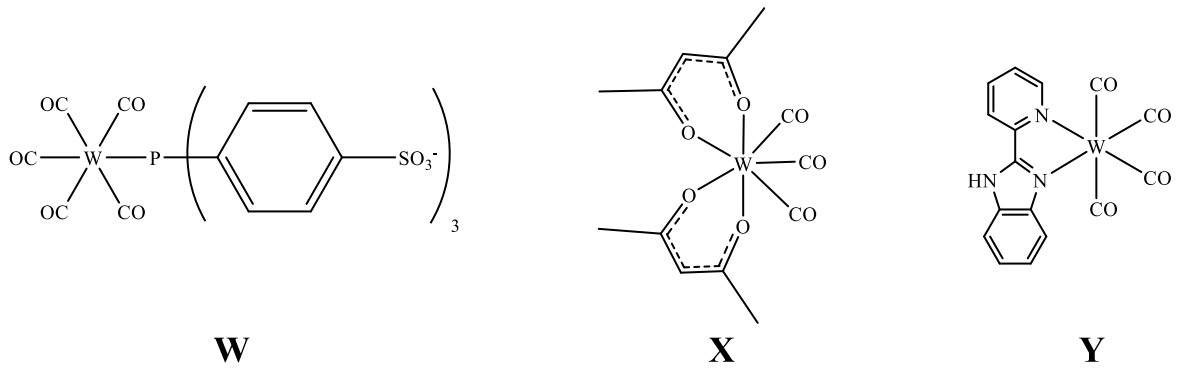

W **X** **Y**

Figure 1.12: Selected W-based CORMs

You *et al*. coordinated a W(0) aqua, carbonyl complex to the known antibacterial drug, norfloxacin. The complex displayed potent *in vitro* antibacterial activity *against E. coli, B. dysenteriae* and *S. auseus*. The complex was more efficacious than the organic parent drug.[79]

Ditungsten carbonyl Schiff base complexes synthesised by El-Medani *et al*. displayed decent *in vitro* antibacterial activity against *E. coli* and *S. aureus*, but were not as potent as the control antibacterial agent, tetracycline.[80]

1.5 Mechanisms of CO-release from CORMs

CO can be released from an organometallic carbonyl complex in a variety of modes, namely thermal dissociation, by the presence of strong *cis* π-donor ligands, *via* an associative

mechanism, by oxidation of the metal centre, by decomposition by an enzyme, by direct transfer of CO to a haem protein, and by photochemical release.[81]

Most metal-carbonyl compounds will release CO upon thermal activation.[81] When heated, the M-CO bond is broken and the gas is released.[81] When this process is dissociative, the vacant coordination site is occupied by a different ligand. This approach is extensively used in the synthesis of organometallic complexes when starting from simple metal-carbonyls, such as $Fe(CO)_5$ and $Mo(CO)_6$.[81] However, the use of thermally activated CORMs in biological systems is limited, owing to the high temperatures needed for dissociation to occur.[81] For thermal dissociation of CO to occur at 37°C, it would require the complex to be fairly unstable at room temperature.

Strong π-donor ligands in a *cis* position to the CO labilises the CO, allowing dissociation under mild conditions.[82] A few examples of strong π-donor ligands are O^{2-}, OH^-, OR^-, NHR^- and NR_2^-.[82] These ligands are formed by deprotonation in basic media of the coordinated ligands OH^-, H_2O, HOR, NH_2R and NR_2H, respectively.[82] Due to strong π-donor ligands being formed by deprotonation, the dissociation of CO is considered pH dependent, and can be used for release of CO into specific tissues.[81] For example, a CORM could be orally ingested and move through the stomach without dissociation, and only release CO when it reaches the intestine, where the pH is higher and deprotonation occurs.[81]

CO dissociation *via* an associative mechanism occurs when an incoming ligand forms a new metal-ligand bond with the metal centre. When this takes place, the coordination number of the complex increases and one of the M-CO bonds elongates and breaks.[83] CO gas is then released and a new metal-ligand bond is fully formed.[83]

In biological systems, the most common oxidant is dissolved molecular oxygen, which can interact directly with the metal centre.[81] The metal is oxidised by the transferral of electrons from the metal centre to the O_2, weakening the metal-carbonyl bond, and eventually breaking it.[81] Thus, if a co-ligand of an organometallic carbonyl complex is displaced under physiological conditions, dissolved O_2 can occupy the free coordination site and induce metal oxidation and subsequently, CO-release.[81] This mechanism could be used to target specific tissues, owing to the increased lability of some co-ligands after protonation (e.g. histidine and pyridine).[81] Reactive oxygen species and reactive NO species (NOS) may also act as oxidants and lead to CO-release.[81]

CO can be released due to the decomposition of the complex by enzymes or proteins *in vivo*. Certain ligands will be metabolised by enzymes thus triggering the decomposition of the organometallic carbonyl complex and subsequent release of CO.[81] Esterase-mediated release of CO from a cyclohexadienyl-acetate tricarbonyl-iron CORM is shown in **Scheme 1.2**. Ligands that are good substrates for a specific enzyme could be chosen to exert some control over the CO-release.[81]

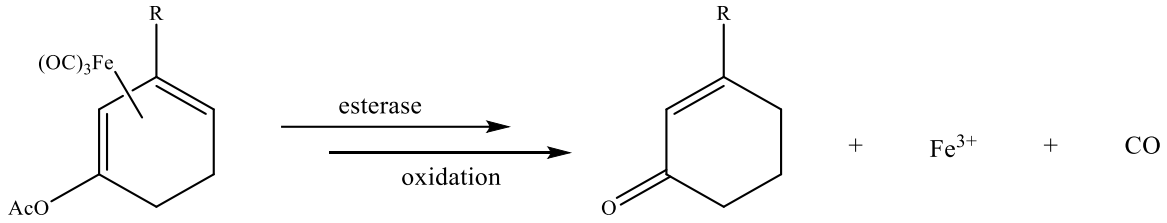

Scheme 1.2: Esterase-mediated CO-release[81]

Release mechanisms that are of particular interest are those which allow a certain degree of control over the time and place of CO-release. Using CORMs that release CO upon irradiation with light (photo-CORMs) is an approach that permits this controlled, specific delivery.

1.6 Photo-CORMs

Photo-CORMs present a way to achieve precise spatial and temporal control of the biological activity of CORMs. These photo-CORMs release CO only upon irradiation with a specific wavelength of electromagnetic radiation, and thus can be stored and transported in aqueous aerated solution as long as it is not exposed to light.[9] Additionally, the amount of CO released is directly dependent on the amount of light delivered to the target. Therefore, the dosage of CO can be defined.[84] The general reaction scheme for photoactivated CO dissociation is shown in **Scheme 1.3**.

Scheme 1.3: General reaction for photoactivated CO-release

The first visible-light-activated CORM to display a potent antimicrobial effect against Escherichia coli was synthesised by Ward and co-workers, and is shown in **Figure 1.13**.[85]

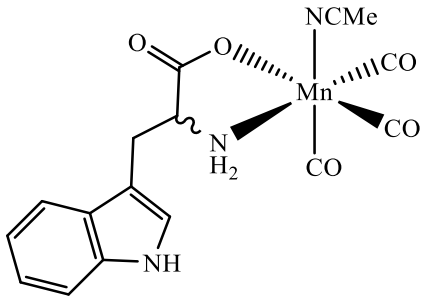

Figure 1.13: Tryptophan-containing Mn(I) tricarbonyl acetonitrile core[85]

There are certain desirable properties that a photo-CORM should possess. It should be:

- Soluble in aqueous solution or DMSO (commonly used for drug delivery)[84]
- Stable in aerated aqueous media at physiological temperatures. Although spontaneous decay of CORMs at known rates is expected, a photoCORM should only release CO when triggered by light.[84]
- Photoreactive at wavelengths of light where transmission is optimal. Penetrative depth of electromagnetic radiation into tissue is strongly dependent on the wavelength of light. Short wavelength radiation is the least penetrative, and the depth peaks in the near infrared region of the spectrum (700 – 1100 nm).[84]

Nagel and co-workers synthesised a manganese(I)-tricarbonyl CORM with a tridentate tris(2-picolyl)amine ligand and a bromide counter-ion (**Figure 1.14**). The CORM displayed no antimicrobial activity against Escherichia coli in the absence of light, although it was internalised by the microbe. Subsequently, after photoactivation, a reduction in growth rate of the bacteria was observed. This suggests that the complex is not toxic to the bacteria, but rather that the CO released after photoactivation has antimicrobial activity.[9]

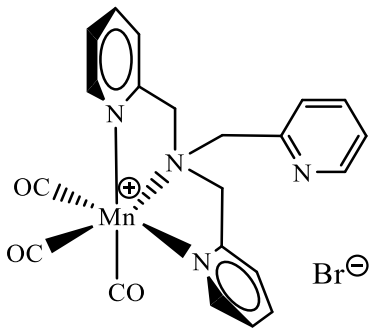

Figure 1.14: Manganese-based photo-CORM[9]

A manganese(I)-tricarbonyl complex with tridentate tris(pyrazolyl)methane ligand and a PF_6^- counter-ion displayed photoinduced cytotoxicity towards HT29 colon cancer cells comparable

to that of the established anticancer agent 5-fluorouracil, while having no effect when kept in the dark.[86]

1.7 CO Detection

Detecting the rate and amount of CO released from a CORM is an important part of the characterisation process of the complex. Proper targeting of the CORM requires a suitable half-life profile for CO-release so that the CORM can reach the intended site.[16]

Ideally, quantification of the amount of CO released by a CORM should be done *in vitro* or *in vivo*.[84]

Quantum yield for CO-release (φ_{CO}) at the excitation wavelength (λ_{ex}) is the most quantitative parameter with regard to the photoreactivity of a CORM.[84] φ_{CO} would be reported in units of moles of CO released per Einstein of light (one mole of photons) absorbed.[84] Although, from a therapeutic standpoint, a more important parameter would be the rate of CO production, because this establishes the number of moles of CO released per unit time.[84]

Apart from practical methods of CO-release measurements, theoretical approaches were found to give accurate evaluations for CO-release. This method used density functional theory, a computational quantum mechanical model, to determine the rates of CO-release from CORMs.[87]

There are a variety of methods that can be utilised to determine the amount and rate of CO released from a CORM, some of which are discussed below.

1.7.1 Gas Chromatography

Gas chromatography can be used to separate CO from other volatile compounds, in order for accurate quantitation of CO to be performed. In gas chromatography, the mixture is passed through a heated column that is packed with a sorbent or with molecular sieves. An inert gas (carrier gas) phase elutes the CO and other volatile compounds in succession, based on their molecular size and/or absorption coefficients specific for each packing material.[88] A detector at the end of the column quantifies the amount of CO released. There are a number of different types of detectors available for quantitation of CO using gas chromatography.

Gas chromatography coupled to mass spectrometry (GC-MS) can be used for CO-release quantitation.[84, 88] This type of detector is based on the vapour-phase molecules emerging from the column with a stream of high-energy electrons, which convert some of the molecules to ions that are then accelerated in an electric field.[88] The ions are separated according to their mass to charge ratio (*m/z*). Bartolucci and co-workers used a programmed temperature vaporising injector, a porous layer open tubular column with molecular sieves and a programmable temperature oven for CO detection.[89] By monitoring the *m/z* = 28 peak, they demonstrated low detection limits (10 ng/g) and a dynamic range (50 – 2500 ng/g), due to the sensitivity of the detector and the good separation of gases in the column.[84]

The flame ionisation detector (FID) is the most common detector used in a gas chromatographic system. It is based on the combustion of organic compounds in a flame. For analysis of CO, the samples must first be dried, pre-concentrated and then separated from hydrocarbons on a pre-column, due to the fact that hydrocarbons will be detected by the FID. The sample is directed through the analytical column and the emerging CO is reduced to CH_4 in a heated catalytic reduction tube (methaniser), which can then be quantitated using the FID detector.[88]

1.7.2 Manometric Techniques

The evolution of CO gas from a compound can be measured in a manometric fashion. The gas is evolved in a closed container and the volume is measured using a manometer.[58]

1.7.3 Myoglobin

By far the most common technique used to determine the amount of CO released from a CORM is the myoglobin assay.[17, 88] With this method, CO reacts with myoglobin to form carboxymyoglobin. The electronic spectrum changes significantly and can be visualised using ultraviolet-visible spectrophotometry (UV-Vis).[90] Due to the reactivity of myoglobin with molecular oxygen (O_2), the measurements must be performed in the presence of dithionite, a reducing agent.[8] Myoglobin reacts rapidly with CO, and removes free CO quickly from the solution. If the loss of CO from the CORM is reversible, this could affect the rate of CO-release.[8] The assay is conducted under physiological conditions (pH 7.4 and 37°C). The absorbance at 540 nm is measured and the proportion of myoglobin that has converted to carboxymyoglobin can be determined.[90]

1.7.4 CO Electrode

A CO electrode has been produced by World Precision Instruments and has been used to determine the concentration of CO in solution.[40, 91] The electrode is calibrated using $Na_2[H_3BCO_2]$ (CORM-A1).[92] The electrode consumes CO throughout the measurement and the resulting data corresponds to the liberation of CO from the CORM.[8]

1.8 Dendrimers

Dendrimers are repetitively highly branched macromolecules. Dendrimers have a well-defined shape, a central core, and branches emanating from the core.[93] An extensive range of functionalities can be contained within the dendritic framework.

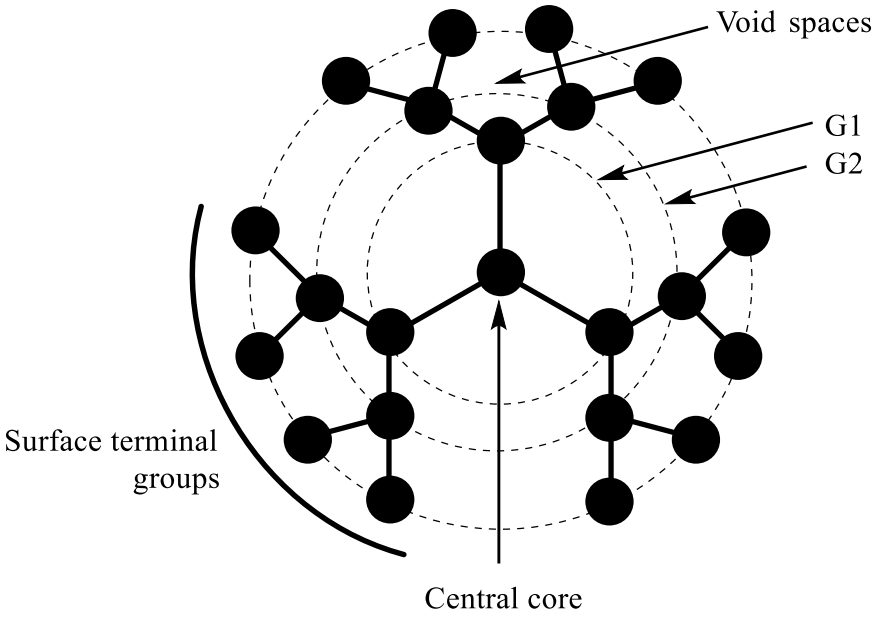

Figure 1.15: General schematic of a dendritic scaffold[94]

A dendritic scaffold has four key regions: the core, the repeating branching units, terminal groups, and void spaces (**Figure 1.15**).[94] The void spaces can encapsulate molecular cargo, and the surface terminal groups bear reactive groups that are easily functionalised to suit the intended use of the dendrimer.[94] G1 and G2 refer to the generation of the dendrimer (Gn), which can range from G1 to G12.[94] The dendrimer diameter increases linearly with the generation, whereas the number of surface terminal groups increase exponentially with the generation.[94]

The active moiety is usually covalently attached to the terminal groups of the dendrimer, which brings about a multinuclear compound, often resulting in improved biological activity when compared to the mononuclear compound.[95] This increase in activity could be due to favourable modulation of the stability, solubility and/or lipophilicity of the drug.[95]

Dendrimers are able to passively target malignant tissue as a result of the pathophysiological properties of solid tumours, such as leaky vasculature and impaired drainage. This leads to a property of dendrimers, and, in fact, most nanoparticles, called the enhanced permeability and retention effect.[60, 96] Consequently, nanoparticles, such as dendrimers, can improve site-specific drug delivery and subsequently reduce systemic exposure to the drug, reducing side effects.[96]

Due to the ease of control of the size, surface chemistry and shape of dendrimers, they offer various drug-design opportunities and a suitable approach for the delivery of metal-based drugs.[94]

1.8.1 Metallodendrimers as Biological Agents

Functionalising dendrimers with metals to form so-called metallodendrimers can increase the potency of the dendrimer as a biological agent. Furthermore, this multinuclear method often bears the potential drug with an increase in activity and efficacy over their mononuclear analogues.[97]

Many studies have been performed by Smith and co-workers that give insight into the therapeutic potential of metallodendrimers. These studies include functionalising dendrimers with a number of different metal moieties, including ruthenium-arene complexes,[98] osmium-arene complexes,[99] manganese- and rhenium-Cp and Cp* complexes,[100, 101] and rhodium- and iridium-Cp* complexes.[102]

Following the success of the Pt-based anticancer drug Cisplatin, researchers turned their attention to synthesising and evaluating the biological potential of multinuclear Pt-based drugs, such as the trinuclear complex synthesised by Boegler *et al.*[103] (**Figure 1.16A**) and the tetranuclear complex synthesised by Brouwer *et al.*[104] (**Figure 1.16B**). Both potential drugs displayed potent activity against a variety of cell lines.

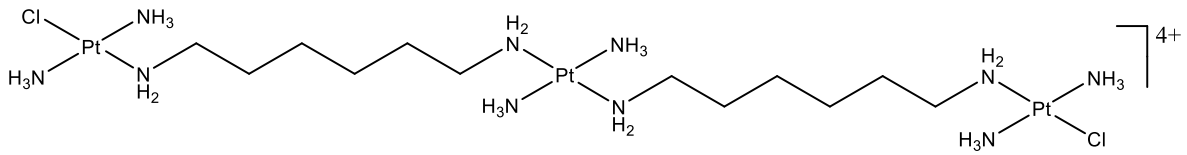

A

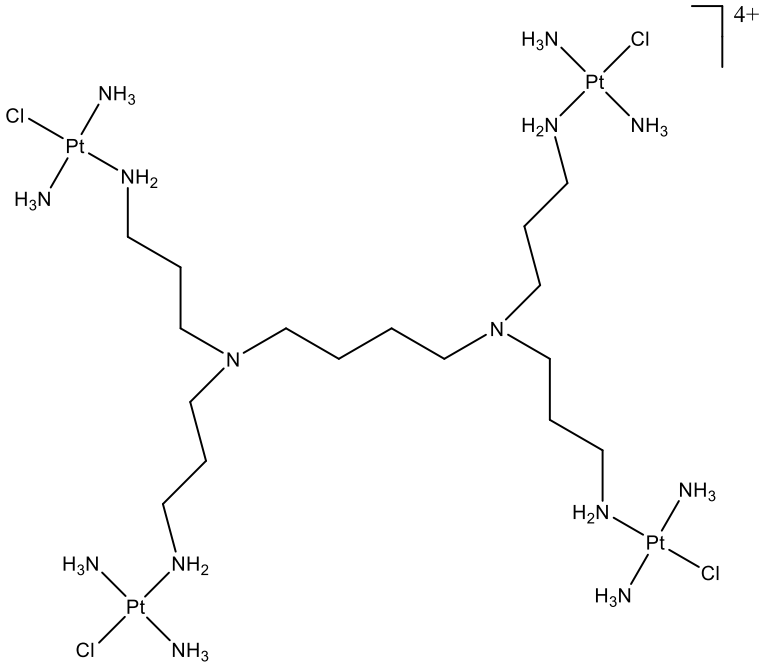

B

Figure 1.16: Structures of two multinuclear Pt-based anticancer drugs

1.8.2 Metallodendrimers as Photo-CORMs

Macromolecular systems have been used as CORM carriers in attempts to improve pharmacokinetic properties.[16] Tetranuclear and octanuclear (G1 and G2, respectively) $[Mn(CO)_3]$-functionalised metallodendrimers were synthesised by Smith *et al.* (**Figure 1.17**).[105]

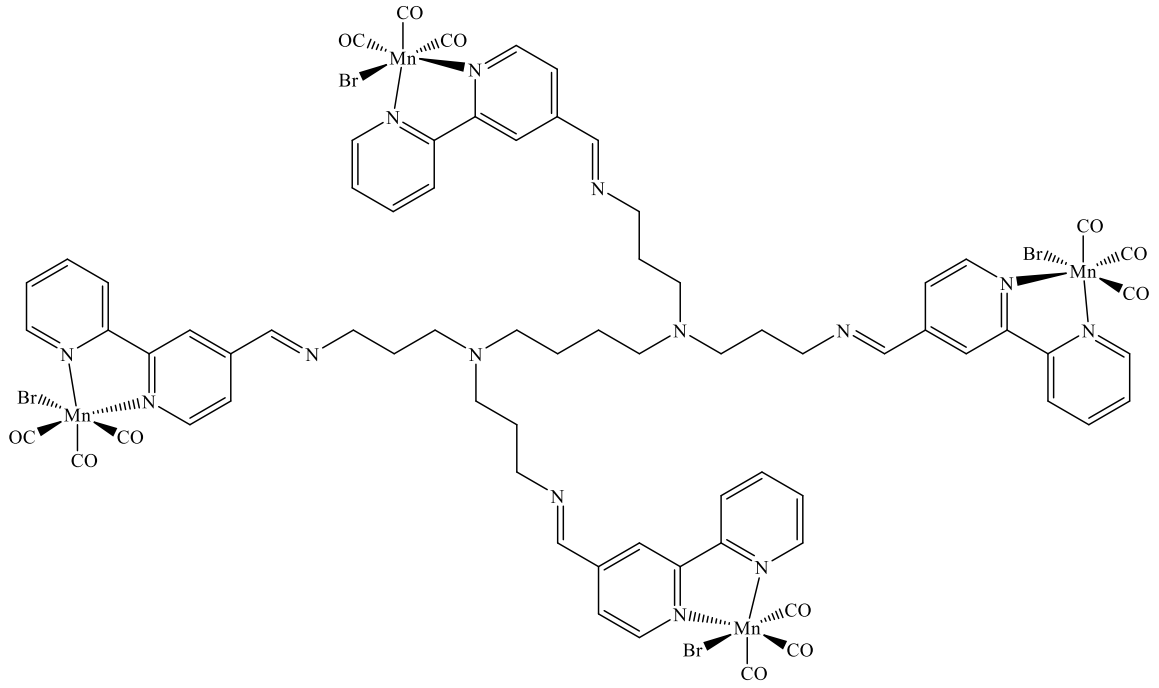

Figure 1.17: Poly(propyleneimine) dendrimer functionalised with photoreactive [$Mn(CO)_3$] moieties[105]

These metallodendrimers are the only example of photo-CORMs on a dendritic scaffold. The CO-release properties of the dendrimers were investigated, and showed that with an increase in dendrimer generation, there was an increase the equivalents of CO released, as expected. The study also showed that percentage of CO released increased from the monomer to the dendrimer, which could indicate that there is some cooperative CO release, and that higher generation dendrimers will release a higher percentage of CO.

1.9 Nuclear Medicine

It is apparent that non-invasive detection and therapy of solid tumours at an early stage is extremely beneficial.[106] Technologies that enable this will move diagnosis and treatment to an earlier point in the tumour progression, preventing the spread of cancer to other parts of the body, and minimising patient inconvenience and incapacitation.[106] Radiopharmaceuticals, a radioactive compound combined with a new molecule or a molecule of identified biological conduct, can be used to visualise solid tumours.[107]

Radioactivity occurs when the nucleus of an atom is unstable, and during the decomposition of the nucleus, electromagnetic radiation or particles are emitted in the form of alpha, beta, or

gamma rays.[108-110] Nucleons (protons and neutrons) in the nucleus of an atom experience a binding force stronger than that of the repulsive force due to charge. The competition between this nuclear binding force and the electrostatic repulsion determines the stability of the nucleus.[111]

In the 1930s phosphorus-32, a beta-emitting cyclotron-produced radionuclide, was used for the treatment of patients with haematological diseases for the first time. Since then, the use of radioisotopes in medicine has expanded dramatically, and they are used for both diagnostic imaging (tissue penetration of gamma rays from nuclear decay of positron annihilation) and targeted therapy (toxicity of non-penetrating alpha and beta particles).[109]

1.9.1 Therapeutic Radiopharmaceuticals

Therapeutic radiopharmaceuticals are designed to deliver a therapeutic dose of ionising radiation to a specific site. Preferably, the molecule should localise at the desired site in an adequate concentration to deliver a cytotoxic dose of radiation. The radiopharmaceutical should also clear itself from the blood stream and other organs in a period that ensures no radiation damage can occur.[108] Numerous radionuclides are currently used for the treatment of malignancies, almost all of which are alpha- and beta-emitters. Some of the beta-emitting radionuclides used for medical applications in oncology are ^{32}P, ^{89}Sr, ^{90}Y, ^{166}Ho, ^{186}Re and ^{188}Re.[108]

1.9.2 Diagnostic Radiopharmaceuticals

Diagnostic radiopharmaceuticals are used for imaging and consist of molecules labelled with gamma- or positron-emitting radionuclides. Single photon emission computed tomography (SPECT) and positron emitted tomography (PET) are the two imaging techniques used to visualise the radionuclide and provide metabolic and functional information.

Technetium-99m, a metastable isotope of technetium-99, emits γ-radiation with a half-life of 6.02 hours.[109] It is, and has been for some decades, the radioisotope used in the largest number of radionuclide scans, due to its suitable half-life and gamma-energy (140 keV), which are beneficial for effective imaging and patient safety viewpoints.[108, 109] The distribution problems posed by the short half-life of ^{99m}Tc are overcome by transporting it in the form of ^{99}Mo ($t_{1/2}$ = 60 hours).[109] ^{99m}Tc is then generated from ^{99}Mo using a ^{99m}Tc generator.[109]

Rhenium-186 and rhenium-188 are of great interest to researchers as therapeutic analogues of ^{99m}Tc radiopharmaceuticals.[109] Although rhenium and technetium behave differently in certain conditions, for example, the bisphosphonate complexes,[112] the tricarbonyl complexes are similar in structure and reactivity.[109]

Along with the enhanced permeability and retention effect of dendrimers, ^{99m}Tc-based moieties on dendritic scaffolds could be used to image solid tumours and, if the complexes are found to aggregate in microbes, microbial infections.[113]

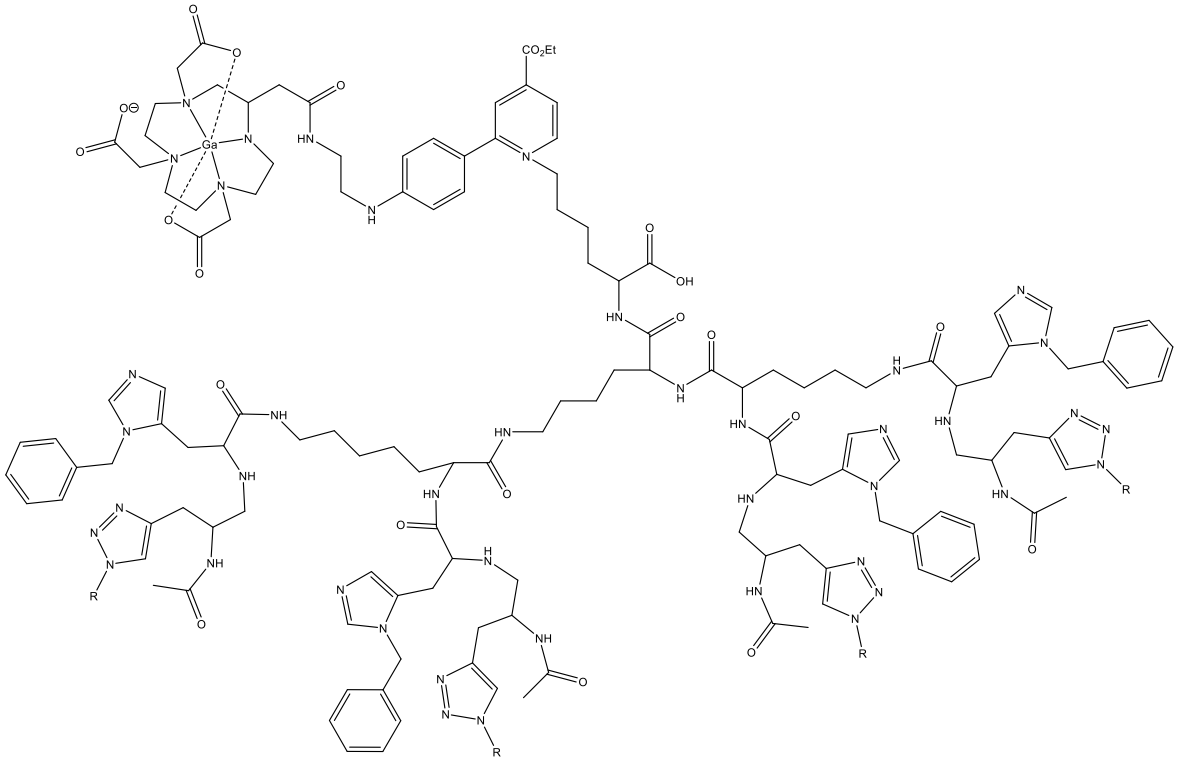

Figure 1.18: Structure of ^{68}Ga-radiolabelled metallodendrimer[114]

^{111}In is a radionuclide that is clinically available for imaging using gamma-scintigraphy. It has a half-life of 2.8 days and decays by electron capture (whereby an electron from a low electron shell is absorbed by the nucleus to pair with a proton, which becomes a neutron, resulting in the release of an electron neutrino), releasing two gamma-photon emissions at 173 and 247 keV.[108] ^{111}In was first introduced as a tumour imaging agent, due to its dispersal in the intracellular and extracellular spaces of tumours.[115] ^{111}In-labelled complexes are often used as imaging substitutes for dosimetry determination and biodistribution of ^{90}Y congeners, due to their similar coordination chemistry.

^{125}I is a radioisotope of iodine with a half-life of 60 days and a gamma-ray photon energy of 28 keV. It is used primarily in radioimmunoassays and other *in vitro* tests. Other iodine isotopes are used for thyroid SPECT (^{123}I), hormonal disorders or cancerous thyroid pathology observed by PET (^{124}I) or SPECT (^{131}I) imaging.[108]

^{68}Ga is used as a non-physiological metallic positron emitter for clinical PET imaging. Its use stems from the availability of ^{68}Ga from an on-site generator, eliminating the need for a cyclotron. It has a half-life of 68 minutes, and decays by 89 % through a positron emission of 1.92 MeV.[108] **Figure 1.18** shows the structure of a radiolabelled metallodendrimer synthesised by Fukase and co-workers.[114]

1.10 Non-invasive Nuclear Imaging Modalities

SPECT and PET are the two techniques used to visualise the radionuclide *in vivo*. The different techniques come with pros and cons, but, in general, PET is preferred over SPECT due to the higher resolution that it is possible to achieve using PET.[116]

In SPECT imaging, the radiation is measured by gamma-ray cameras, with gamma-emitting radionuclides with energies of approximately 75 – 360 keV.[117] SPECT is usually used in combination with other imaging techniques, such as magnetic resonance contrast. SPECT/CT scans are the most common, where a computed tomography scan (CT) is first performed, followed by the SPECT scan, and the images are merged.

PET imaging also uses the detection of gamma-rays to image the radionuclides. In PET imaging, the gamma-rays are formed from the annihilation of positrons. The unstable atom lowers its energy by emitting ionising radiation. The emitted particle loses its energy by collisions with the atoms in the adjacent tissue.[116] When the particle has reached a sufficiently low energy, it collides with a free electron, producing two photons of equal energy (511 keV) travelling in almost opposite directions, which are detected by the PET camera.[116]

The most important advantage that PET imaging has over SPECT imaging is the higher sensitivity. PET imaging is more sensitive by two or three orders of magnitude, meaning that the detector can detect a higher percentage of emitted events.[117]

Due to the longer half-life of single photon emitters, SPECT has a widened observational window when compared to PET. This allows biological processes to be observed *in vivo* over a period of hours or days.[118]

1.11 Aims and Objectives

1.11.1 General Aims

The general aims of this project were to:

- Design, synthesise and characterise two series of mono-, tris- and dendritic picolylamine ligands
- Synthesise the metal precursors and coordinate them to the ligands to form the respective metallodendrimers
- Evaluate the CO-release properties of the complexes
- Radiolabel the ligands with ^{99m}Tc

1.11.2 Specific Objectives

- To synthesise a series of monomeric and dendritic ligands functionalised with 2-picolylamine and 4-picolylamine

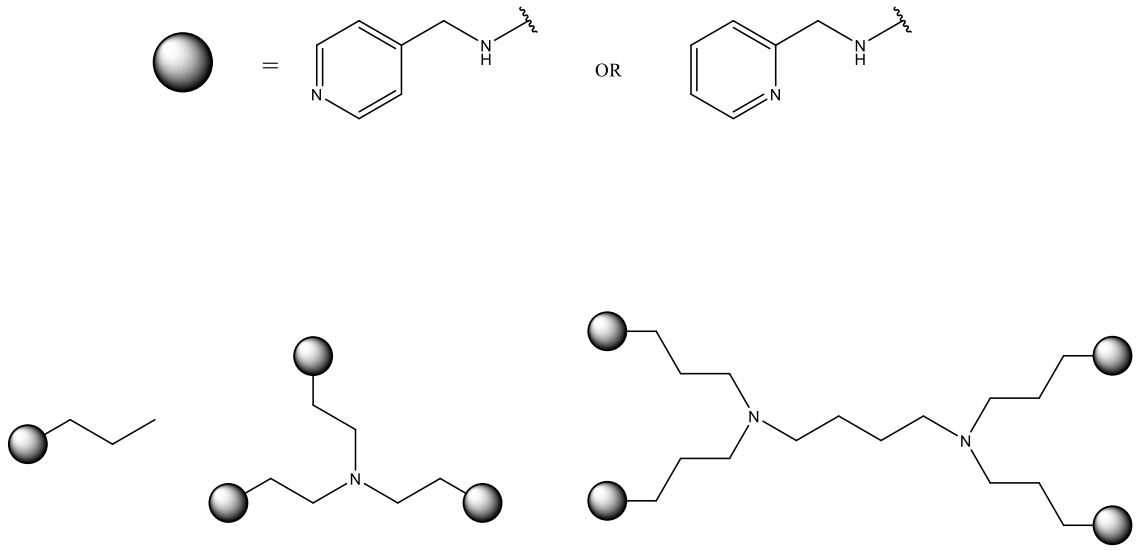

Figure 1.19: General structure of the 2-picolylamine and 4-picolylamine ligands

- To coordinate the synthesised 4-picolylamine ligands to carbonyl-bipyridyl Mn and Re to form the tricarbonyl products

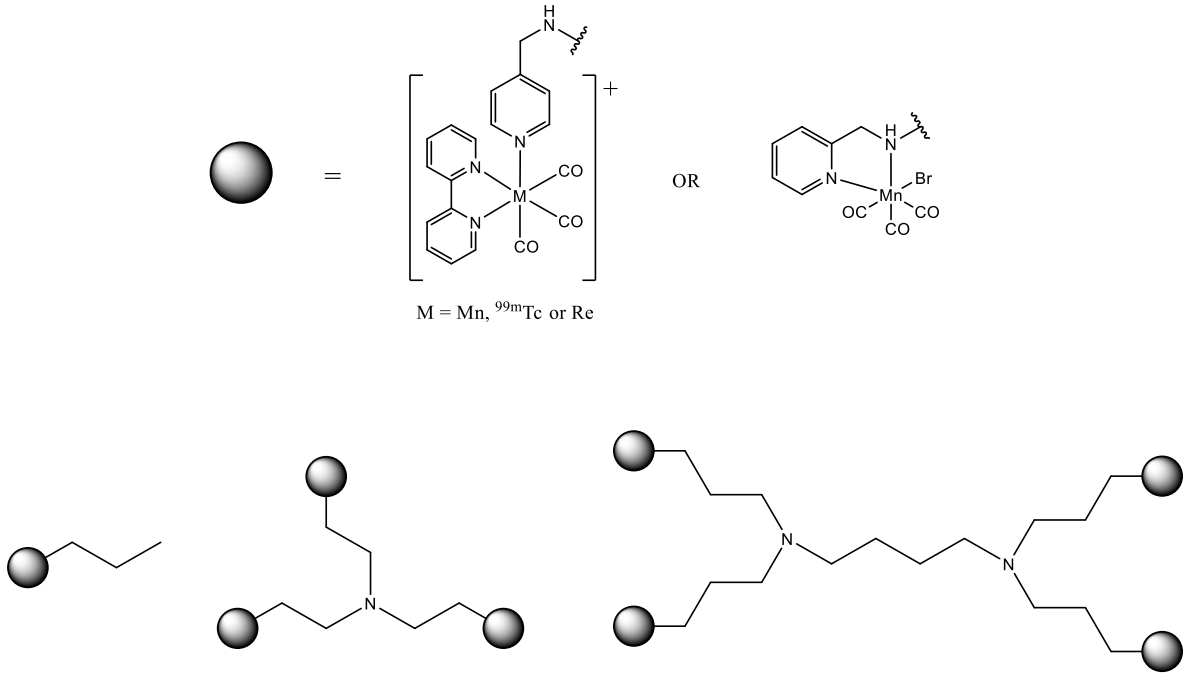

Figure 1.20: General structure of the manganese, technetium-99m and rhenium metallodendrimers

- To radiolabel the ligands with ^{99m}Tc using the isoLink® method
- To determine the CO-release properties of the Mn(I) tricarbonyl complexes

References

1. L. S. Nobre, J. D. Seixas, C. C. Romao and L. M. Saraiva, *Antimicrob. Agents Chemother.*, 2007, **51**, 4303-4307.
2. T. Sjostrand, *Nature*, 1949, **164**, 580-580.
3. B. E. Mann and R. Motterlini, *Chem. Commun.*, 2007, **41**, 4197-4208.
4. R. Alberto and R. Motterlini, *Dalton Trans.*, 2007, **17**, 1651-1660.
5. G. L. Bannenberg and H. L. A. Vieira, *Expert Opin. Ther. Pat.*, 2009, **19**, 663-682.
6. R. Foresti, M. G. Bani-Hani and R. Motterlini, *Intensive Care Med.*, 2008, **34**, 649-658.
7. R. Motterlini, B. E. Mann and R. Foresti, *Expert Opin. Invest. Drugs*, 2005, **14**, 1305-1318.
8. B. E. Mann, in *Top. Organometal. Chem.*, 2010, vol. 32, pp. 247-285.
9. C. Nagel, S. McLean, R. K. Poole, H. Braunschweig, T. Kramer and U. Schatzschneider, *Dalton Trans.*, 2014, **43**, 9986-9997.

10. M. Desmard, R. Foresti, D. Morin, M. Dagoussat, A. Berdeaux, E. Denamur, S. H. Crook, B. E. Mann, D. Scapens, P. Montravers, J. Boczkowski and R. Motterlini, *Antioxid. Redox Signaling*, 2012, **16**, 153-163.
11. M. Desmard, K. S. Davidge, O. Bouvet, D. Morin, D. Roux, R. Foresti, J. D. Ricard, E. Denamur, R. K. Poole, P. Montravers, R. Motterlini and J. Boczkowski, *FASEB J.*, 2009, **23**, 1023-1031.
12. K. Sato, J. Balla, L. Otterbein, R. N. Smith, S. Brouard, Y. Lin, E. Csizmadia, J. Sevigny, S. C. Robson, G. Vercellotti, A. M. Choi, F. H. Bach and M. P. Soares, *J. Immunol.*, 2001, **166**, 4185-4194.
13. M. Lavitrano, R. T. Smolenski, A. Musumeci, M. Maccherini, E. Slominska, E. di Florio, A. Bracco, A. Mancini, G. Stassi, M. Patti, R. Giovannoni, A. Froio, F. Simeone, M. Forni, M. L. Bacci, G. D'Alise, E. Cozzi, L. E. Otterbein, M. H. Yacoub, F. H. Bach and F. Calise, *FASEB J.*, 2004, **18**, 1093-1109.
14. B. S. Zuckerbraun, B. Y. Chin, B. Wegiel, T. R. Billiar, E. Czsimadia, J. Rao, L. Shimoda, E. Ifedigbo, S. Kanno and L. E. Otterbein, *J. Exp. Med.*, 2006, **203**, 2109-2119.
15. S. Lee, S. J. Lee, A. A. Coronata, L. E. Fredenburgh, S. W. Chung, M. A. Perrella, K. Nakahira, S. W. Ryter and A. M. Choi, *Antioxid. Redox Signaling*, 2014, **20**, 432-442.
16. S. Garcia-Gallego and G. J. Bernardes, *Angew. Chem. Int. Ed.*, 2014, **53**, 9712-9721.
17. R. Motterlini, J. E. Clark, R. Foresti, P. Sarathchandra, B. E. Mann and C. J. Green, *Circ. Res.*, 2002, **90**, E17-24.
18. W. H. Organisation, 10 facts on malaria, http://www.who.int/features/factfiles/malaria/en/, October, 2017).
19. A. Bosman and K. N. Mendis, *Am. J. Trop. Med. Hyg.*, 2007, **77**, 193-197.
20. *World Malaria Report 2016: Summary*, World Health Organisation, Geneva, 2017.
21. C. Biot, W. Castro, C. Y. Botte and M. Navarro, *Dalton Trans.*, 2012, **41**, 6335-6349.
22. P. L. Trigg and A. V. Kondrachine, *Malaria: Parasite biology, pathogenesis and protection*, ASM Press, Washington D.C., 1 edn., 1998.
23. E. A. Ashley, M. Dhorda, R. M. Fairhurst, C. Amaratunga, P. Lim, S. Suon, S. Sreng, J. M. Anderson, S. Mao, B. Sam, C. Sopha, C. M. Chuor, C. Nguon, S. Sovannaroth, S. Pukrittayakamee, P. Jittamala, K. Chotivanich, K. Chutasmit, C. Suchatsoonthorn, R. Runcharoen, T. T. Hien, N. T. Thuy-Nhien, N. V. Thanh, N. H. Phu, Y. Htut, K. T. Han, K. H. Aye, O. A. Mokuolu, R. R. Olaosebikan, O. O. Folaranmi, M. Mayxay, M. Khanthavong, B. Hongvanthong, P. N. Newton, M. A. Onyamboko, C. I. Fanello, A.

K. Tshefu, N. Mishra, N. Valecha, A. P. Phyo, F. Nosten, P. Yi, R. Tripura, S. Borrmann, M. Bashraheil, J. Peshu, M. A. Faiz, A. Ghose, M. A. Hossain, R. Samad, M. R. Rahman, M. M. Hasan, A. Islam, O. Miotto, R. Amato, B. MacInnis, J. Stalker, D. P. Kwiatkowski, Z. Bozdech, A. Jeeyapant, P. Y. Cheah, T. Sakulthaew, J. Chalk, B. Intharabut, K. Silamut, S. J. Lee, B. Vihokhern, C. Kunasol, M. Imwong, J. Tarning, W. J. Taylor, S. Yeung, C. J. Woodrow, J. A. Flegg, D. Das, J. Smith, M. Venkatesan, C. V. Plowe, K. Stepniewska, P. J. Guerin, A. M. Dondorp, N. P. Day and N. J. White, *N. Engl. J. Med.*, 2014, **371**, 411-423.

24. F. Dubar, T. J. Egan, B. Pradines, D. Kuter, K. K. Ncokazi, D. Forge, J. F. Paul, C. Pierrot, H. Kalamou, J. Khalife, E. Buisine, C. Rogier, H. Vezin, I. Forfar, C. Slomianny, X. Trivelli, S. Kapishnikov, L. Leiserowitz, D. Dive and C. Biot, *ACS Chem. Biol.*, 2011, **6**, 275-287.
25. F. Dubar, J. Khalife, J. Brocard, D. Dive and C. Biot, *Molecules*, 2008, **13**, 2900-2907.
26. To Evaluate the Efficacy of a Single Dose Regimen of Ferroquine and Artefenomel in Adults and Children With Uncomplicated Plasmodium Falciparum Malaria (FALCI), https://clinicaltrials.gov/ct2/show/NCT02497612, (accessed October, 2017).
27. H. Torres-Gomez, E. Hernandez-Nunez, I. Leon-Rivera, J. Guerrero-Alvarez, R. Cedillo-Rivera, R. Moo-Puc, R. Argotte-Ramos, C. Rodriguez-Gutierrez Mdel, M. J. Chan-Bacab and G. Navarrete-Vazquez, *Bioorg. Med. Chem. Lett.*, 2008, **18**, 3147-3151.
28. P. Toro, A. H. Klahn, B. Pradines, F. Lahoz, A. Pascual, C. Biot and R. Arancibia, *Inorg. Chem. Commun.*, 2013, **35**, 126-129.
29. A. Ferreira, J. Balla, V. Jeney, G. Balla and M. P. Soares, *J. Mol. Med.*, 2008, **86**, 1097-1111.
30. A. Ferreira, I. Marguti, I. Bechmann, V. Jeney, A. Chora, N. R. Palha, S. Rebelo, A. Henri, Y. Beuzard and M. P. Soares, *Cell*, 2011, **145**, 398-409.
31. A. Pamplona, A. Ferreira, J. Balla, V. Jeney, G. Balla, S. Epiphanio, A. Chora, C. D. Rodrigues, I. P. Gregoire, M. Cunha-Rodrigues, S. Portugal, M. P. Soares and M. M. Mota, *Nat. Med. (N. Y., NY, U. S.)*, 2007, **13**, 703-710.
32. G. Silva, V. Jeney, A. Chora, R. Larsen, J. Balla and M. P. Soares, *J. Biol. Chem.*, 2009, **284**, 29582-29595.
33. R. T. Figueiredo, P. L. Fernandez, D. S. Mourao-Sa, B. N. Porto, F. F. Dutra, L. S. Alves, M. F. Oliveira, P. L. Oliveira, A. V. Graca-Souza and M. T. Bozza, *J. Biol. Chem.*, 2007, **282**, 20221-20229.

34. R. Gozzelino, V. Jeney and M. P. Soares, *Annu. Rev. Pharmacool. Toxicol.*, 2010, **50**, 323-354.
35. E. Seixas, R. Gozzelino, A. Chora, A. Ferreira, G. Silva, R. Larsen, S. Rebelo, C. Penido, N. R. Smith, A. Coutinho and M. P. Soares, *Proc. Natl. Acad. Sci. U. S. A.*, 2009, **106**, 15837-15842.
36. S. McLean, R. Begg, H. E. Jesse, B. E. Mann, G. Sanguinetti and R. K. Poole, *Antioxid. Redox Signaling*, 2013, **19**, 1999-2012.
37. F. Gullotta, A. di Masi and P. Ascenzi, *IUBMB Life*, 2012, **64**, 378-386.
38. K. S. Davidge, G. Sanguinetti, C. H. Yee, A. G. Cox, C. W. McLeod, C. E. Monk, B. E. Mann, R. Motterlini and R. K. Poole, *J. Biol. Chem.*, 2009, **284**, 4516-4524.
39. A. Kastl, S. Dieckmann, K. Waehler, T. Voelker, L. Kastl, A. L. Merkel, A. Vultur, B. Shannan, K. Harms, M. Ocker, W. J. Parak, M. Herlyn and E. Meggers, *ChemMedChem*, 2013, **8**, 924-927.
40. R. Motterlini, P. Sawle, J. Hammad, S. Bains, R. Alberto, R. Foresti and C. J. Green, *FASEB J.*, 2005, **19**, 284-286.
41. A. Leonidova and G. Gasser, *ACS Chem. Biol.*, 2014, **9**, 2180-2193.
42. *USA Pat.*, WO2002092075A2, 2002.
43. A. Kooli, E. Kermorvant-Duchemin, F. Sennlaub, M. Bossolasco, X. Hou, J.-C. Honore, P. A. Dennery, P. Sapieha, D. Varma, P. Lachapelle, T. Zhu, S. Tremblay, P. Hardy, K. Jain, M. Balazy and S. Chemtob, *Free Radical Biol. Med.*, 2008, **44**, 815-825.
44. J. Megias, J. Busserolles and M. J. Alcaraz, *Br. J. Pharmacol.*, 2007, **150**, 977-986.
45. H. O. Pae, B. M. Choi, G. S. Oh, M. S. Lee, D. G. Ryu, H. Y. Rhew, Y. M. Kim and H. T. Chung, *Mol. Pharmacol.*, 2004, **66**, 122-128.
46. J. L. Wilson, H. E. Jesse, B. Hughes, V. Lund, K. Naylor, K. S. Davidge, G. M. Cook, B. E. Mann and R. K. Poole, *Antioxid. Redox Signaling*, 2013, **19**, 497-509.
47. J. C. Obirai, S. Hamadi, A. Ithurbide, C. Wartelle, T. Nyokong, J. Zagal, S. Top and F. Bedioui, *Electroanalysis*, 2006, **18**, 1689-1695.
48. A. Yabluchanskiy, P. Sawle, S. Homer-Vanniasinkam, C. J. Green, R. Foresti and R. Motterlini, *Crit. Care Med.*, 2012, **40**, 544-552.
49. I. J. S. Fairlamb, A. K. Duhme-Klair, J. M. Lynam, B. E. Moulton, C. T. O'Brien, P. Sawle, J. Hammad and R. Motterlini, *Bioorg. Med. Chem. Lett.*, 2006, **16**, 995-998.
50. *USA Pat.*, WO2007085806A2, 2007.

51. D. Scapens, H. Adams, T. R. Johnson, B. E. Mann, P. Sawle, R. Aqil, T. Perrior and R. Motterlini, *Dalton Trans.*, 2007, **43**, 4962-4973.
52. P. Dorkov, I. N. Pantcheva, W. S. Sheldrick, H. Mayer-Figge, R. Petrova and M. Mitewa, *J. Inorg. Biochem.*, 2008, **102**, 26-32.
53. M. X. Li, C. L. Chen, D. Zhang, J. Y. Niu and B. S. Ji, *Eur. J. Med. Chem.*, 2010, **45**, 3169-3177.
54. M. Damercheli, D. Dayyani, M. Behzad, B. Mehravi and M. S. Ardestani, *J. Coord. Chem.*, 2015, **68**, 1500-1513.
55. D. P. Singh, K. Kumar and C. Sharma, *Eur. J. Med. Chem.*, 2010, **45**, 1230-1236.
56. B.-W. Sun, X. Chen, Z.-Y. Chen, K. Katada and G. Cepinskas, *Chin. Med. J.*, 2007, **87**, 3148-3151.
57. Q. Xi, D. Tcheranova, H. Parfenova, B. Horowitz, C. W. Leffler and J. H. Jaggar, *Am. J. Physiol.*, 2004, **286**, H610-H618.
58. *Portugal Pat.*, WO2007073226A1, 2007.
59. *USA Pat.*, WO2008003953A2, 2008.
60. N. E. Brueckmann, M. Wahl, G. J. Reiss, M. Kohns, W. Waetjen and P. C. Kunz, *Eur. J. Inorg. Chem.*, 2011, **29**, 4571-4577.
61. K. I. Ansari, J. D. Grant, S. Kasiri, G. Woldemariam, B. Shrestha and S. S. Mandal, *J. Inorg. Biochem.*, 2009, **103**, 818-826.
62. P. V. Simpson, C. Nagel, H. Bruhn and U. Schatzschneider, *Organometallics*, 2015, **34**, 3809-3815.
63. Y. K. Yan, S. E. Cho, K. A. Shaffer, J. E. Rowell, B. J. Barnes and I. H. Hall, *Pharmazie*, 2000, **55**, 307-313.
64. A. W. T. Choi, M. W. Louie, S. P. Y. Li, H. W. Liu, B. T. N. Chan, T. C. Y. Lam, A. C. C. Lin, S. H. Cheng and K. K. W. Lo, *Inorg. Chem.*, 2012, **51**, 13289-13302.
65. A. Kermagoret, G. Morgant, J. d'Angelo, A. Tomas, P. Roussel, G. Bastian, P. Collery and D. Desmaële, *Polyhedron*, 2011, **30**, 347-353.
66. C. S. Parson, V.; Krauss, C.; Banerjee, H.N.; Reilly, C.; Krause, J.A.; Wachira, J.M.; Giri, D.; Winstead, A.; Mandal, S.K., *Br. J. Pharm. Res.*, 2014, **4**, 362-367.
67. N. A. Illan-Cabeza, A. R. Garcia-Garcia, M. N. Moreno-Carretero, J. M. Martinez-Martos and M. J. Ramirez-Exposito, *J. Inorg. Biochem.*, 2005, **99**, 1637-1645.
68. I. Machado, S. Fernandez, L. Becco, B. Garat, J. S. Gancheff, A. Rey and D. Gambino, *J. Coord. Chem.*, 2014, **67**, 1835-1850.
69. A. Leonidova and G. Gasser, *ACS Chem. Biol.*, 2014, **9**, 2180-2193.

70. F. Zobi, O. Blacque, R. A. Jacobs, M. C. Schaub and A. Y. Bogdanova, *Dalton Trans.*, 2012, **41**, 370-378.
71. N. A. Illan-Cabeza, A. R. Garcia-Garcia, M. N. Moreno-Carretero, J. M. Martinez-Martos and M. J. Ramirez-Exposito, *J. Inorg. Biochem.*, 2005, **99**, 1637-1645.
72. W. Q. Zhang, A. J. Atkin, R. J. Thatcher, A. C. Whitwood, I. J. Fairlamb and J. M. Lynam, *Dalton Trans.*, 2009, **22**, 4351-4358.
73. L. Glans, D. Taylor, C. de Kock, P. J. Smith, M. Haukka, J. R. Moss and E. Nordlander, *J. Inorg. Biochem.*, 2011, **105**, 985-990.
74. *Portugal Pat.*, WO2007073225A1, 2007.
75. *Portugal Pat.*, WO2008130261A1, 2008.
76. A. A. Abdel Aziz, *J. Mol. Struct.*, 2010, **979**, 77-85.
77. D. Jesudurai and S. Vancheesan, *Indian J. Chem., Sect. A: Inorg., Bio-inorg., Phys., Theor. Anal. Chem.*, 2003, **42**, 1609-1616.
78. R. D. Rimmer, H. Richter and P. C. Ford, *Inorg. Chem.*, 2010, **49**, 1180-1185.
79. X.-B. Chen, Q. Ye, Q. Wu, Y.-M. Song, R.-G. Xiong and X.-Z. You, *Inorg. Chem. Commun.*, 2004, **7**, 1302-1305.
80. R. G. Mohamed, F. M. Elantabli, N. H. Helal and S. M. El-Medani, *Synth. React. Inorg., Met.-Org., Nano-Met. Chem.*, 2015, **45**, 1839-1850.
81. C. C. Romao, W. A. Blaettler, J. D. Seixas and G. J. L. Bernardes, *Chem Soc Rev*, 2012, **41**, 3571-3583.
82. D. J. Darensbourg, J. D. Draper, D. L. Larkins, B. J. Frost and J. H. Reibenspies, *Inorg. Chem.*, 1998, **37**, 2538-2546.
83. J. A. S. Howell and P. M. Burkinshaw, *Chem. Rev.*, 1983, **83**, 557-599.
84. R. D. Rimmer, A. E. Pierri and P. C. Ford, *Coord. Chem. Rev.*, 2012, **256**, 1509-1519.
85. J. S. Ward, J. M. Lynam, J. Moir and I. J. Fairlamb, *Chemistry*, 2014, **20**, 15061-15068.
86. J. Niesel, A. Pinto, H. W. P. N'Dongo, K. Merz, I. Ott, R. Gust and U. Schatzschneider, *Chem. Commun.*, 2008, **15**, 1798-1800.
87. S. V. C. Vummaleti, D. Branduardi, M. Masetti, M. De Vivo, R. Motterlini and A. Cavalli, *Chemistry - A European Journal*, 2012, **18**, 9267-9275.
88. H. J. Vreman, R. J. Wong and D. K. Stevenson, in *Carbon Monoxide and Cardiovascular Functions*, ed. R. Wang, CRC Press, 2001.
89. G. Bartolucci, E. Droghetti, C. Focardi, M. Bambagiotti-Alberti, M. Nocentini and G. Smulevich, *J. Mass Spectrom.*, 2010, **45**, 1041-1045.

90. A. J. Atkin, J. M. Lynam, B. E. Moulton, P. Sawle, R. Motterlini, N. M. Boyle, M. T. Pryce and I. J. S. Fairlamb, *Dalton Trans.*, 2011, **40**, 5755-5761.
91. *USA Pat.*, WO8304095A1, 1983.
92. *USA Pat.*, WO2005114161A1, 2005.
93. G. E. Oosterom, J. N. H. Reek, P. C. J. Kamer and P. van Leeuwen, *Angew. Chem. Int. Ed.*, 2001, **40**, 1828-1849.
94. S. El Kazzouli, N. El Brahmi, S. Mignani, M. Bousmina, M. Zablocka and J. P. Majoral, *Curr. Med. Chem.*, 2012, **19**, 4995-5010.
95. L. C. Sudding, R. Payne, P. Govender, F. Edafe, C. M. Clavel, P. J. Dyson, B. Therrien and G. S. Smith, *J. Organomet. Chem.*, 2014, **774**, 79-85.
96. G. Doerdelmann, H. Pfeiffer, A. Birkner and U. Schatzschneider, *Inorg. Chem.*, 2011, **50**, 4362-4367.
97. R. K. Tekade, P. V. Kumar and N. K. Jain, *Chem. Rev.*, 2009, **109**, 49-87.
98. P. Govender, N. C. Antonels, J. Mattsson, A. K. Renfrew, P. J. Dyson, J. R. Moss, B. Therrien and G. S. Smith, *J. Organomet. Chem.*, 2009, **694**, 3470-3476.
99. P. Govender, F. Edafe, B. C. E. Makhubela, P. J. Dyson, B. Therrien and G. S. Smith, *Inorg. Chim. Acta*, 2014, **409**, 112-120.
100. W. Hu, J. Hoyer, I. Neundorf, P. Govender, G. S. Smith and U. Schatzschneider, *Eur. J. Inorg. Chem.*, 2015, **2015**, 1505-1510.
101. L. C. Sudding, R. Payne, P. Govender, F. Edafe, C. M. Clavel, P. J. Dyson, B. Therrien and G. S. Smith, *J. Organomet. Chem.*, 2014, **774**, 79-85.
102. R. Payne, P. Govender, B. Therrien, C. M. Clavel, P. J. Dyson and G. S. Smith, *J. Organomet. Chem.*, 2013, **729**, 20-27.
103. C. Billecke, S. Finniss, L. Tahash, C. Miller, T. Mikkelsen, N. P. Farrell and O. Boegler, *Neuro Oncol.*, 2006, **8**, 215-226.
104. B. A. J. Jansen, J. van der Zwan, J. Reedijk, H. den Dulk and J. Brouwer, *Eur. J. Inorg. Chem.*, 1999, **1999**, 1429-1433.
105. P. Govender, S. Pai, U. Schatzschneider and G. S. Smith, *Inorg. Chem.*, 2013, **52**, 5470-5478.
106. A. I. Kassis, H. Korideck, K. Wang, P. Pospisil and S. J. Adelstein, *Molecules*, 2008, **13**, 391-404.
107. R. Alberto, in *Bioorganometallics: Biomolecules, Labeling, Medicine*, ed. G. Jaouen, Wiley-VCH, Weinheim, Germany, 2006, pp. 97-124.

108. C. Ghobril, G. Lamanna, M. Kueny-Stotz, A. Garofalo, C. Billotey and D. Felder-Flesch, *New J. Chem.*, 2012, **36**, 310-323.
109. P. J. Blower, *Dalton Trans.*, 2015, **44**, 4819-4844.
110. E. M. Jagoda, L. X. Lang, V. Bhadrasetty, S. Histed, M. Williams, G. Kramer-Marek, E. Mena, L. Rosenblum, J. Marik, J. N. Tinianow, M. Merchant, L. Szajek, C. Paik, F. Cecchi, K. Raffensperger, J. M. Jose-Dizon, D. P. Bottaro and P. Choyke, *J. Nucl. Med.*, 2012, **53**, 1592-1600.
111. E. Rutherford, *The Newer Alchemy*, Cambridge University Press, Cambridge, UK, 1937.
112. R. Torres Martin de Rosales, C. Finucane, S. J. Mather and P. J. Blower, *Chem. Commun. (Cambridge, U. K.)*, 2009, **32**, 4847-4849.
113. S. Vinjamuri, A. V. Hall, K. K. Solanki, J. Bomanji, Q. Siraj, E. Oshaughnessy, S. S. Das and K. E. Britton, *Lancet*, 1996, **347**, 233-235.
114. K. Tanaka, E. R. O. Siwu, K. Minami, K. Hasegawa, S. Nozaki, Y. Kanayama, K. Koyama, W. C. Chen, J. C. Paulson, Y. Watanabe and K. Fukase, *Angew. Chem. Int. Ed.*, 2010, **49**, 8195-8200.
115. H. M. Abdeldayam, A. M. Elkousy, E. V. Leslie and V. A. Panaro, *Radiology*, 1975, **114**, 403-406.
116. D. Brasse and A. Nonat, *Dalton Trans.*, 2015, **44**, 4845-4858.
117. A. Rahmim and H. Zaidi, *Nucl. Med. Commun.*, 2008, **29**, 193-207.
118. S. R. Meikle, P. Kench, M. Kassiou and R. B. Banati, *Phys. Med. Biol.*, 2005, **50**, R45-R61.

Chapter 2 Synthesis and Characterisation of Ligands and Complexes

2.1 Introduction

Considering the success of metal-based drugs in the treatment of various illnesses, a range of ligands and their group 7 complexes have been synthesised and researched as biologically active molecules. Group 7 carbonyl complexes have shown promise as potential anticancer,[1-6] antibacterial,[7] antifungal[8] and antiplasmodial agents.[9, 10]

2.2 Synthesis and Characterisation of 4-Picolylamine Ligands

The 4-picolylimine ligand precursors, **4**, **5** and **6**, were synthesised using known methods.[11-13] The ligand precursors were prepared by reacting 4-pyridinecarboxaldehyde with the suitable dendritic scaffold *via* a Schiff base condensation reaction (general mechanism shown in **Scheme 2.2**), followed by reduction of the imine using $NaBH_4$ to afford the desired ligand (**Scheme 2.1**).

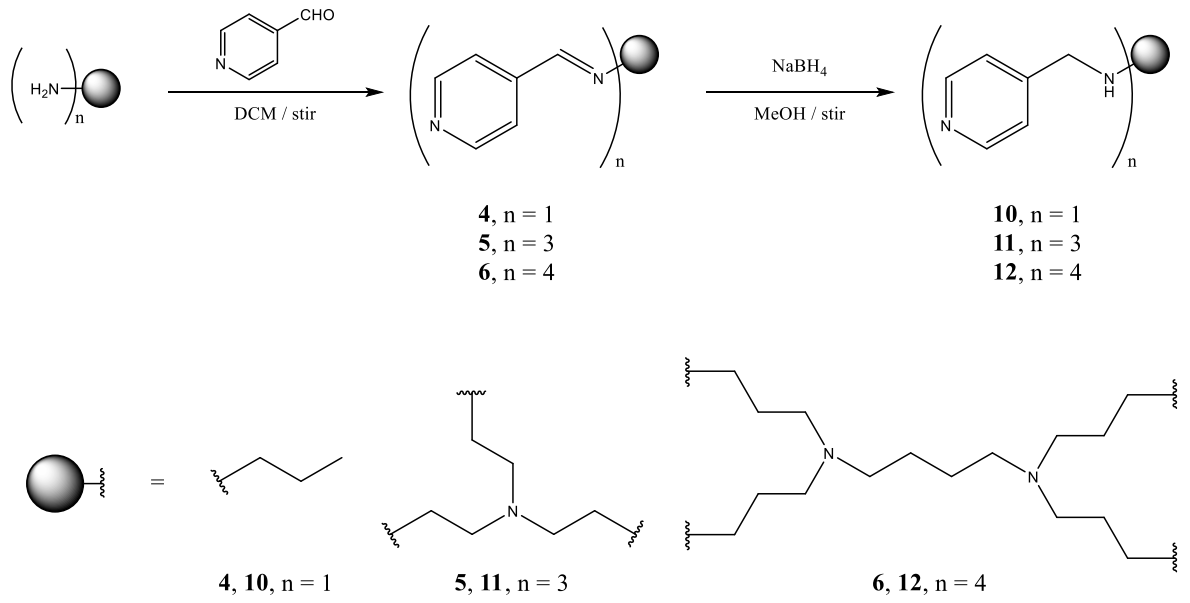

Scheme 2.1: Synthesis of 4-picolylamine ligands

The Schiff base reaction was performed in DCM in the presence of $MgSO_4$, used as a drying agent to remove the water, which is formed as a by-product (see **Scheme 2.2**), and prevents the reverse reaction from occurring, as all steps in the Schiff-base formation are reversible. The reduction was performed in methanol by $NaBH_4$. The 4-picolylamine ligands were isolated as brown oils in good to moderate overall yields (**Table 2.1**).

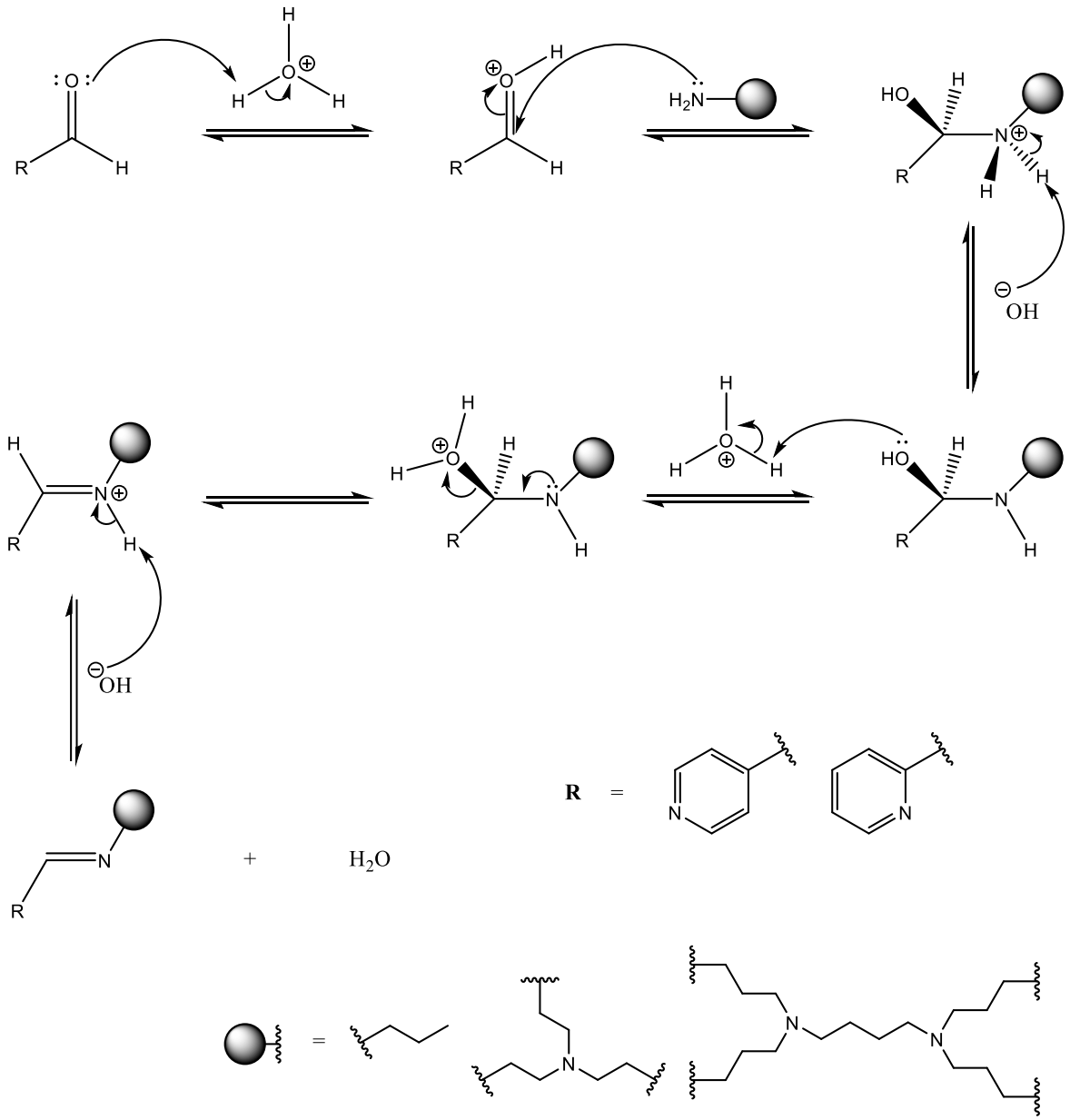

Scheme 2.2: Mechanistic outline of a general Schiff base condensation reaction in water

Table 2.1: Physical appearance and overall yield for 4-picolylamine ligands

Compound	Physical Appearance	Overall yield (%)
10	Yellow oil	48
11	Dark brown oil	76
12	Light brown oil	41

The 4-picolylamine ligands **10** – **12** are non-hygroscopic, stable in air at room temperature, and soluble in acetone, acetonitrile, dichloromethane, methanol, ethanol and dimethylsulfoxide.

2.2.1 ^{1}H and ^{13}C{^{1}H} NMR Spectroscopy

Analysis of the ^{1}H and ^{13}C{^{1}H} spectra of compounds **4** – **6** and **10** – **12** confirmed that the proposed compounds were attained. **Figure 2.1** shows the ^{1}H NMR spectrum of ligand precursor **6**.

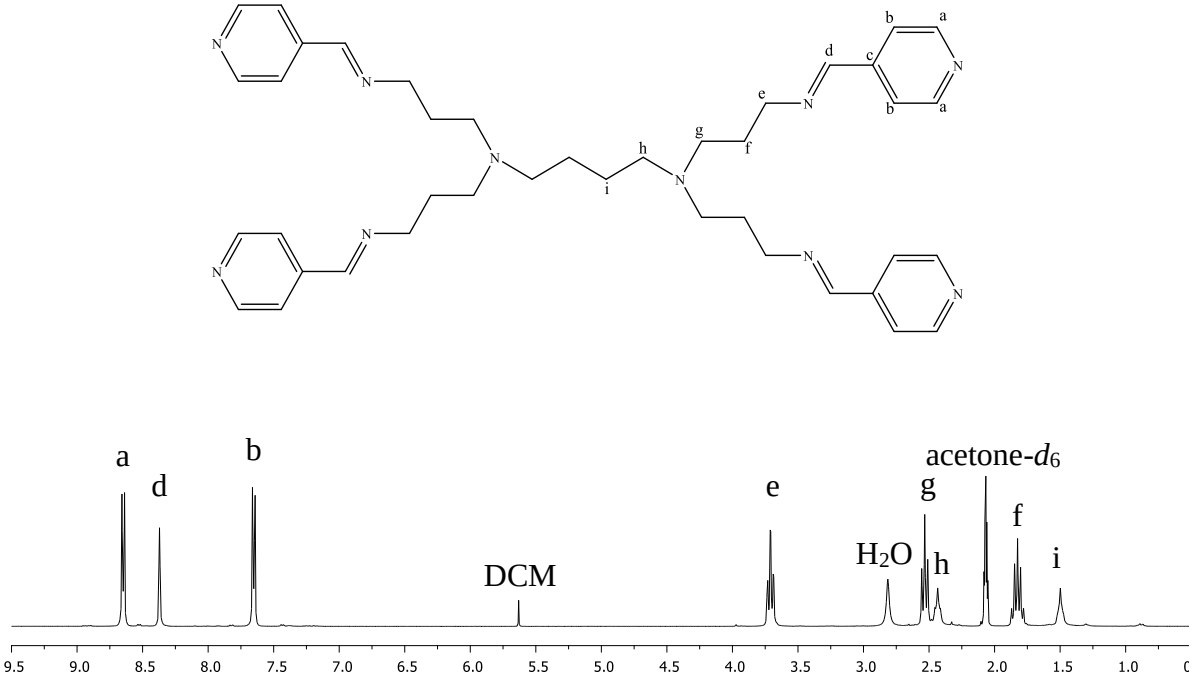

Figure 2.1: ^{1}H NMR spectrum of ligand precursor **6**

In the ^{1}H NMR spectrum of compound **6**, protons H_a and H_b appear as a pair of doublet of doublets at 8.65 and 7.65 ppm, respectively. The imine proton, H_d, appears in the expected region as a singlet at 8.37 ppm. A cross peak is observed in the COSY spectrum, indicating coupling between the imine proton and H_e, but, at this resolution, the imine proton is observed

as a singlet. COSY and HSQC NMR experiments were performed to assign proton and carbon signals.

Figure 2.2 shows the stacked ^{1}H NMR spectra for ligands **10**, **11** and **12**, all recorded in acetone-d_6.

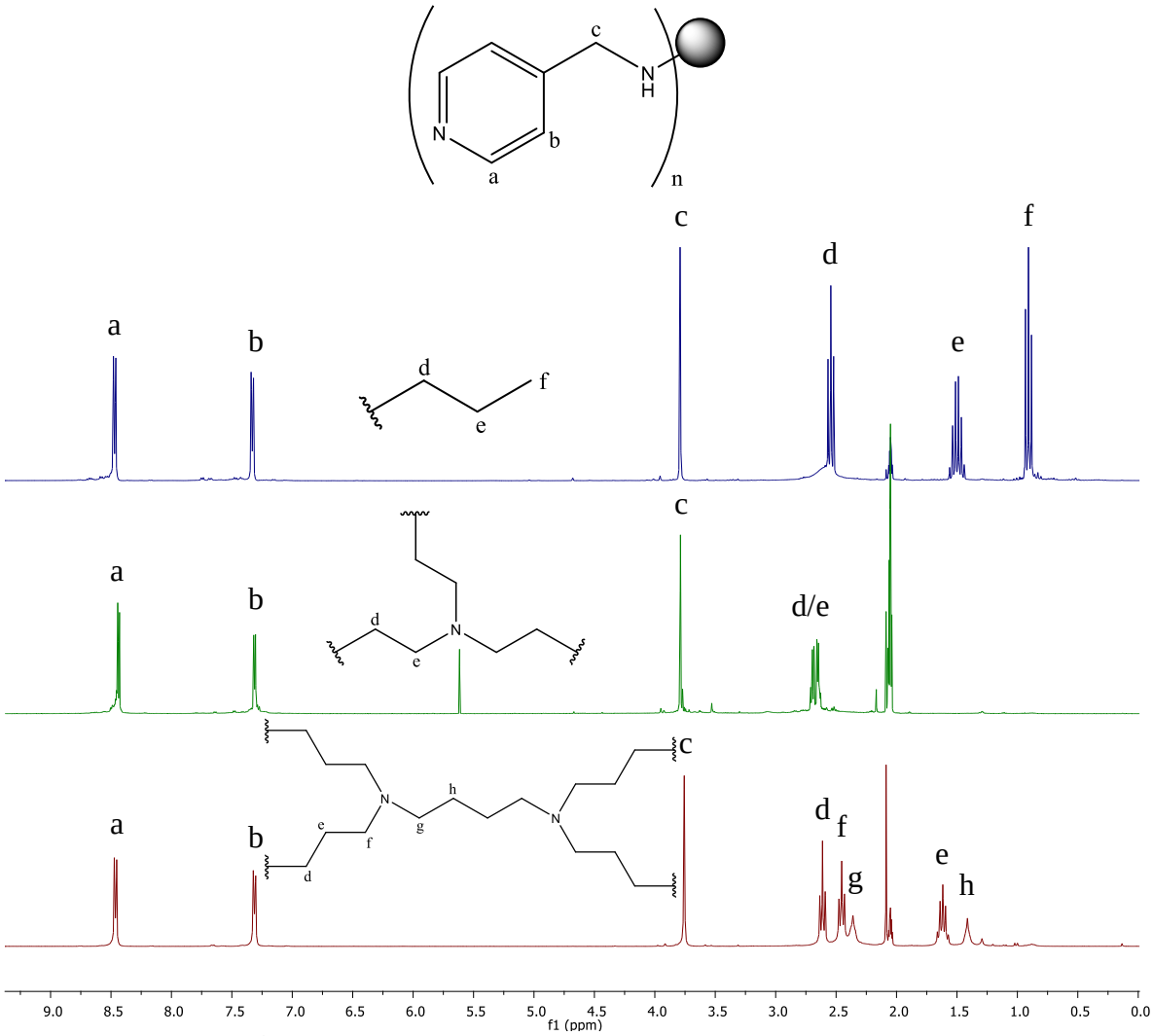

Figure 2.2: Stacked ^{1}H NMR spectra of ligands **10**, **11** and **12**

From **Figure 2.2** it is clear that there is no imine peak, which is observed as a singlet at approximately 8.35 ppm in the ^{1}H NMR spectra of ligand precursors **4**, **5** and **6** (see **Figure 2.1**). This, along with the new methylene singlet (H_c) at *ca.* 3.80 ppm in each of the spectra, is evidence that the reduction was successfully performed.

In each ^{1}H NMR spectrum, two doublets are observed in the aromatic region, due to the four protons on the pyridyl ring. Only two peaks are observed due to the local symmetry in the pyridyl ring. No NH signal is observed in acetone-d_6, but is observed in DMSO-d_6.

$^{13}C\{^{1}H\}$ NMR experiments were performed, accompanied by COSY and HSQC 2-D NMR experiments, to aid in the assignment of proton and carbon signals. The $^{13}C\{^{1}H\}$ spectra display all of the expected peaks in the expected ranges.

2.2.2 Infrared Spectroscopy

The infrared spectra of 4-picolylamine ligands **10** – **12** were recorded as pure oils using the attenuated total reflectance sampling technique, which allows the user to examine the sample directly without further preparation. Two characteristic absorption bands for the aromatic C=N stretching vibration and the NH stretching band are displayed. **Table 2.2** shows important absorption bands in the infrared spectrum of the 4-picolylamine ligands.

Table 2.2: Important infrared absorption bands for 4-picolylamine ligands

Compound	$C=N_{aromatic}$ (cm^{-1})	NH (cm^{-1})
10	1600	3274
11	1600	3270
12	1602	3270

The infrared absorption bands arise in the expected regions for both the C=N ring stretch and the NH stretching bands.

2.2.3 Mass Spectrometry

Mass spectrometry was utilised to further confirm the presence of the proposed structures.

Table 2.3: EI mass spectrometry results for 4-picolylamine ligands

Compound	*m/z*	Fragment
10	149.07	$[M-H]^+$
11	419.26	$[M]^+$
12	678.45	$[M-H]^+$

Table 2.3 displays the mass spectrometry results for 4-picolylamine ligands. These results, accompanied by the other characterisation techniques used, suggest that the proposed structures were obtained.

2.3 Synthesis and Characterisation of 2-Picolylamine Ligands

The 2-picolylamine ligands (**13**, **14** and **15**) were synthesised in a similar manner to that of the 4-picolylamine ligands, following literature procedures (see **Scheme 2.3**): Schiff base reaction in DCM to afford the ligand precursors,[11, 12, 14] **7**, **8** and **9**, followed by reduction with $NaBH_4$ to yield the desired ligands. The ^1H NMR spectra of the 2-picolylamine ligands are shown in **Figure 2.4**.

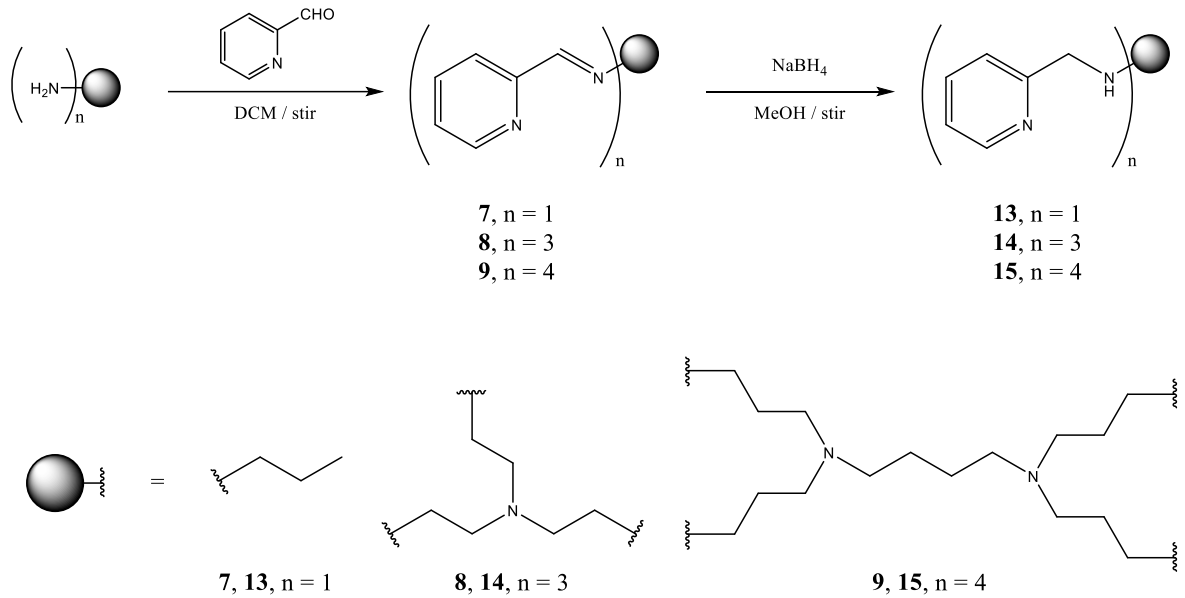

Scheme 2.3: Synthesis of 2-picolylamine ligands

Similarly to the synthesis and purification of the 4-picolylamine ligands, the imine formation was performed in DCM, and purification was accomplished by washing the DCM layer with copious amounts of water. The reduction was performed in methanol using sodium borohydride as the reducing agent, under Ar, after which the excess $NaBH_4$ was quenched with water, and a liquid-liquid extraction (DCM/water) was employed to remove the remaining starting material. The 2-picolylamine ligands were isolated as brown oils in moderate to low overall yields (**Table 2.3**).

Table 2.3: Physical appearance and overall yield for 2-picolylamine ligands

Compound	Physical Appearance	Overall yield (%)
13	Yellow oil	31
14	Dark brown oil	62

15	Dark brown oil	61

Ligands **13** – **15** are air-stable at room temperature, are soluble in methanol, ethanol, acetone, DCM, chloroform and DMSO, and sparingly soluble in water.

2.3.1 ^{1}H and $^{13}C\{^{1}H\}$ NMR Spectroscopy

^{1}H and $^{13}C\{^{1}H\}$ NMR experiments were performed to ascertain whether the desired products were present. **Figure 2.3** shows an assigned ^{1}H NMR spectrum for ligand precursor **7**, as a representative for the ligand precursors **7** – **9**.

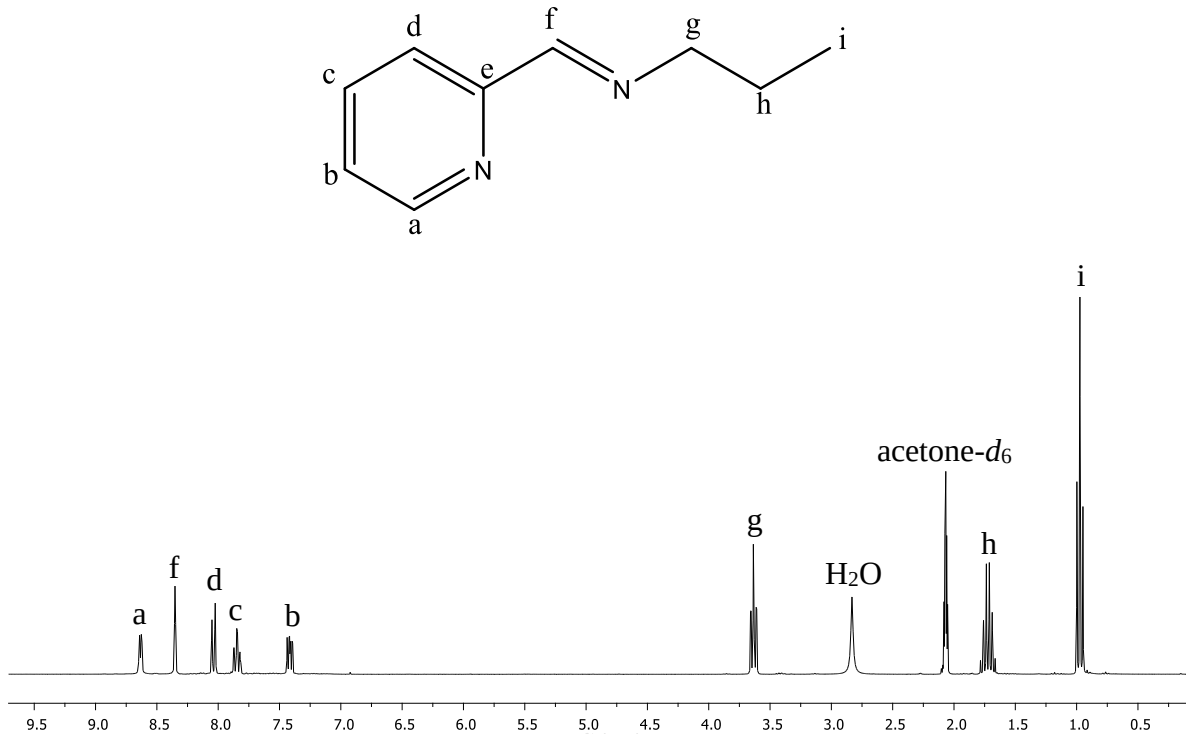

Figure 2.3: ^{1}H NMR spectrum of ligand precursor **7**

^{1}H and $^{13}C\{^{1}H\}$ NMR spectroscopy were used to confirm that the proposed structures were obtained. **Figure 2.3** shows the ^{1}H NMR spectrum of ligand precursor **7**. The characteristic imine peak, H_f, integrates for one proton, and is observed as a doublet at 8.35 ppm, due to coupling to proton H_g, as confirmed by a COSY NMR experiment. Unlike the 4-pyridyl ligands and ligand precursors, there is no local symmetry in the pyridyl ring, resulting in four separate aromatic peaks (H_a, H_b, H_c and H_d), each integrating for one proton. The aliphatic proton peaks are in the expected region and integrate for the projected number of protons.

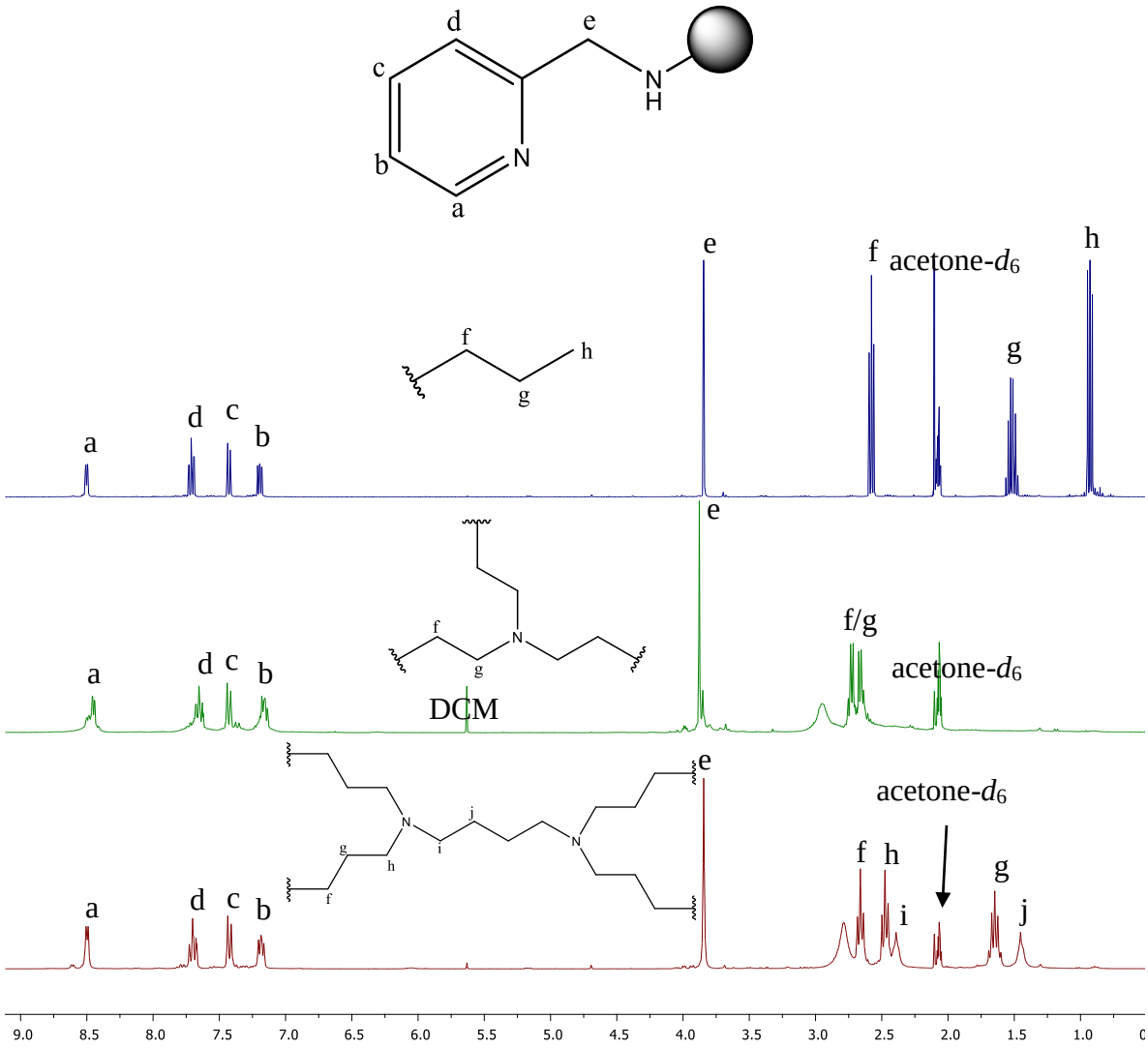

Figure 2.4: stacked ^{1}H NMR spectra of ligands **13**, **14** and **15**

The lack of a sharp imine proton signal at *ca.* 8.35 ppm in all the spectra in **Figure 2.4**, in conjunction with the formation of a new methylene peak observed at approximately 3.80 ppm, signifies the reduction of the imine to form the desired amine.

The aromatic peaks are due to the four non-equivalent protons on the pyridyl ring. The four peaks each integrate for one proton, which is consistent with the proposed structures. The aliphatic peaks are typical of the respective cores.

In the ^{13}C{^{1}H} NMR spectra of the ligands, the aromatic peaks arise between 121 and 161 ppm, as expected, while the aliphatic peaks are observed in the range of 11 – 55 ppm. COSY and HSQC NMR experiments were performed to assign the proton and carbon NMR spectra.

2.3.2 Infrared Spectroscopy

Infrared spectroscopy was used as further evidence to demonstrate the formation of the desired ligands. The 2-picolylamine ligands display two characteristic absorption bands: the C=N stretching band, and the NH stretching band. The important absorption bands are summarised in **Table 2.4**, all of which lie in the expected regions.

Table 2.4: Important infrared absorption bands for 2-picolylamine ligands

Compound	$C=N_{aromatic}$ (cm^{-1})	NH (cm^{-1})
13	1592	3290
14	1591	3291
15	1591	3288

2.3.3 Mass Spectrometry

EI mass spectrometry was utilised to further confirm the structural integrity of the proposed ligands. The data are summarised in **Table 2.5**.

Table 2.5: EI mass spectrometry results for 4-picolylamine ligands

Compound	*m/z*	Fragment
13	149.08	$[M-H]^+$
14	419.90	$[M]^+$
15	679.44	$[M-H]^+$

2.4 Re(I)(bpy) [2 + 1] Complexes

The Re(I)(bpy) [2 + 1] complexes **16 - 18** were formed by abstracting the chloride ion from $[Re(bpy)Cl(CO)_3]$ (synthesised by reaction of $[ReCl(CO)_5]$ with 2,2'-bipyridyl) using silver triflate before the addition of the appropriate ligand in the appropriate stoichiometric ratio (**Scheme 2.4**). Anion exchange was then performed using ammonium hexafluorophosphate. The [2 + 1] strategy is a useful tool to impart desired properties on a complex. The monodentate and bidentate moiety can be modified to give the molecule appealing characteristics, such as solubility in aqueous media.

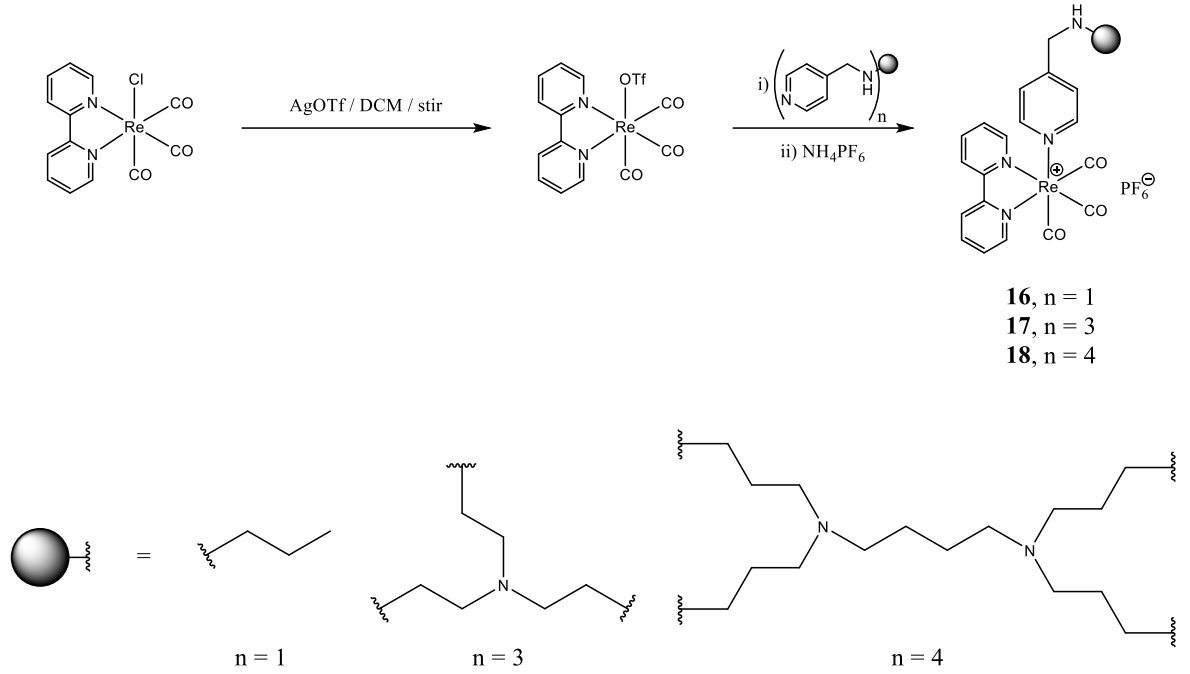

Scheme 2.4: Synthesis of Re(I)(bpy) monodentate complexes **16**, **17** and **18**.

The [2 + 1] Re(I) complexes were isolated in very low yields as brown powders (**Table 2.6**).

Table 2.6: Physical appearance and yield for Re(I) [2 + 1] complexes

Compound	Physical Appearance	Yield (%)
16	Brown powder	19
17	Brown powder	12
18	Brown powder	11

The Re(I) complexes 1**6**, **17** and **18** are air-stable, and soluble in DCM, methanol, ethanol, acetone and DMSO.

2.4.1 ^{1}H and $^{13}C\{^{1}H\}$ NMR Spectroscopy

Complex **16** was synthesised by abstracting the chloride from $[Re(bpy)Cl(CO)_3]$ before addition of ligand **10**. An anion exchange was then performed using ammonium hexafluorophosphate. The ^{1}H NMR spectrum for complex **16** is shown in **Figure 2.5**.

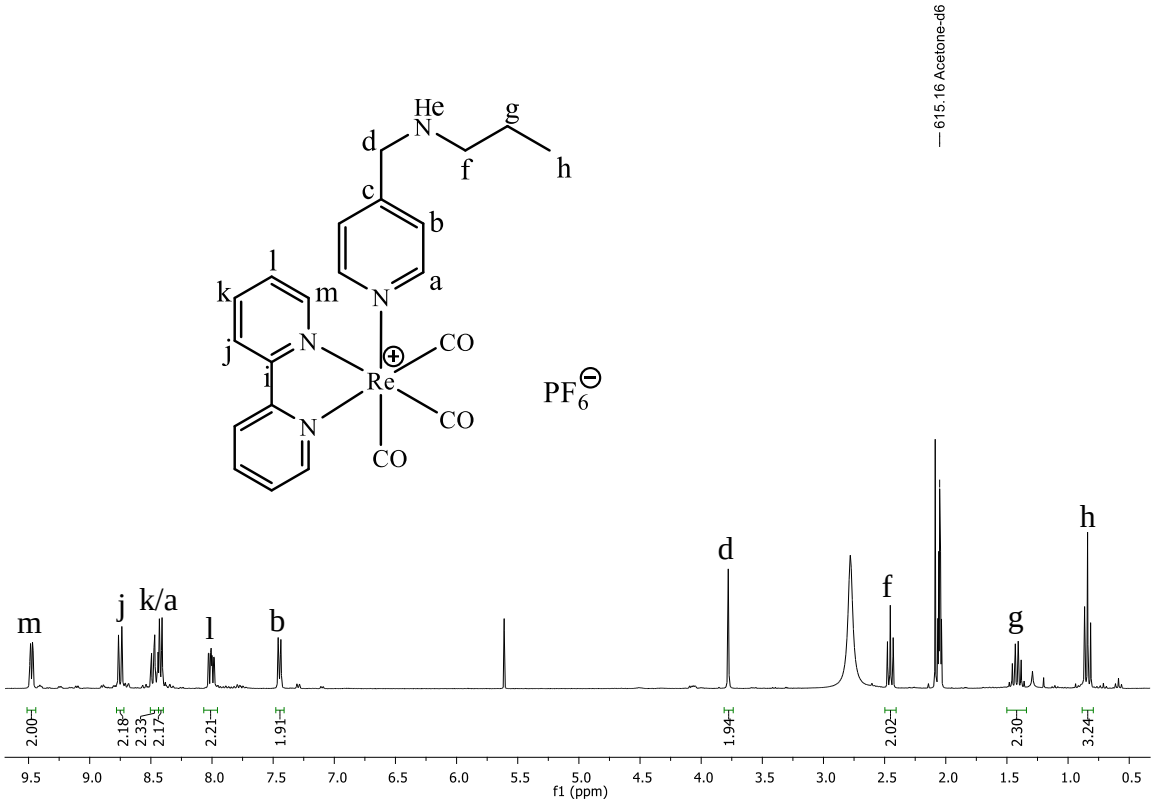

Figure 2.5: ^{1}H NMR spectrum of complex **16**

Integration of the aromatic proton signals shows that the bipyridyl moiety and ligand **10** have been added in a one-to-one ratio, suggesting the presence of the desired complex. The characteristic peak assigned to H_d appears at 3.78 ppm compared to 3.80 ppm in the ligand, which suggests complexation *via* the pyridyl nitrogen, as opposed to the secondary amine nitrogen. The proton peaks attributed to the bipyridyl moiety, as well as the pyridine moiety appear in the region from 7.45 – 9.48 ppm. Overlap of signals H_a and H_k result in a multiplet at 8.45 ppm.

The ^{13}C{^{1}H} NMR spectrum shows all the expected peaks, which have been assigned using HSQC NMR methodology.

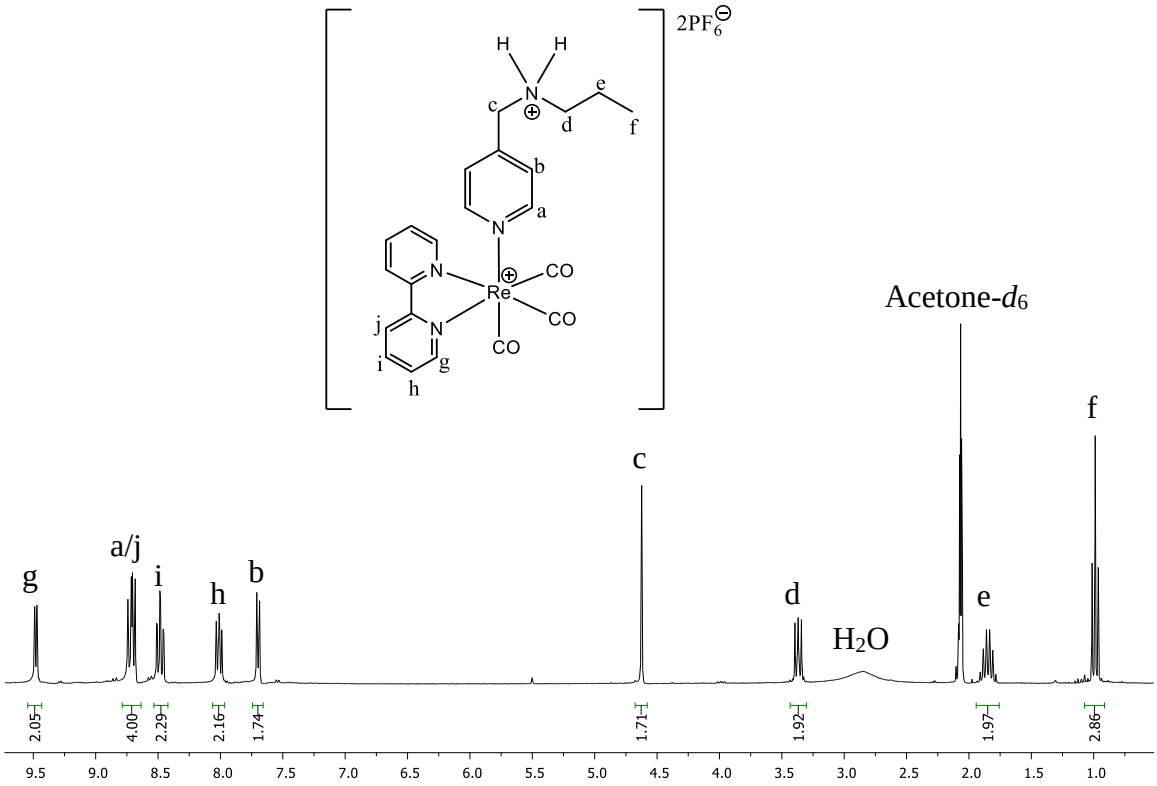

Figure 2.6: ^{1}H NMR spectrum of complex **16b**

The complexation reaction to form complex **16b** was performed in methanol instead of DCM.

As can be seen from **Figure 2.6**, the characteristic proton signal H_d appears as a singlet at 4.62 ppm, compared to 3.78 ppm in complex **16**. This difference between the two complexes (**16** and **16b**) is attributed to solvent effects or protonation of the secondary amine. The protonation hypothesis is substantiated by the presence of two PF_6 anions in the molecular structure (see **Section 2.3.4**). The aromatic proton peaks are all present, with the correct integration and multiplicity.

Complexation of ligand **11** with [Re(bpy)$(CO)_3$Cl] was performed in DCM to afford the tri-functionalised complex **17**. The ^{1}H NMR spectrum for complex **17** is shown in **Figure 2.7**.

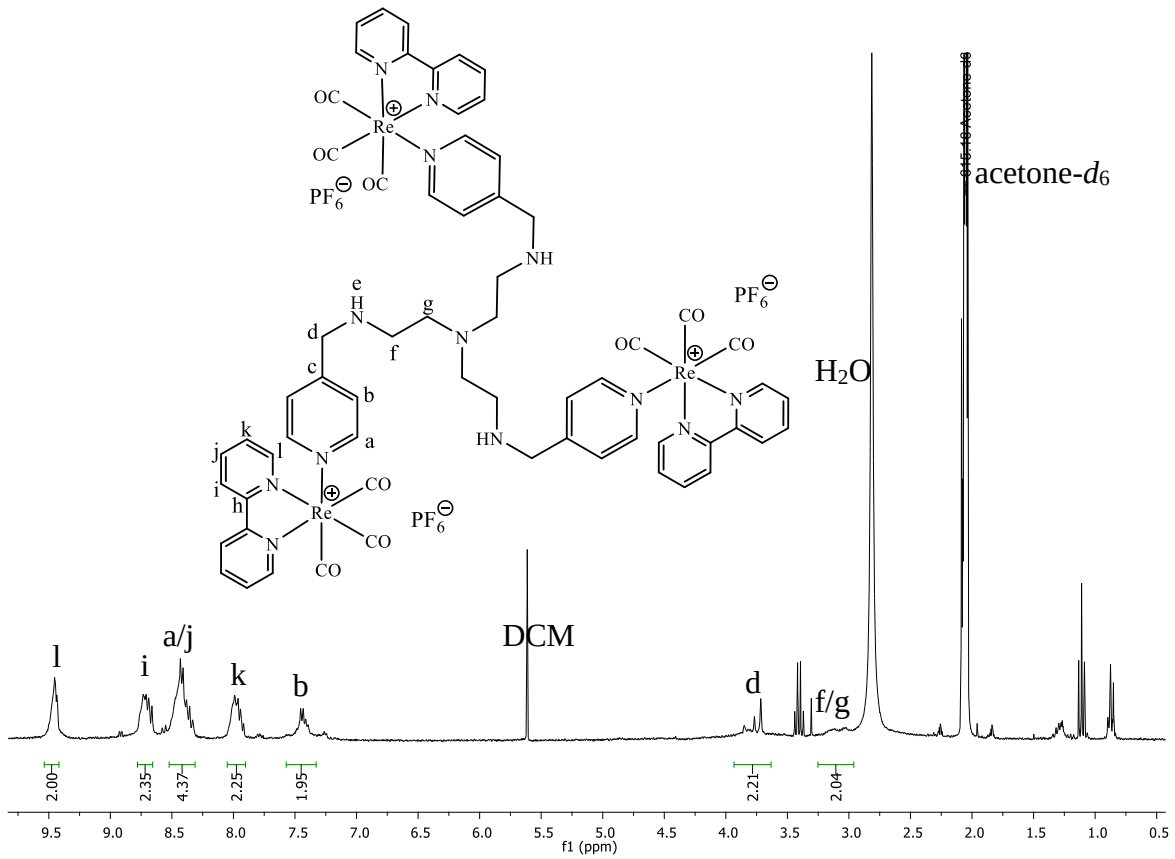

Figure 2.7: Assigned NMR spectrum of trifunctionalised complex **17**

Figure 2.7 shows that integration of the aromatic proton signals matches that of the proposed structure. Upon coordination, there is no significant shift of aromatic proton peak H_a, as expected, whereas there is a slight downfield shift of proton peak H_b from 7.30 ppm to 7.43 ppm upon coordination. Proton H_d remains unshifted upon coordination, suggesting that complexation has occurred *via* the pyridyl nitrogen and not the secondary amine nitrogen.

The peaks are not well-defined, which may indicate a mixture of mono-, di-, and tri-functionalised complexes present. Excess metal precursor was used for the reaction, and the reaction time was increased to 72 hours without effect.

The $^{13}C\{^1H\}$ spectrum (**Figure 2.8**) displays all of the expected peaks in the expected regions. The peaks were assigned using an HSQC NMR experiment.

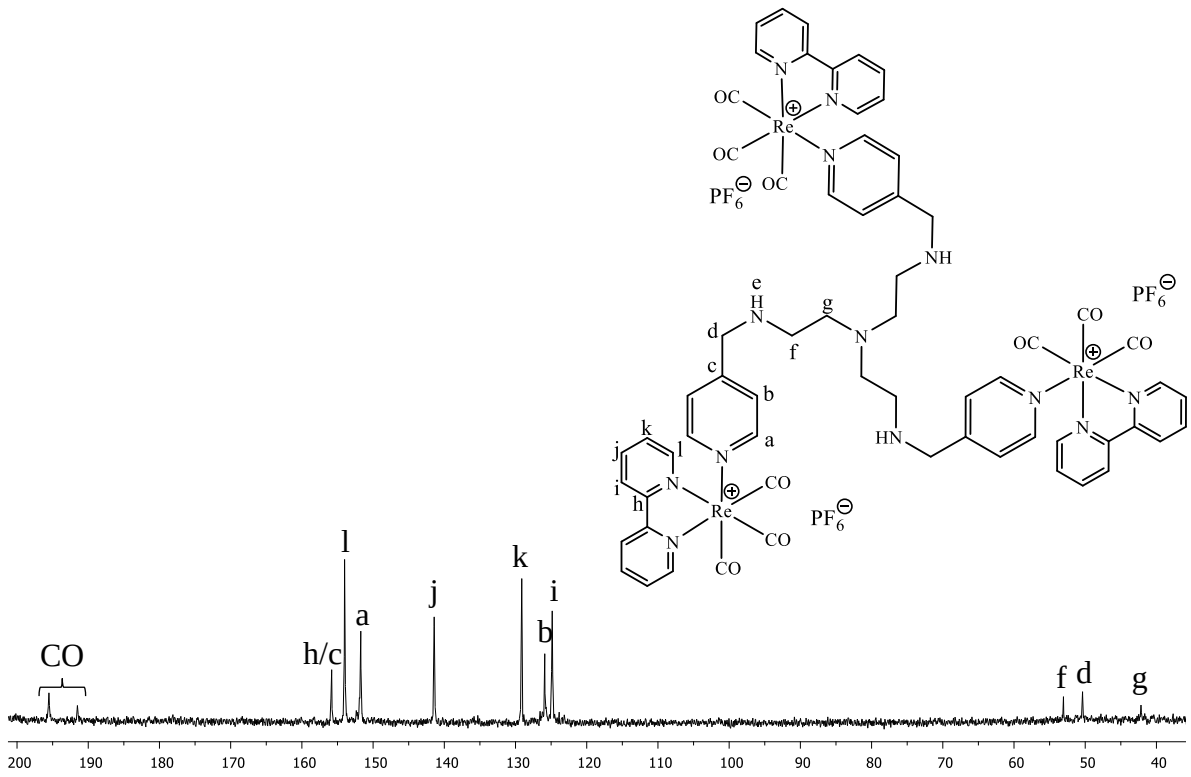

Figure 2.8: Assigned $^{13}C\{^{1}H\}$ spectrum of complex **17**

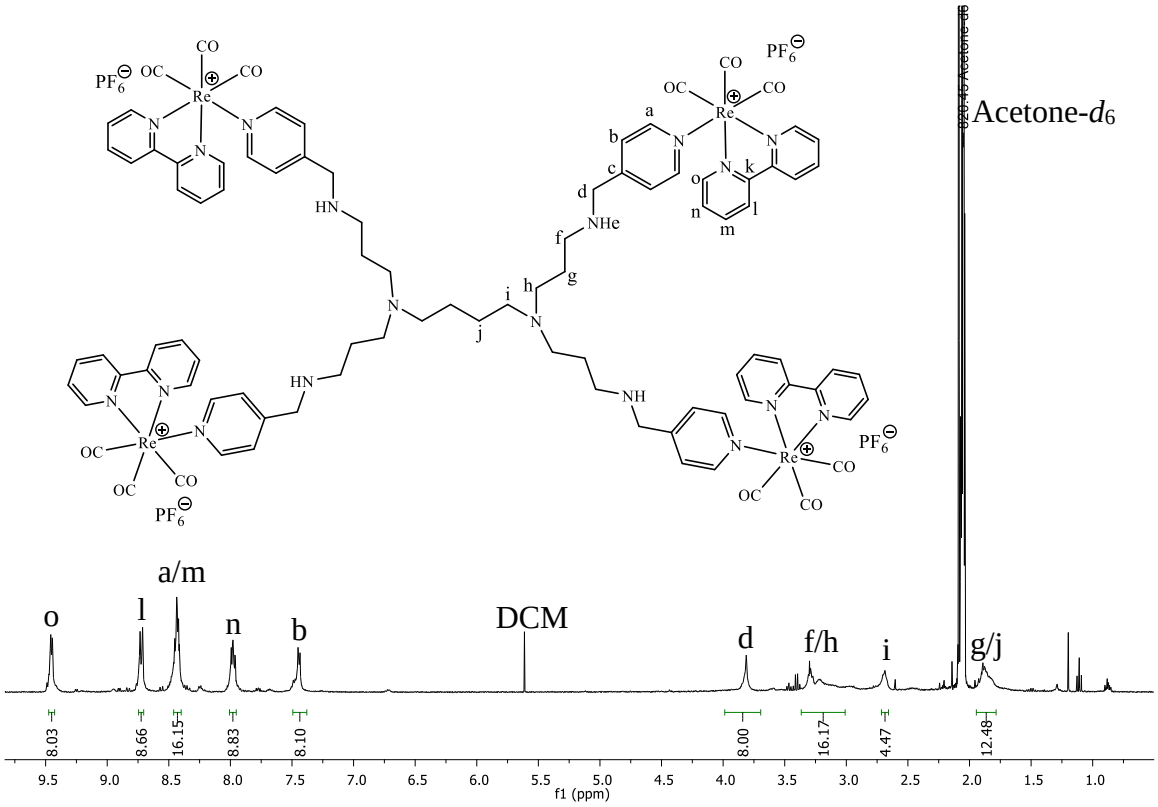

Figure 2.9: Assigned NMR spectrum of tetrafunctionalised complex **18**

Figure 2.9 shows that the aromatic proton peaks of complex **18** are similar to that of complexes **16** and **17**, displaying five peaks with H_a and H_m as an overlapping multiplet. The picolyl methylene protons are visible as a singlet at 3.83 ppm (shifted from 3.78 ppm in the ligand). The DAB core signals are not as well defined as the aromatic proton signals, exhibiting overlap of proton signals for H_f and H_h, as well as H_g and H_j.

The complexation of the DAB ligand **12** with [Re(bpy)$(CO)_3$Cl] was attempted multiple times with different solvents and work up procedures. Using methanol for the complexation reaction was found to decompose the product, while DCM and toluene gave similar results.

Figure 2.10 is a comparison of the three Re(I) tricarbonyl complexes, **16**, **17** and **18**.

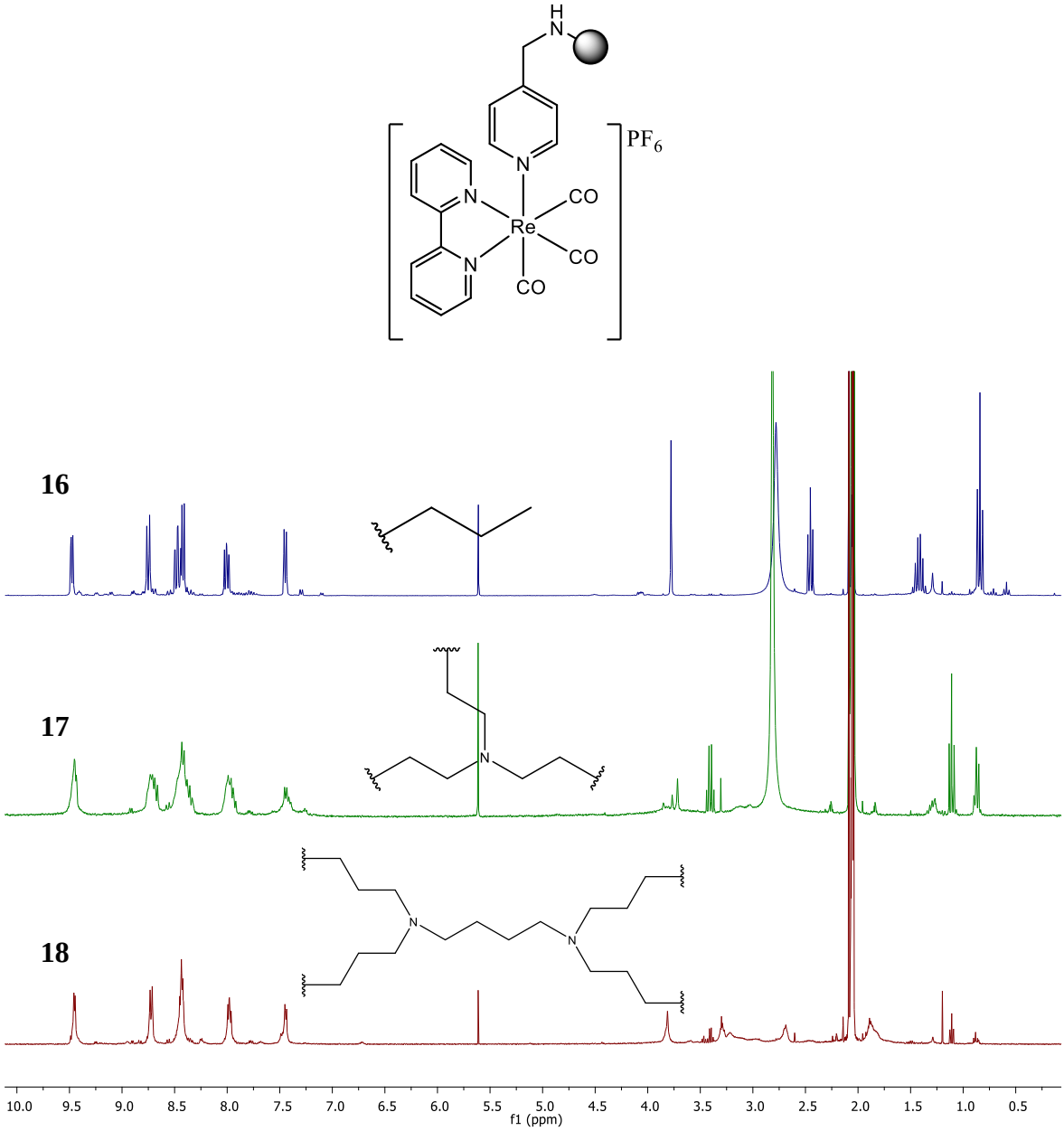

Figure 2.10: Comparison of ^{1}H NMR spectra of the three Re(I) complexes **16**, **1**7 and **18**.

Using **Figure 2.10**, it can be seen that the aromatic proton peaks, in addition to the picolyl methylene peaks, are in similar positions for the three Re(I) complexes. The major differences between the complexes lie in the core aliphatic protons. This suggests that the bonding mode is the same for all three complexes.

^{31}P{^{1}H} experiments were performed on complexes **16** – **18** to confirm the presence of the PF_6 counterion. The resulting signal was a heptet at *ca*. -144.30 ppm, with a coupling constant of *ca*. 708.5 Hz for all of the complexes.

2.4.2 Infrared Spectroscopy

In conjunction with the ^{1}H and $^{13}C\{^{1}H\}$ NMR spectroscopy, infrared spectroscopy was utilised to indicate the formation of the desired products. Absorption bands attributed to the carbonyl moiety, as well as shifts in the pyridyl C=N absorption band are characteristic of complexation. **Table 2.7** shows the significant absorption bands for the Re(I)(bpy) complexes.

Table 2.7: Important infrared absorption bands for the Re(I)(bpy) complexes

Compound	$C=N_{aromatic}$ (cm^{-1})	CO (cm^{-1})
16	1619	2025 / 1899
17	1619	2031 / 1907
18	1619	2028 / 1901

The carbonyl stretching bands appear in the region of approximately 2030 – 1900 cm^{-1}, which indicate a *facial* coordination of the carbonyl groups.

The shift of the C=N stretching band to higher wavenumbers from approximately 1600 cm^{-1} in the ligand to 1619 cm^{-1} upon complexation is likely due to the accumulation of positive charge on the pyridyl nitrogen, which decreases aromaticity and increases the bond order of the C=N bond.[15] This shift of the C=N band in pyridine moieties to higher wavenumbers upon complexation has been observed in other pyridine complexes.[16] This confirms that coordination occurred *via* the pyridyl nitrogen.

2.4.3 Elemental Analysis and Mass Spectrometry

High resolution ESI mass spectrometry experiments were used to confirm the proposed structure of the Re(I) [2 + 1] complexes **16**, **17** and **18**, the data of which is displayed in **Table 2.8**. ESI+ is a 'soft ionisation' technique, meaning that there is little fragmentation. Owing to this, the observed fragments have lost only carbonyl groups, which are the most labile.

Elemental analysis was used to further confirm the structural integrity and purity of the complexes. All results were in reasonable limits, confirming high purity of the samples. For complex **18**, several solvent molecules were present in the sample, as confirmed by ^{1}H NMR. This is acceptable as dendrimers are known to incorporate solvent molecules and are notoriously difficult to dry.[17]

Table 2.8: HR-ESI+ mass spectrometry results for Re(I) complexes

Complex	*m/z*	Fragment
16	577.12	$[M\text{-}PF_6]^+$
17	566.07	$[M\text{-}3PF_6]^{3+}$
18	590.08	$[M\text{-}CO\text{-}4PF_6]^{4+}$

2.4.4 Single-crystal X-ray Crystallography

The molecular structure of the mononuclear complex **16b** was determined by single crystal X-ray diffraction. The crystal was grown by the slow evaporation of methanol. The molecular structure is displayed in **Figure 2.11**.

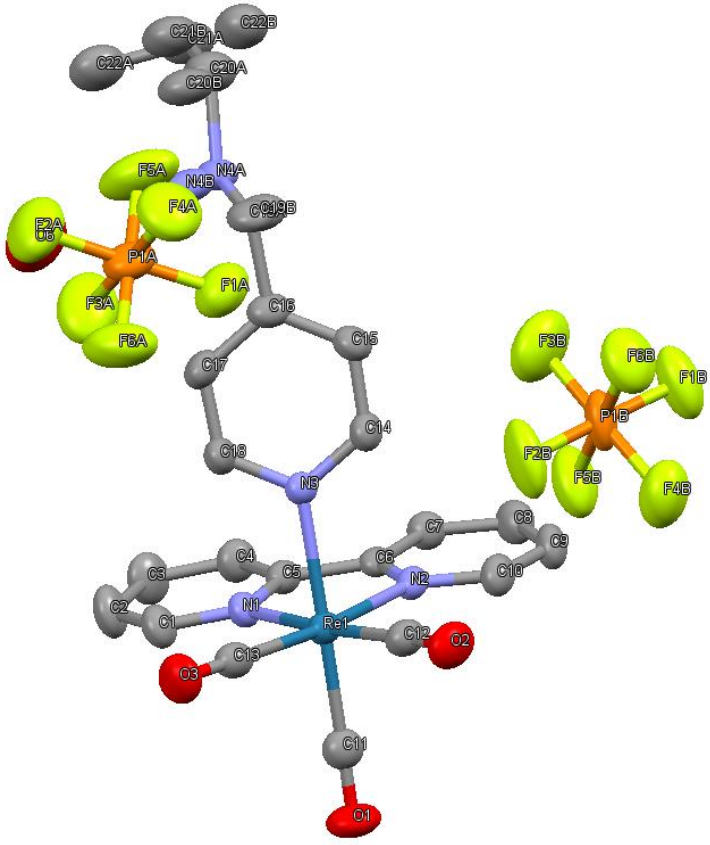

Figure 2.11: Representation of the molecular structure of complex **16b**. Ellipsoids are drawn at the 50 % probability level.

Complex **16b** crystallised in the triclinic, centrosymmetric space group $P\overline{1}$,with two formula units per cell (Z = 2). The molecular structure of complex **16b** is represented in **Figure 2.11**,

together with the numbering scheme. **Table 2.9** and **Table 2.10** show the general X-ray diffraction data and geometrical parameters of complex **16b**.

Table 2.9: X-ray diffraction data of complex **16b**

Empirical formula	$C_{22}H_{22}N_4O_3Re$, 2(PF_6), 3(O)
Formula weight	914.59
Crystal system	Triclinic
Space Group	$P\overline{1}$
a (Å)	8.3609(5)
b (Å)	10.5475(6)
c (Å)	18.7131(11)
α (°)	95.917(1)
β (°)	94.552(1)
γ (°)	93.283(1)
V (Å^3)	1632.71(17)
D_{calc}(mg.cm^{-3})	1.860
μ (mm^{-1})	3.929
F(000)	886
T (K)	173
Crystal colour	Yellow
θ range (°)	2.6 – 28.4
Index ranges	h = -11 to 11
	k = -13 to 14
	l = -25 to 25
Reflections collected	51611
Independent reflections	8155
R_{int}	0.061
R indices	R_1 = 0.0346, wR_2 = 0.0939
ρ_{max} and ρ_{min} (e Å^3)	2.13, -0.73

Table 2.10: Selected bond lengths and bond angles for complex **16b**

Selected bond angles	**Bond angle (°)**	**Selected bond lengths**	**Bond length (Å)**
C(11)-Re(1)-N(3)	176.61(16)	Re(1)-C(11)	1.927(5)
C(12)-Re(1)-N(1)	174.02(16)	Re(1)-C(12)	1.937(4)
C(13)-Re(1)-N(2)	171.89(15)	Re(1)-C(13)	1.924(5)
N(1)-Re(1)-N(3)	83.80(13)	Re(1)-N(1)	2.173(3)
N(2)-Re(1)-N(3)	83.48(12)	Re(1)-N(2)	2.179(3)
	Bite angle (°)	Re(1)-N(3)	2.213(3)
N(1)-Re(1)-N(2)	74.79(12)		

The coordination of the 2,2'-bipyridyl forms a five-membered ring with the Re(I) atom. The three carbonyl groups are coordinated *facially* to the metal centre. The geometry around the Re(I) atom is distorted octahedral. The *trans* angles given to the Re-CO (C(11)-Re(1)-N(3), C(12)-Re(1)-N(1), C(13)-Re(1)-N(2)) range between 171.89(15) and 176.61(16) °, which is a slight deviation from the perfect octahedral angles of 180.00°. The bite angle of the 2,2'-bipyridyl ancillary ligand (N(1)-Re(1)-N(2)) is 74.79(12) °, which is between the ideal bite angle of 90.00 ° for the octahedral geometry and 72.00 ° for the five-membered ring.

No substantial *trans* influence is observed as all the ligands *trans* to the carbonyls are nitrogens in pyridyl rings. The Re-C_{CO} bond distances range between 1.924(5) and 1.937(4) Å.

The molecular structure obtained exhibits two hexafluorophosphate anions for every Re(I) centre. This could be due to protonation of the nitrogen (N(4)), although this cannot be proven using SCXRD, due to disorder in the packing of the molecule in the crystal structure, and the low scattering of X-rays by hydrogen atoms. Protonation of the nitrogen (N(4)) could explain the downfield shift observed in the ^{1}H NMR spectrum of complex **16b** compared to that of **16** (discussed in **Section 2.3.1**).

Calculated hydrogen bonds show a hydrogen bond between nitrogen N(4) and the oxygen of a water molecule located in the crystal lattice.

2.5 Mn(I)(bpy) [2 + 1] Complexes

The manganese [2 + 1] complexes, **19**, **20** and **21**, were synthesised in a similar manner to the Re(I) monodentate complexes. The precursor [Mn(bpy)Br(CO)$_3$] was synthesised by reaction of [MnBr(CO)$_5$] with 2,2'-bipyridyl. The bromide anion was abstracted with silver triflate from [Mn(bpy)Br(CO)$_3$], before addition of the appropriate ligand in the appropriate stoichiometric ratio. An anion exchange was then performed using ammonium hexafluorophosphate to afford the PF_6 salt. The synthesis is shown in **Scheme 2.5**.

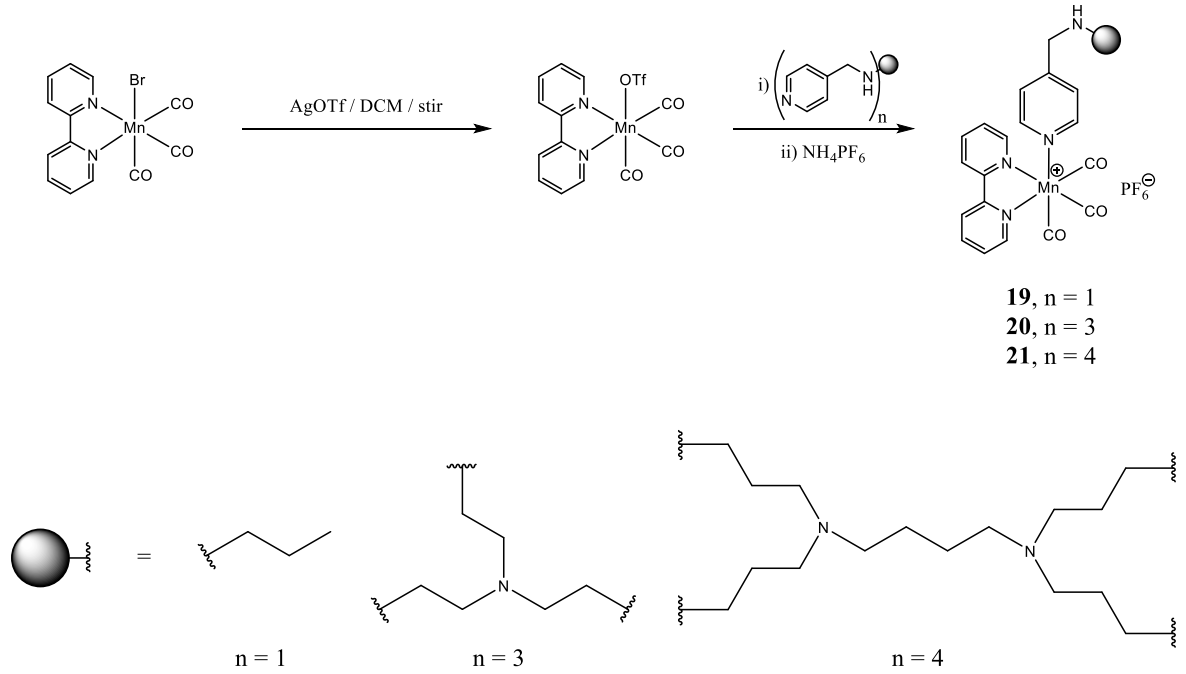

Scheme 2.5: Synthesis of Mn(I)(bpy) monodentate complexes **19**, **20** and **21**.

The Mn(I) [2 + 1] complexes **19** – **21** were isolated in moderate to low yields, all as yellow powders or residues (**Table 2.11**).

Table 2.11: Physical appearance and yield for the [2 + 1] Mn(I)(bpy) tricarbonyl complexes

Compound	Physical Appearance	Yield (%)
19	Yellow/orange residue	66
20	Pale yellow powder	31
21	Pale yellow powder	40

The Mn(I) [2 + 1] complexes **19** – **21** are air-stable, light sensitive, and soluble in methanol, ethanol, acetone, DCM, chloroform and DMSO.

2.5.1 ^{1}H and $^{13}C\{^{1}H\}$ NMR Spectroscopy

^{1}H and ^{13}C NMR spectroscopy techniques were used to verify the formation of the desired products. The ^{1}H NMR spectrum for monomeric complex **19** is shown in **Figure 2.12**.

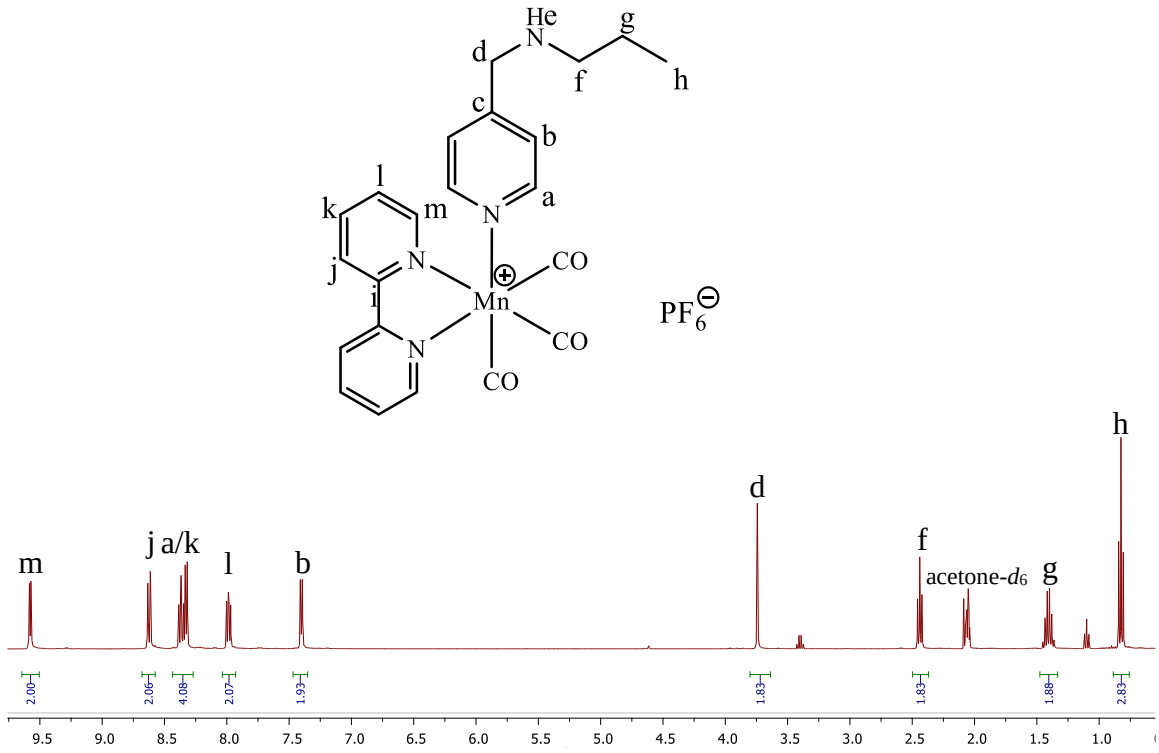

Figure 2.12: Assigned ^{1}H NMR spectrum of complex **19**

The presence of the bipyridyl peaks in the aromatic region, in addition to the peaks expected for ligand **10** gives evidence that complexation has occurred. Proton H_a displays an upfield shift from 8.49 ppm in ligand **10** to 8.33 pm in the complex. This is likely due to the electropositive metal ion acting as an electron-withdrawing group, deshielding the nearby protons. This shift in the proton peak upfield, along with the lack of shift of the picolylamine methylene peak H_d serves as proof that complexation has occurred *via* the picolylamine nitrogen and not the secondary amine nitrogen.

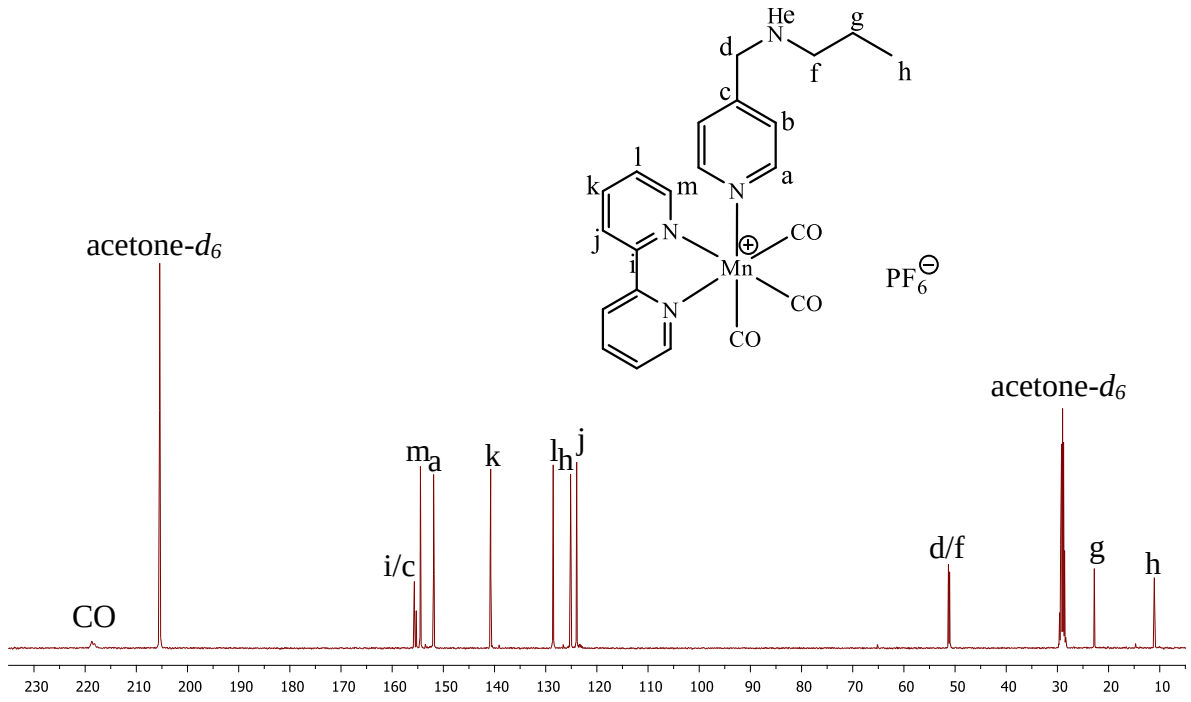

Figure 2.13: Assigned $^{13}C\{^{1}H\}$ NMR spectrum of complex **19**

A $^{13}C\{^{1}H\}$ NMR spectrum of complex **19** was obtained (**Figure 2.13**), and displayed all of the expected peaks. In the ^{13}C spectrum, the carbonyl carbons are observed as two singlets at 218.72 ppm and 218.15 ppm. This is due to the local symmetry around the metal centre, in which the two carbonyl *trans* to the bipyridyl moiety are equivalent, and the carbonyl *trans* to the picolylamine nitrogen is in a different magnetic environment. These, as well as the proton peaks, were assigned using HSQC and COSY 2-D NMR spectroscopy experiments.

The presence of the hexafluorophosphate anion was confirmed with $^{31}P\{^{1}H\}$ NMR, which displayed a heptet at -144.12 ppm.

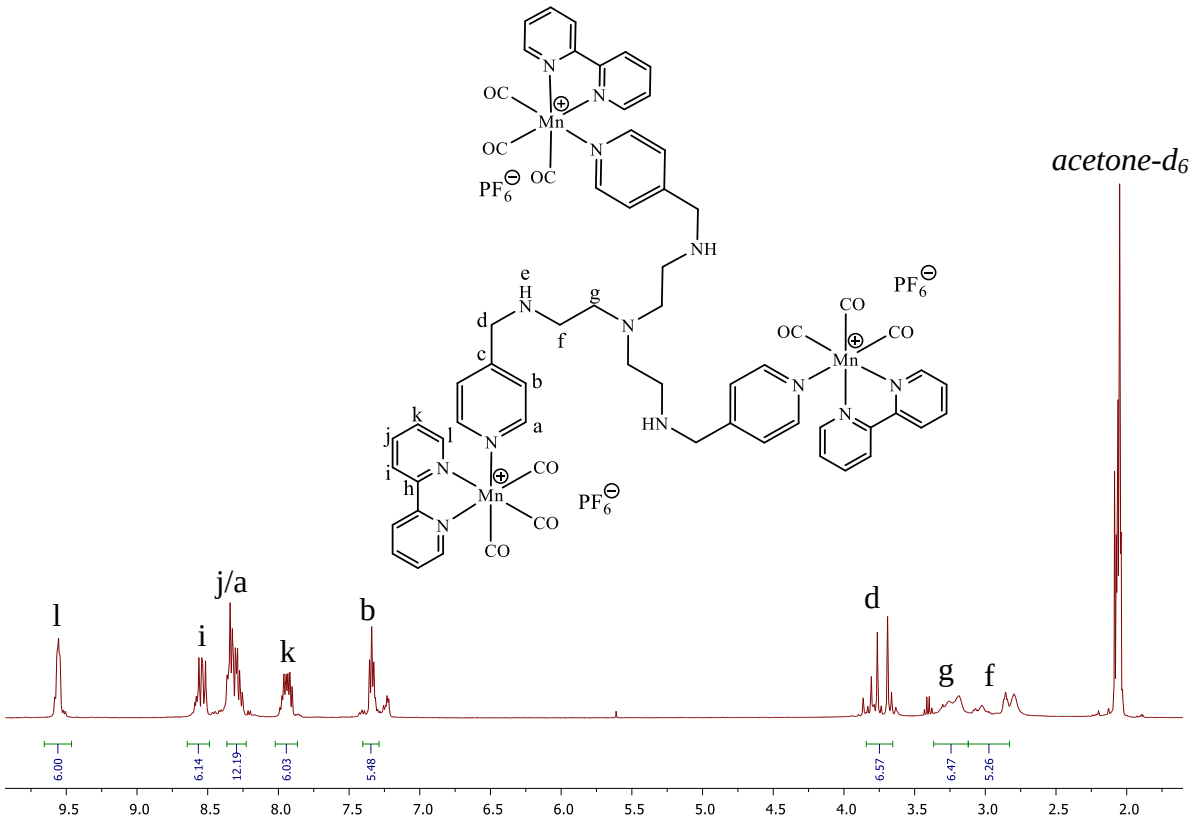

Figure 2.14: Assigned ^{1}H NMR spectrum of complex **20**

Figure 2.14 displays the assigned ^{1}H NMR spectrum of Mn(I) [2 + 1] complex **20**. The peaks for the 2,2'-bipyridyl and the picolylamine moiety of the ligand are present in the correct ratios, which is shown by the correct integration of the peaks. It is clear from the small doublet observed at approx. 7.23 ppm that unreacted ligand is present. It is likely that there is a mixture of mono-, di- and tri-functionalised ligand. Due to this, the peak corresponding to proton H_d appears as a series of singlets, rather than a single singlet. This is observed in the analogous tris Re(I) complex (**Figure 2.7**, **Section 2.3.1**), and could indicate that, as well as not being fully functionalised, the molecule has restricted movement around single bonds in the ligand core, bringing about different magnetic environments for the same proton. This is evidenced by the HSQC experiment, which displays multiple crosspeaks for the singlets attributed to H_d, which all correspond to a single peak in the carbon spectrum.

The aromatic carbon peaks in the $^{13}C\{^{1}H\}$ NMR spectrum for complex **20** are displayed in the region of 124 – 157 ppm. There is no peak in the $^{13}C\{^{1}H\}$ spectrum attributed to carbon C_f, but its presence is confirmed by a crosspeak observed in the HSQC spectrum.

The presence of a heptet (J = 708.7 Hz) at -144.13 ppm in the ^{31}P NMR spectrum confirms the presence of the PF_6 anions.

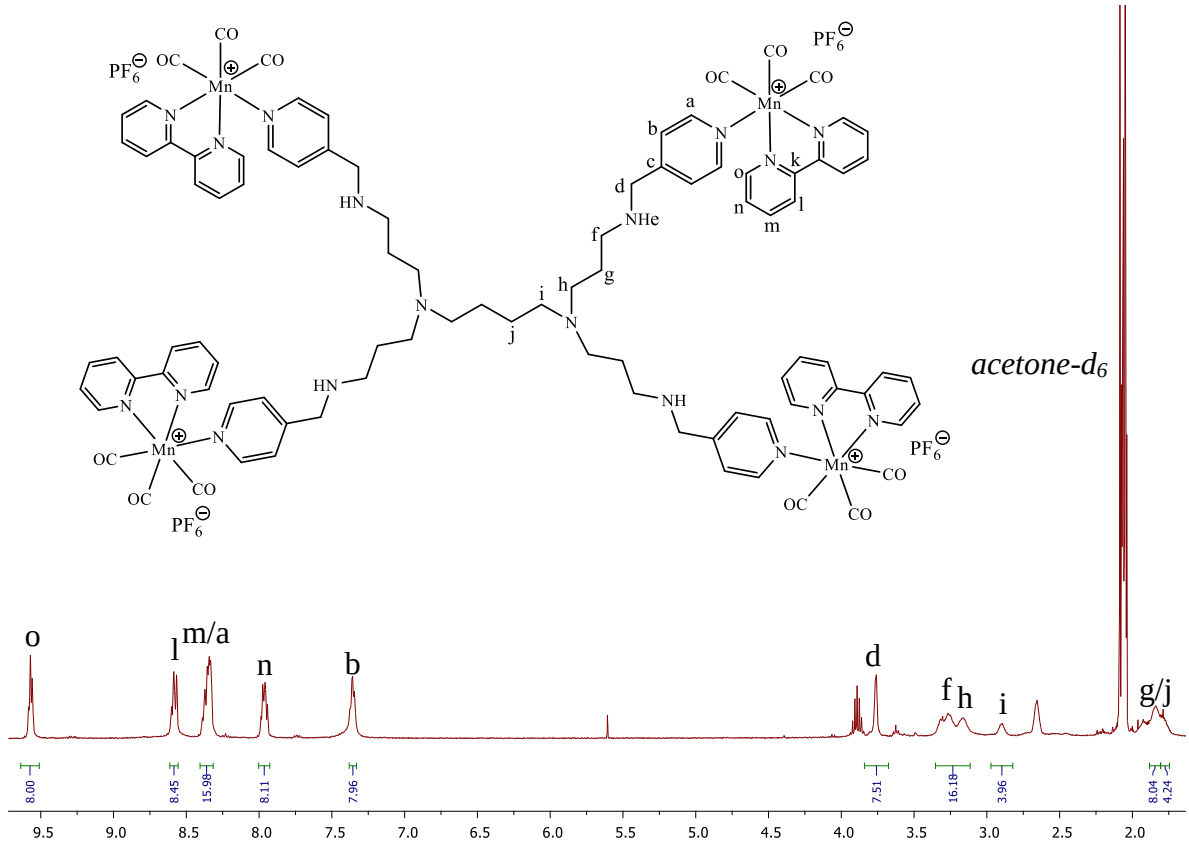

Figure 2.15: Assigned ^{1}H NMR spectrum of complex **21**

Figure 2.15 shows the ^{1}H NMR spectrum of the tetranuclear Mn(I) [2 + 1] complex. The aromatic proton peaks arise in the same region as for Mn(I) complexes **19** and **20**. Protons H_l-H_o of the bipyridyl moiety are observed as multiplets in the aromatic region. The peak attributed to H_m overlaps with proton peak H_a to form an overlapping multiplet at 8.28 – 8.42 ppm. The diagnostic peak attributed to methylene protons H_d appear as a doublet at 3.76 ppm. The doublet is formed from the coupling of H_d to protons H_b, with a coupling constant of 3.3 Hz. The coupling was confirmed using a 2-D COSY NMR experiment. The aliphatic proton peaks attributed to the DAB-G1 core appear in the expected regions, and integrate for the expected number of protons.

The presence of the PF_6 anion was confirmed using a $^{31}P\{^{1}H\}$ NMR experiment, which resulted in a heptet at -144.13 ppm (J = 708.7 Hz).

In the $^{13}C\{^{1}H\}$ spectrum, the carbonyl carbons are observed as two singlets at 218.98 ppm and 219.65 ppm, due to the symmetry discussed earlier. The aromatic carbon signals appear from 124 – 156 ppm, and the aliphatic carbon signals, attributed to carbon C_d and the carbons in the DAB scaffold are in the range of 21 – 55 ppm. 2-D NMR experiments, namely COSY and HSQC, were used to assign the peaks in the proton and carbon spectra.

2.5.2 Infrared Spectroscopy

Fourier transform infrared spectroscopy experiments were used in combination with the other techniques to confirm the formation of the desired products. The characteristic carbonyl stretching bands are observed in the expected region, from 1900 – 2050 cm^{-1}, confirming that complexation has occurred. Furthermore, a shift to higher wavenumbers in the C=N stretching band of the picolyl moiety from approximately 1600 cm^{-1} in the ligands to 1619 – 1622 cm^{-1} upon complexation due to the back-bonding mentioned in **Section 2.3.1** and **Section 2.3.2** confirms complexation *via* the pyridyl nitrogen.[16] **Figure 2.16** displays the infrared traces of complexes **19** – **21**.

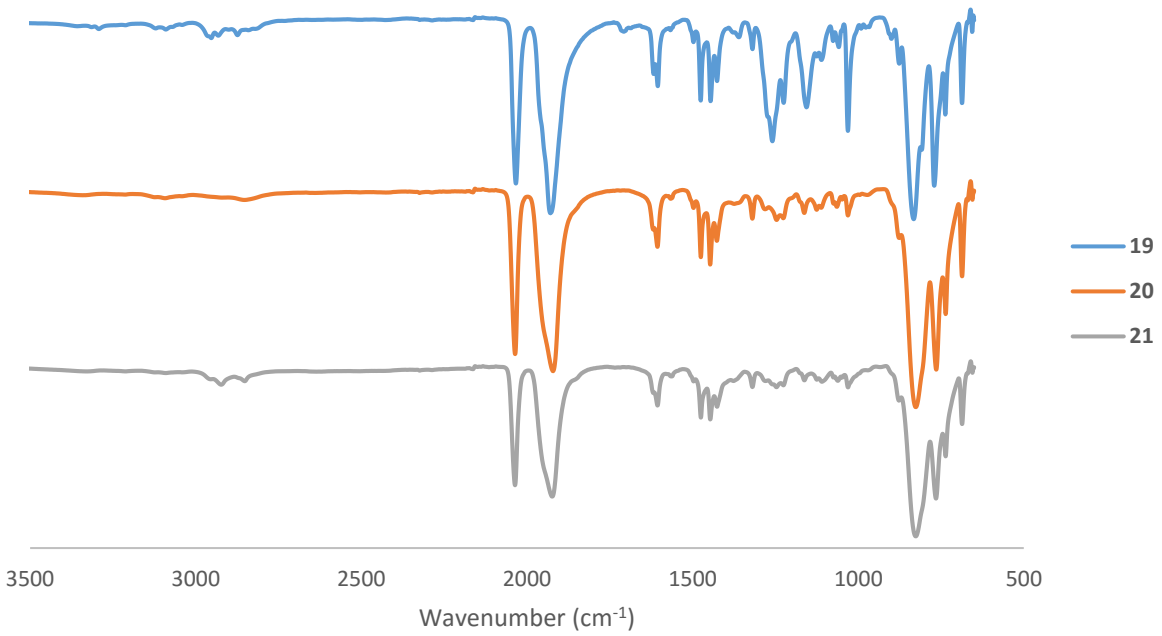

Figure 2.16: FT-IR traces of Mn(I) complexes **19** – **21**

2.5.3 Elemental Analysis and Mass Spectrometry

Elemental analysis and HR-ESI mass spectrometry experiments were used to further confirm the structural integrity of the Mn(I) [2 + 1] complexes. The mass spectral data for the complexes is summarisked in **Table 2.12**. Elemental analysis results confirmed the presence of the desired products in high purity. The unusual fragmentation pattern observed for complex **22** is likely due to exposure to light, either during or before the mass spectrometry analysis, hence the loss of the carbonyls.

Table 2.12: ESI mass spectrometry results for Mn(I) [2 + 1] complexes

Compound	*m/z*	Fragment
19	445.11	$[M\text{-}PF_6]^+$
20	434.06	$[M\text{-}3PF_6]^{3+}$
21	964.90	$[M\text{-}8CO\text{-}2PF_6]^{2+}$

2.6 Mn(I) Bidentate Complexes

The complexation reaction was achieved by stirring the metal precursor and the appropriate ligand at the appropriate stoichiometric ratio in DCM at room temperature. The general scheme for the formation of the Mn(I) bidentate complexes is shown in **Scheme 2.6**.

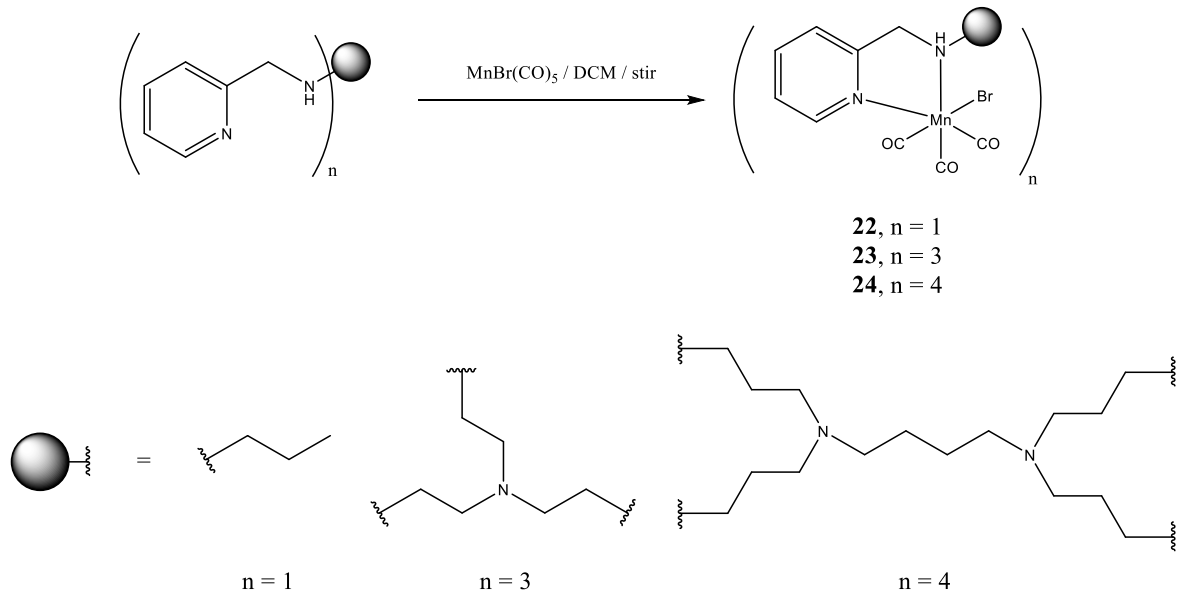

Scheme 2.6: Synthesis of Mn(I)(bpy) monodentate complexes **22**, **23** and **24**.

The Mn(I) bidentate tricarbonyl complexes were isolated in good yields as orange powders (**Table 2.13**). They are all air-stable, light sensitive powders, which are soluble in methanol, ethanol, DCM, chloroform and DMSO.

Table 2.13: Physical appearance and yield for the bidentate Mn(I) tricarbonyl complexes

Compound	Physical Appearance	Yield (%)
22	Orange powder	76
23	Light orange powder	65
24	Light orange powder	71

2.6.1 ^{1}H and $^{13}C\{^{1}H\}$ NMR Spectroscopy

The proposed chelation of the pyridyl and secondary amino nitrogens to form the bidentate (*N*,*N*)-Mn(I) complexes was confirmed by ^{1}H NMR spectroscopy. The ^{1}H NMR spectra of Mn(I) bidentate complexes **22** – **24** were recorded in deuterated acetone, and display characteristic peaks due to complexation, most notably splitting of the diastereotopic methylene peaks closest to the secondary amine, due to the formation of a chiral centre on the Mn(I) centre. The ^{1}H NMR spectrum for complex **22** is shown in **Figure 2.17**.

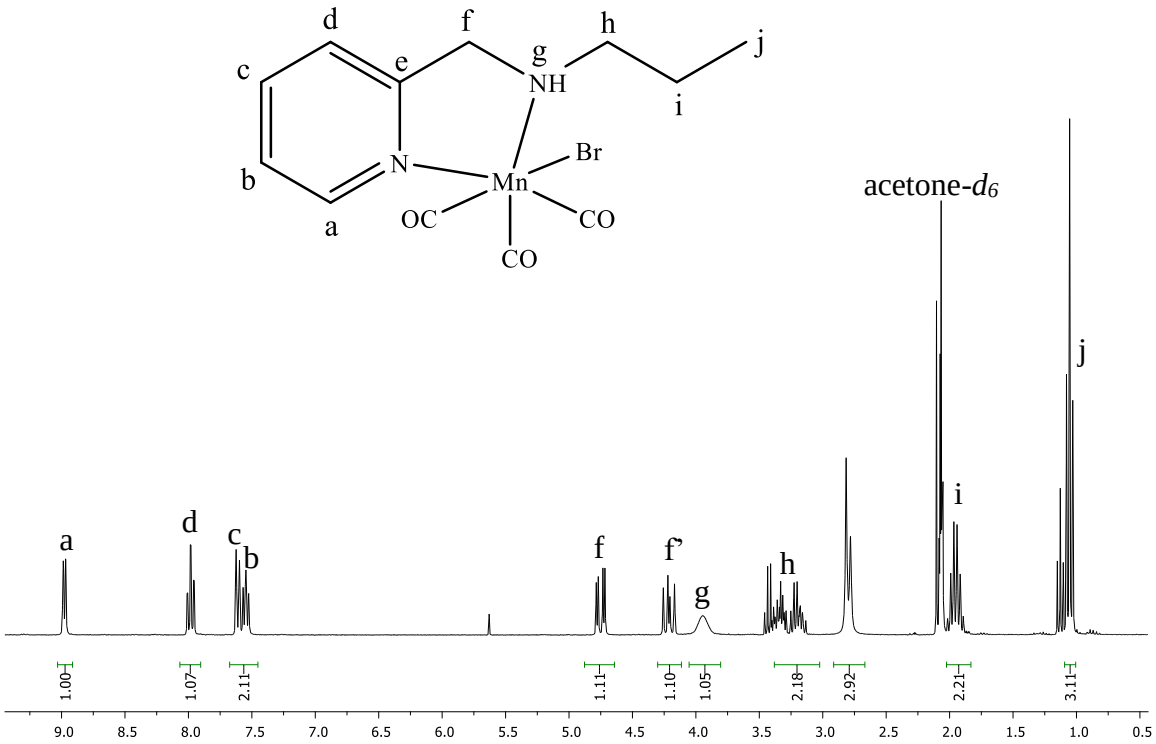

Figure 2.17: Assigned ^{1}H NMR spectrum for complex **22**

Complexation can be confirmed by the splitting of proton signal H_f into two doublet of doublets. This occurs because the bonding mode holds those two protons in magnetically non-equivalent positions. Protons H_h have also split into two signals, showing that they too are held in magnetically non-equivalent positions.

The $^{13}C\{^1H\}$ NMR spectrum displays all the expected peaks and was assigned using an HSQC NMR spectrum.

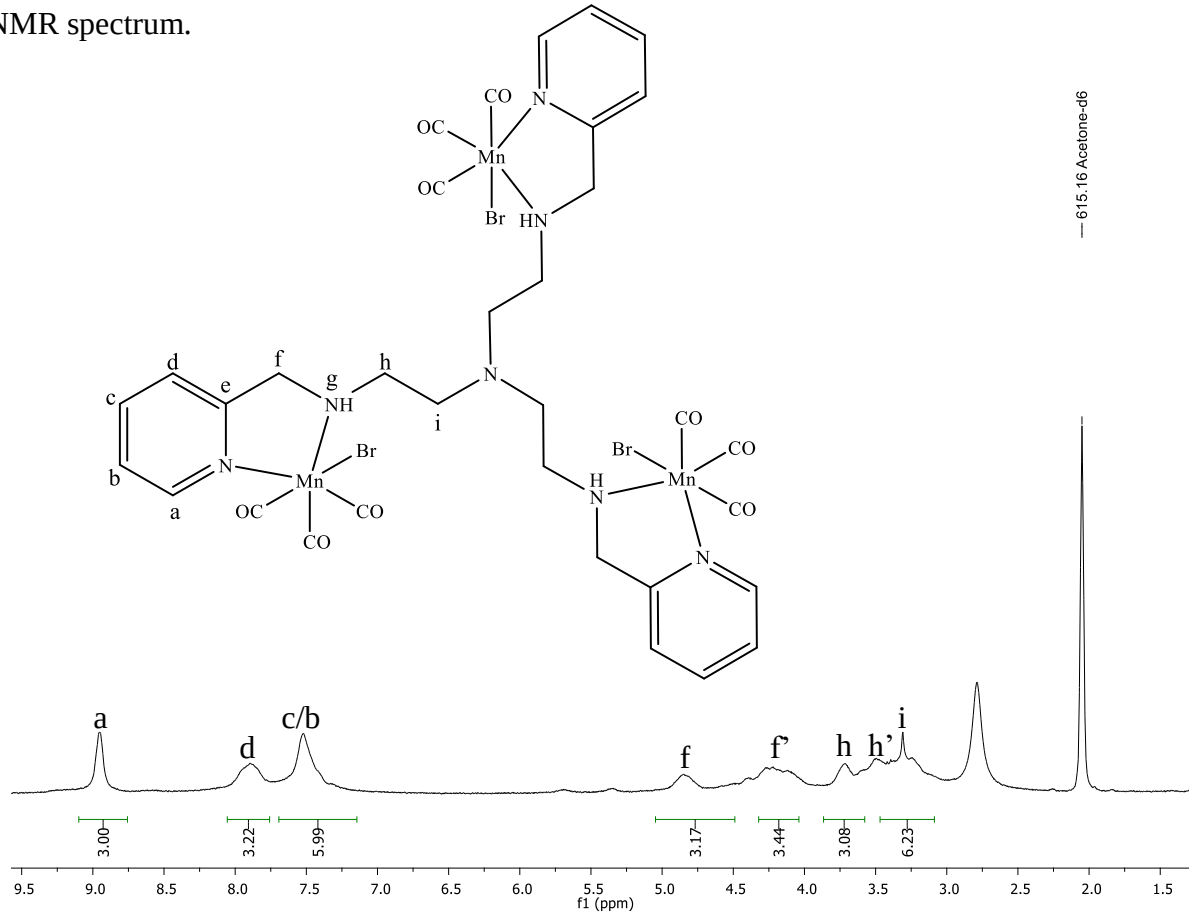

Figure 2.18: Assigned ^1H NMR spectrum for complex **23**

Figure 2.18 displays the assigned ^1H NMR spectrum of the trimeric Mn(I) complex **23**. The splitting of the proton signals H_f and H_h confirm coordination and formation of the five-membered ring. In a similar manner to complex **22**, the methylene protons H_f and H_h are held in magnetically non-equivalent environments.

The $^{13}C\{^1H\}$ NMR spectrum for complex **23** displays all the expected peaks, but extra peaks are visible in the aliphatic region. This could be due to the strained nature of the trimeric core, resulting in the carbon atoms residing in magnetically non-equivalent environments.

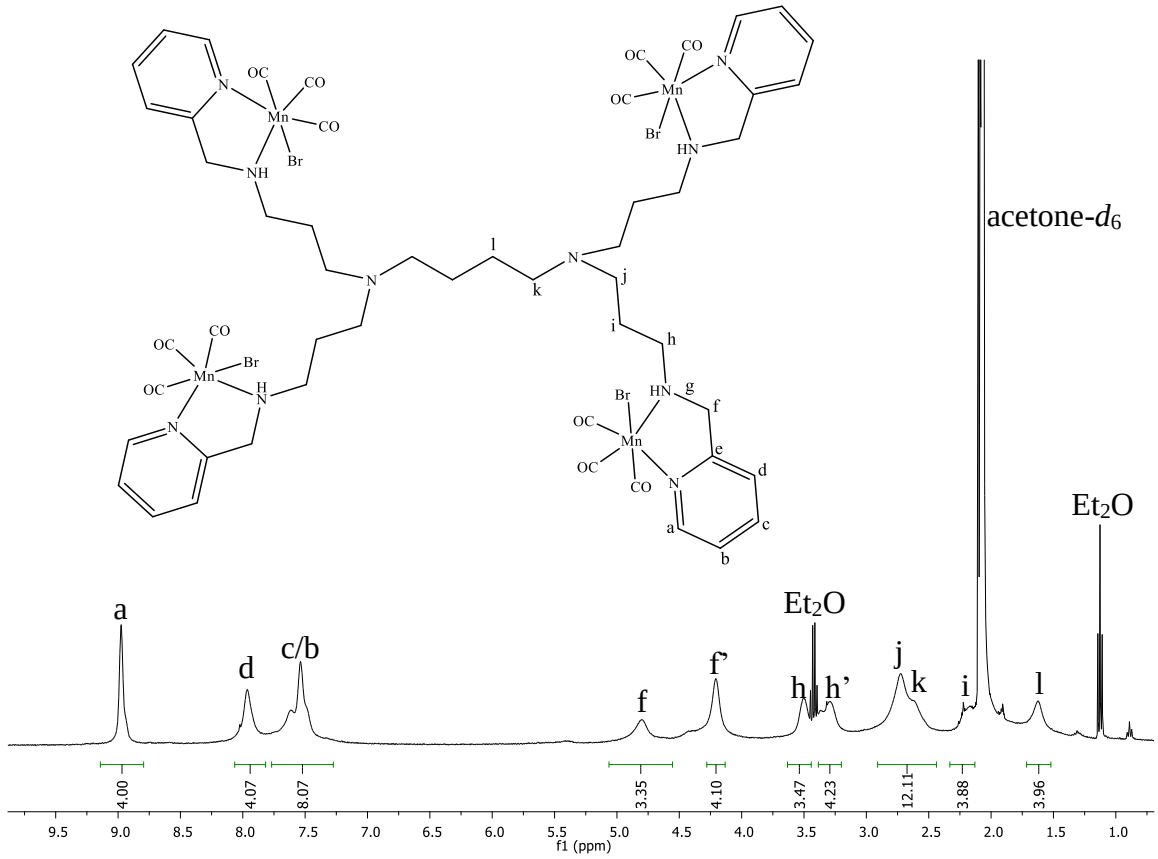

Figure 2.19: Assigned ^{1}H NMR spectrum for complex **24**

The assigned ^{1}H NMR spectrum of the bidentate Mn(I) complex **24** is displayed in **Figure 2.19**. The splitting of proton signals H_f and H_h into H_f, $H_{f'}$, H_h and $H_{h'}$ confirms coordination of the $MnBr(CO)_3$ moiety. The butyl core and propyl chain proton signals are visible in the expected region with the anticipated integration. The peak for proton H_i is slightly overlapping with the acetone-d_6 signal.

The $^{13}C\{^{1}H\}$ NMR spectrum displays the desired peaks, which were assigned using HSQC NMR techniques.

2.6.2 Infrared Spectroscopy

Infrared technology was used in conjunction with the other spectroscopic techniques to confirm the presence of the desired product. **Table 2.14** gives a summary of the significant absorption bands in the infrared spectra of the Mn(I) bidentate complexes.

Table 2.14: Important infrared absorption bands for the Mn(I) bidentate complexes

Compound	$C=N_{aromatic}$ (cm^{-1})	CO (cm^{-1})
22	1609	2013 / 1886
23	1609	2020 / 1895
24	1609	2020 / 1889

2.6.3 Elemental Analysis and Mass Spectrometry

ESI-mass spectrometry was used to confirm the presence of the desired complexes. The data are consistent with the proposed structures, and are summarised in **Table 2.15**. Elemental analysis was used to further confirm the structural integrity of the products in high purity.

Table 2.15: ESI mass spectrometry data for Mn(I) bidentate complexes

Complex	*m/z*	Fragment
22	283.90	$[M - 3CO]^+$
23	995.88	$[M - Br]^+$
24	1472.97	$[M - Br]^+$

2.6.4 Single-crystal X-Ray Crystallography

The molecular structure of the monomeric model manganese complex **22** was determined by X-ray diffraction, the results of which are shown in **Figure 2.19**. The single crystal was obtained by evaporation of DCM. The data attained from the SCXRD was used to confirm that complexation did occur with the correct bonding mode, and that the carbonyls are in a *facial* arrangement around the manganese centre. The geometry around the Mn(I) centre is pseudo-octahedral.

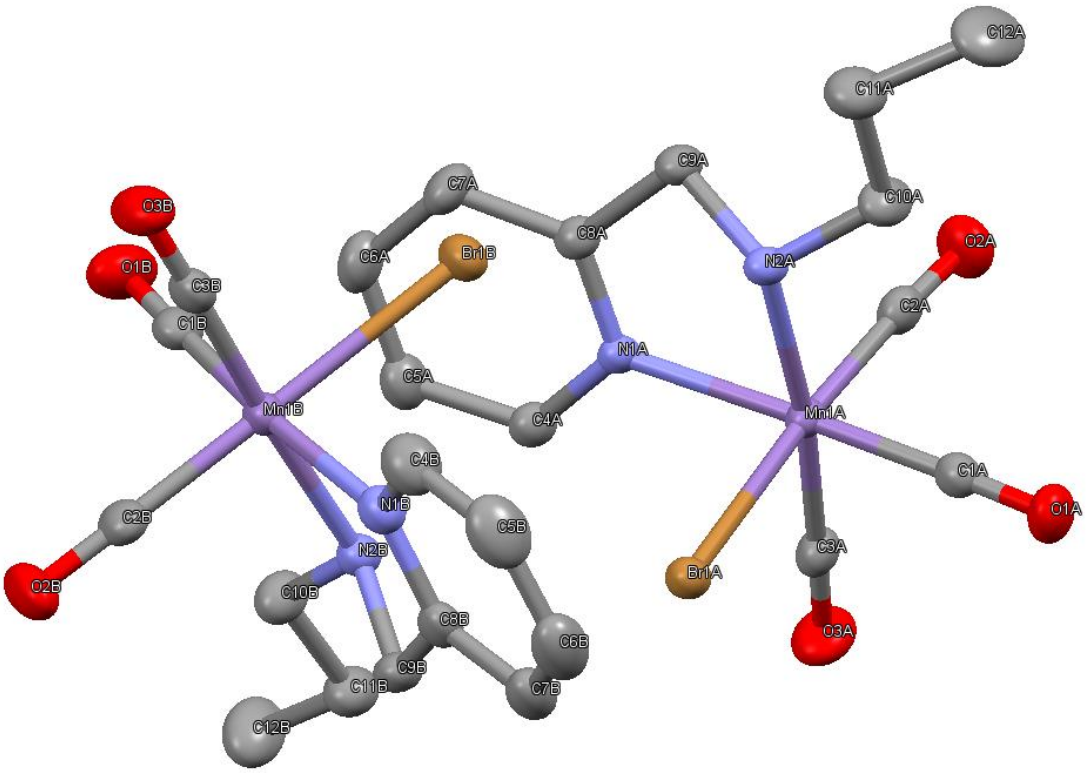

Figure 2.19: Molecular structure of Mn(I) complex **22**

Complex **22** crystallises in the centrosymmetric space group $P\overline{1}$, with four formula units per cell (Z = 4). The asymmetric unit contains two independent molecules positioned centrosymmetrically. The molecular structure of complex **22** is represented in **Figure 2.19** together with the numbering scheme. **Table 2.16** and **Table 2.17** show the general X-ray diffraction data and geometrical parameters corresponding to complex **22**, respectively.

Table 2.16: X-ray diffraction data of complex **22**

Empirical formula	$C_{12}H_{14}BrMnN_2O_3$
Formula weight	369.10
Crystal system	Triclinic
Space Group	P -1
a (Å)	7.5876(5)
b (Å)	12.1743(8)
c (Å)	17.2183(11)
α (°)	73.9730(10)
β (°)	87.105(2)
γ (°)	72.0140(10)
V (Å^3)	1452.94(16)
D_{calc}(mg.cm^{-3})	1.687
μ (mm^{-1})	3.662
F(000)	736
T (K)	173
Crystal colour	Orange
θ range (°)	1.2 – 28.3
Index ranges	h = -10 to 10
	k = -16 to 16
	l = -22 to 22
Reflections collected	30335
Independent reflections	7243
R_{int}	0.049
R indices	R_1 = 0.0304, wR_2 = 0.0647
ρ_{max} and ρ_{min} (e Å^3)	0.56, -0.37

Table 2.17: Selected bond lengths and bond angles for complex **22**

Selected bond angles	**Bond angle (°)**	**Selected bond lengths**	**Bond length (Å)**
Br(1A)-Mn(1A)-C(1A)	84.68(8)	Mn(1A)-C(1A)	1.816(2)
Br(1A)-Mn(1A)-C(2A)	175.80(8)	Mn(1A)-C(2A)	1.797(2)
Br(1A)-Mn(1A)-C(3A)	89.06(8)	Mn(1A)-C(3A)	1.802(2)
Br(1A)-Mn(1A)-N(1A)	87.90(6)	Mn(1A)-Br(1A)	2.5275(5)
Br(1A)-Mn(1A)-N(2A)	87.24(6)	Mn(1A)-N(1A)	2.057(2)
N(1A)-Mn(1A)-C(1A)	170.44(10)	Mn(1A)-N(2A)	2.098(2)
N(2A)-Mn(1A)-C(3A)	173.13(10)	C(8A)-N(1A)	1.343(3)
	Bite angle (°)	C(9A)-N(2A)	1.486(3)
N(1A)-Mn(1A)-N(2A)	78.97(8)	C(10A)-N(2A)	1.496(3)

The coordination of the ligand **13** to the Mn(I) centre *via* the two ligand nitrogen atoms (N(1A), N(2A)) form a five-membered ring. The three carbonyl ligands are coordinated in a *facial* arrangement around the Mn(I) atom, which, together with the bromide anion, form a distorted octahedral arrangement around the metal centre. The carbonyl *trans* angles (Br(1A)-Mn(1A)-C(2A), N(1A)-Mn(1A)-C(1A), N(2A)-Mn(1A)-C(3A)) range from 170.44(10) – 175.80(8) °, which is a minor deviation from the perfect octahedral angle of 180.00 °.

The Mn-C bond lengths range from 1.797(2) – 1.816(2) Å, which is comparable to literature reports. [18-20] [17-19] The bond length for the carbonyl *trans* to the bromide anion is the shortest at 1.797(2) Å. This is unexpected, as one would expect a lengthening of the M-CO bond for the carbonyl *trans* to the Br ligand, as observed in two complexes synthesised by Mascharak *et al.*[21] This may mean that there are more subtle factors at play in this case.

2.7 Summary

Two series of ligands (**10** – **15**), based on *n*-propyl amine, tris(2-aminoethyl)amine and DAB generation one scaffolds, functionalised with 2- and 4-picolyl groups, were designed, synthesised and characterised using a range of spectroscopic and analytical techniques, including ^{1}H and ^{13}C NMR spectroscopy, infrared spectroscopy and EI mass spectrometry.

A new series of Re(I) (**16** – **18**) and Mn(I) (**19** – **21**) tricarbonyl complexes, based on the [2 + 1] approach, were produced and characterised using NMR spectroscopy (^{1}H, ^{13}C, COSY, and HSQC), infrared spectroscopy, ESI mass spectrometry and elemental analysis, all of which correspond well with the proposed structures. A new series of bidentate Mn(I) tricarbonyl complexes (**22** – **24**) were synthesised and characterised using the same techniques mentioned above.

References

1. K. I. Ansari, J. D. Grant, S. Kasiri, G. Woldemariam, B. Shrestha and S. S. Mandal, *J. Inorg. Biochem.*, 2009, **103**, 818-826.
2. Y. K. Yan, S. E. Cho, K. A. Shaffer, J. E. Rowell, B. J. Barnes and I. H. Hall, *Pharmazie*, 2000, **55**, 307-313.
3. A. W. T. Choi, M. W. Louie, S. P. Y. Li, H. W. Liu, B. T. N. Chan, T. C. Y. Lam, A. C. C. Lin, S. H. Cheng and K. K. W. Lo, *Inorg. Chem.*, 2012, **51**, 13289-13302.
4. A. Kermagoret, G. Morgant, J. d'Angelo, A. Tomas, P. Roussel, G. Bastian, P. Collery and D. Desmaële, *Polyhedron*, 2011, **30**, 347-353.
5. C. S. Parson, V.; Krauss, C.; Banerjee, H.N.; Reilly, C.; Krause, J.A.; Wachira, J.M.; Giri, D.; Winstead, A.; Mandal, S.K., *Br. J. Pharm. Res.*, 2014, **4**, 362-367.
6. N. A. Illan-Cabeza, A. R. Garcia-Garcia, M. N. Moreno-Carretero, J. M. Martinez-Martos and M. J. Ramirez-Exposito, *J. Inorg. Biochem.*, 2005, **99**, 1637-1645.
7. *Portugal Pat.*, WO2007073226A1, 2007.
8. P. V. Simpson, C. Nagel, H. Bruhn and U. Schatzschneider, *Organometallics*, 2015, **34**, 3809-3815.
9. P. Toro, A. H. Klahn, B. Pradines, F. Lahoz, A. Pascual, C. Biot and R. Arancibia, *Inorg. Chem. Commun.*, 2013, **35**, 126-129.

10. I. Machado, S. Fernandez, L. Becco, B. Garat, J. S. Gancheff, A. Rey and D. Gambino, *J. Coord. Chem.*, 2014, **67**, 1835-1850.
11. N. Wilhelms, S. Kulchat and J. Lehn, *Helv. Chim. Acta*, 2012, **95**, 2635-2651.
12. M. Wenzel, K. Wichmann, K. Gloe, K. Gloe, H.-J. Buschmann, K. Otho, M. Schröder, A. J. Blake, C. Wilson, A. M. Mills, L. F. Lindoy and P. G. Plieger, *CrystEngComm*, 2010, **12**, 4176.
13. P. Govender, N. C. Antonels, J. Mattsson, A. K. Renfrew, P. J. Dyson, J. R. Moss, B. Therrien and G. S. Smith, *J. Organomet. Chem.*, 2009, **694**, 3470-3476.
14. G. Smith, R. Chen and S. Mapolie, *J. Organomet. Chem.*, 2003, **673**, 111-115.
15. M. Katcka and T. Urbanski, *B. Acad. Pol. Sci-Chim.*, 1964, **12**, 615-&.
16. K. E. Prosser, S. W. Chang, F. Saraci, P. H. Le and C. J. Walsby, *J. Inorg. Biochem.*, 2017, **167**, 89-99.
17. J. F. Jansen, E. M. de Brabander-van den Berg and E. W. Meijer, *Science*, 1994, **266**, 1226-1229.
18. I. Chakraborty, S. J. Carrington, G. Roseman and P. K. Mascharak, *Inorg. Chem.*, 2017, **56**, 1534-1545.
19. J. S. Ward, J. M. Lynam, J. W. B. Moir, D. E. Sanin, A. P. Mountford and I. J. S. Fairlamb, *Dalton Trans.*, 2012, **41**, 10514-10517.
20. T. N. Twala, M. Schutte-Smith, A. Roodt and H. G. Visser, *Dalton Trans.*, 2015, **44**, 3278-3288.
21. S. J. Carrington, I. Chakraborty and P. K. Mascharak, *Dalton Trans.*, 2015, **44**, 13828-13834.

Chapter 3 Physicochemical, Radiolabelling and Biological Evaluations

3.1 Introduction

CO has been found to be an important signalling molecule in mammalian bodies and displays a wide range of protective properties, including antiinflammatory,[1] antiproliferative[2] and antiapoptotic effects.[3, 4] Furthermore, several research groups have shown that CO displays antimalarial effects,[5-7] *via* carboxylation of haem groups of cell-free haemoglobin.[8-11] CO is toxic in even relatively low concentrations, due to its lack of specificity.[12] It was suggested by Green *et al.*, and is now generally accepted, that a useful manner in which to deliver CO with temporal and spatial accuracy, is to use CORMs.[13]

Besides treatment, early diagnosis of solid tumours and bacterial infections is enormously beneficial. One way to achieve this, in a non-invasive manner, is by labelling a molecule with a radioactive isotope, so that the tumour or infection can be imaged. New radiopharmaceuticals are needed that aggregate in solid tumours and microbial infections for imaging of the tumour or infection.

Manganese and rhenium carbonyl complexes have shown promise as potential anticancer agents, with many IC_{50} values in the low micromolar range against a variety of cell lines.[14-22] Several research groups have revealed that using the [2 + 1] approach is a useful tool in the art of rational drug design. In particular, it has been shown that cationic bipyridyl Re(I) tricarbonyl complexes display great potential in the field of anticancer research.[16, 23, 24] In contrast, very little effort has been made towards potential Mn(I) [2 + 1] complexes as potential drugs, and it is a worthwhile research path to follow.

Despite the relative success of Group 7 organometallic complexes as potential antitumour, antifungal and antiparasitic drugs, very little research has been conducted towards testing these compounds for possible antiparasitic activity. With the rapid rise in drug resistance in both cancer and malaria, new drugs with novel mechanisms are needed. This chapter covers the photochemical

properties of the Mn(I) complexes, antiproliferative studies and antiplasmodial studies of the complexes, as well as a preliminary study involving the radiolabelling of ligand **10** with ^{99m}Tc.

3.2 Photochemical Properties of Mn(I) Compounds

Even though manganese tricarbonyl systems are known to release CO under light illumination, it is important to establish whether the compounds release CO, how much CO is released from the complex, and the stability of the complex in the dark. Hence, the CO-release properties of the Mn(I) tricarbonyl complexes **19** – **24** were evaluated. Complex **22** was used as a model complex, and its CO-release properties were assessed using infrared spectroscopy, UV/Vis spectroscopy, and a myoglobin assay. The CO-release properties of complexes **19**, **20**, **21**, **23** and **24** were assessed using UV/Vis spectroscopy.

3.2.1 Long-term Stability of Compounds

Infrared absorption spectroscopy was used to detect the loss of CO from the compound by a decrease in intensity of the CO stretching bands. When compound **22**, as a pure solid, is exposed to natural daylight for as little as 90 minutes, a distinct decrease in the intensity of the CO stretching bands is observed in the infrared spectrum (**Figure 3.1**).

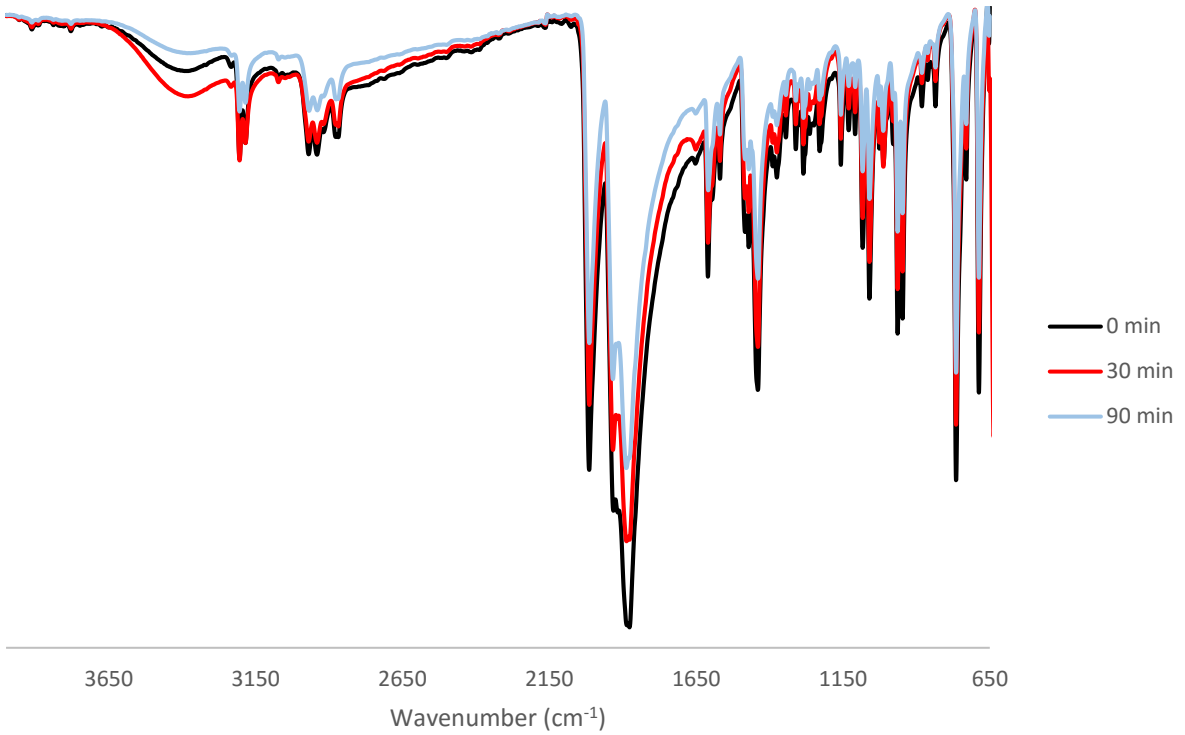

Figure 3.1: Infrared spectrum of complex **22** for a freshly prepared sample (black) and after exposure to natural daylight for 30 minutes (red) and 90 minutes (blue).

The decrease in intensity of the CO stretching bands between 2020 cm^{-1} and 1875 cm^{-1} is indicative of substantial changes in the structure of the metal-carbonyl group, and is the first indication that CO-release is occurring from the compound. Additionally, upon prolonged exposure to natural daylight, solutions of complexes **19** – **24** lose their orange colour and turn to brown with a dark brown precipitate.

3.2.2 Electronic Absorption and CO-release

The absorbance maxima of complexes **19** – **24** were determined in a solution comprised of DMSO and PBS buffer (pH 7.4) (5:95 % *v/v*). Complexes **19** – **21** display two broad bands at ~290 nm and ~380 nm, assigned to the intraligand charge transfer (ILCT) and the metal to ligand charge transfer (MLCT) bands, respectively. Complexes **22** – **24** do not display a ILCT, and display a MLCT in a similar region to complexes **19** – **21** at ~370 nm. Assignments of the ILCT and MLCT bands were made based on structurally similar complexes reported in literature.[25-28] The ILCT absorption band

observed in complexes **19** – **21** is attributed to the spin-allowed π → π* transitions of the 2,2'-bipyridyl moiety.

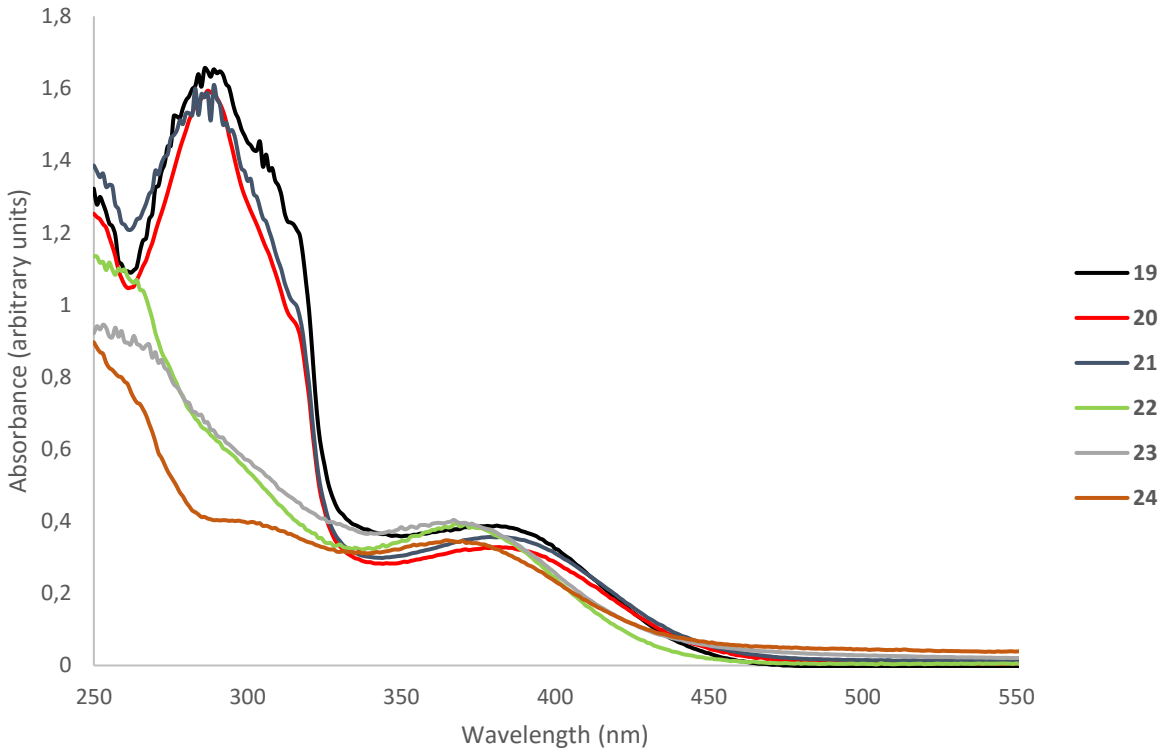

Figure 3.2: Overlay of the electronic absorption spectra of Mn(I) complexes **19** – **24** in DMSO/PBS (5:95 % *v/v*)

3.2.2.1 CO-release

To gain understanding into the photo-induced CO-release and the dark stability of complexes **19** - **24**, the complexes were incubated in a DMSO/PBS (5:95 % *v/v*) solution in the absence of light for 16 hours. The UV/Vis spectrum was recorded every 30 minutes during the stability study (**Figure 3.2**, black). All of the complexes showed good stability in the dark in the aqueous solution, with only insignificant changes in the UV/Vis spectra observed, likely due to precipitation of the complex. The complexes were then irradiated with a custom-made LED array at 365 nm, coincident with the MLCT absorption maxima of the complexes. Irradiation was halted every minute to record the UV/Vis spectra (**Figure 3.3**, red).

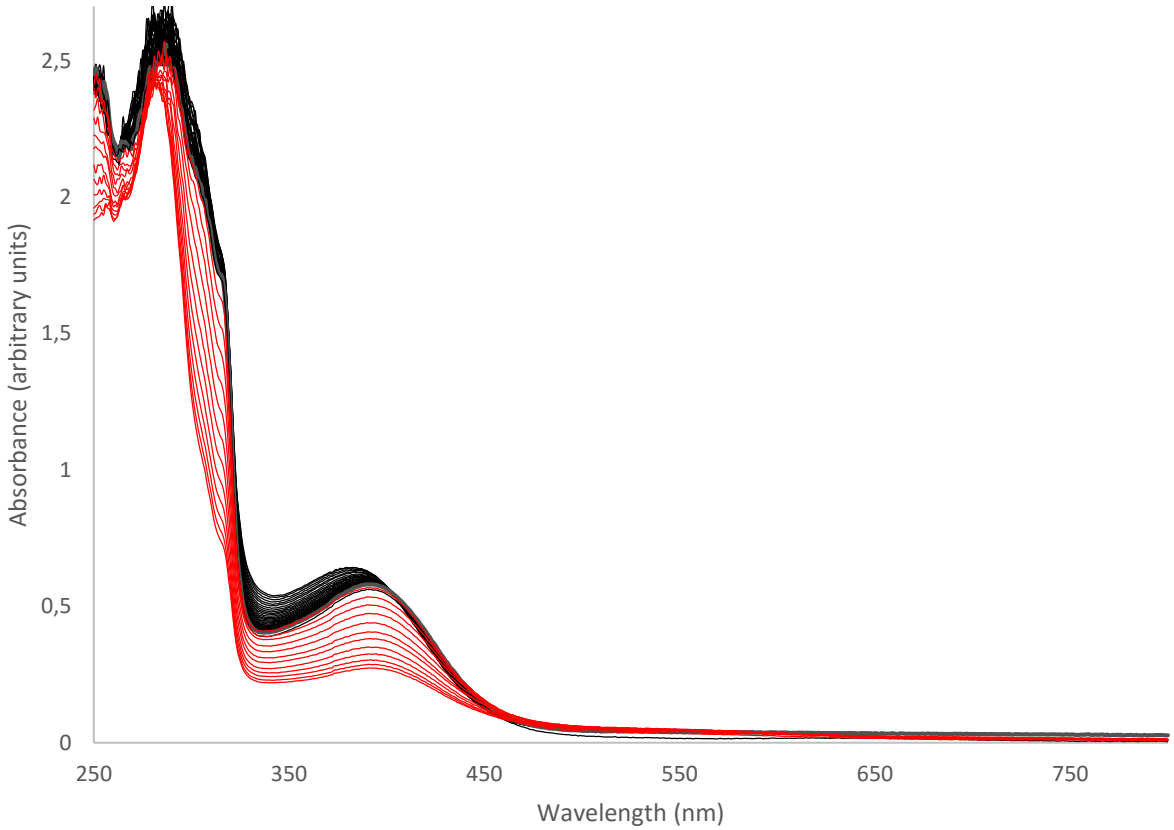

Figure 3.3: UV/Vis spectral traces of tetranuclear complex **21** in DMSO/PBS (5:95 % *v/v*) during incubation in the dark (0 to 16 h, black), followed by photoactivation with an LED cluster at 365 nm for 12 min (red).

Figure 3.3 shows a relatively consistent spectrum in the dark, indicating dark stability, and a marked decrease in the MLCT band upon irradiation with the 365 nm LED cluster. This is indicative of CO-release, and can be visualised as the change in absorbance at 365 nm versus time in **Figure 3.4**. No further spectral changes were observed upon extended irradiation after 10 – 15 minutes.

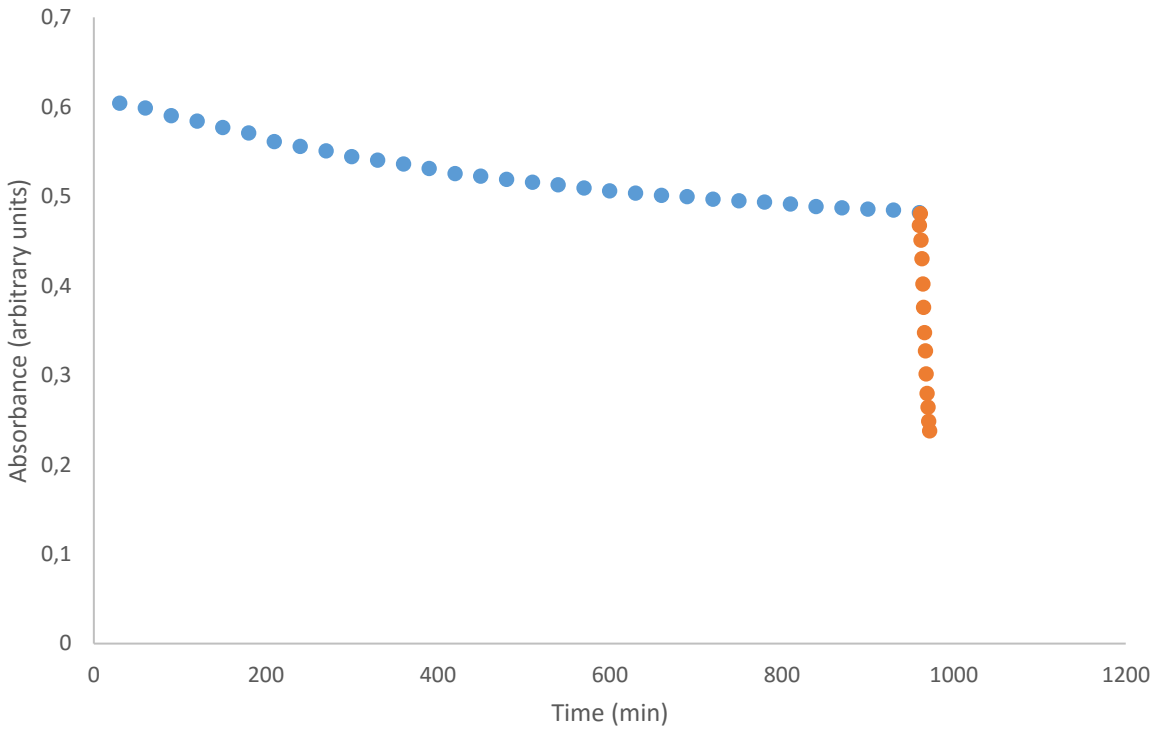

Figure 3.4: Plot of absorption at 365 nm with increasing incubation time in the dark (0 to 16 h, blue), followed by photoactivation with an LED array at 365 nm for 12 min (orange) for a solution of complex **21** in DMSO/PBS (5:95 % *v/v*), monitored by UV/Vis spectroscopy.

All of the Mn(I) tricarbonyl complexes displayed similar trends, that is, good dark stability in a DMSO:PBS (pH 7.4) solution, and a prominent decrease in the MLCT band upon irradiation with the LED cluster.

3.2.3 CO-release using Myoglobin Assay

The amount and rate of CO released from compound **22** was studied using the standard myoglobin assay,[13] with modifications suggested by Fairlamb *et al*.[29] Although the myoglobin assay is not the only method established for quantifying the amount and rate of CO released from compounds, it is the most widely used. In this method, changes in the UV/Vis spectrum of myoglobin, an iron-based oxygen-binding protein, are monitored as it is converted from deoxy-myoglobin (deoxy-Mb) to carboxy-myoglobin (CO-Mb).[13, 29, 30] The conversion occurs by release of CO from the compound, followed by immediate binding of CO to the deoxy-myoglobin (rate constant, k = 0.38

μMs^{-1}),[29] resulting in a drastic change in the Q-band region of the UV/Vis spectrum (**Figure 3.5**). This data can be used to quantify CO-release from a CORM.

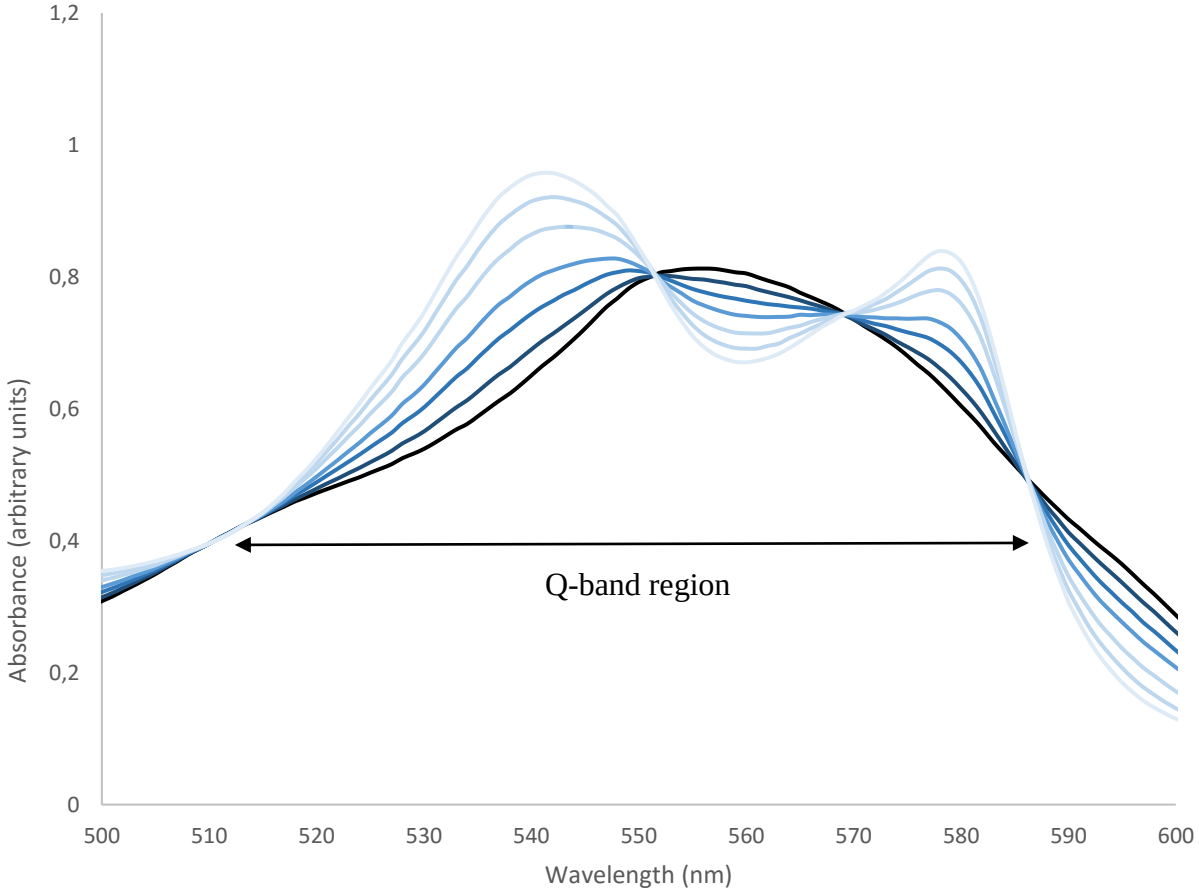

Figure 3.5: UV/Vis spectra of the conversion of deoxy-Mb (black) to CO-Mb (light blue) in a control experiment

Figure 3.5 shows the change in the UV/Vis spectrum of myoglobin as it is converted from deoxy-Mb to CO-Mb. Isosbestic points are observed at 510, 550, 570 and 585 nm, with the Q-band region lying between 510 nm and 585 nm. Deoxy-Mb has one absorption peak in the Q-band region at 557 nm, whereas CO-Mb has two peaks, with maxima at 540 and 577 nm. By measuring the change of absorbance at 540 nm, and correcting for the potential change in absorbance of the compound *vs*. the photo-product by aligning the spectra to intersect at the isosbestic point at 510 nm, CO-release from the compound can be determined.

The concentration of the deoxy-Mb stock solution is determined by using the known extinction coefficient at 557 nm (ε_{557} = 13.8 $mM^{-1}cm^{-1}$), and the concentration of CO-Mb is determined using the known extinction coefficient at 540 nm (15.4 $mM^{-1}cm^{-1}$).[29] Sodium dithionite is used as a reducing agent to reduce the inactive Fe^{3+} version of myoglobin, metmyoglobin (met-Mb), to deoxy-Mb.

3.2.3.1 Dark Stability in Myoglobin Solution

Preceding the irradiation experiments, the stability of complex **22** was monitored under the conditions of the myoglobin assay (10 µM complex **22**, 60 µM myoglobin, sodium dithionite, 0.01 PBS, pH 7.4), to determine whether CO-release would occur in the absence of light. Spectral changes were monitored at 540 nm and 577 nm for the formation of CO-Mb, and 557 for the formation of deoxy-Mb.

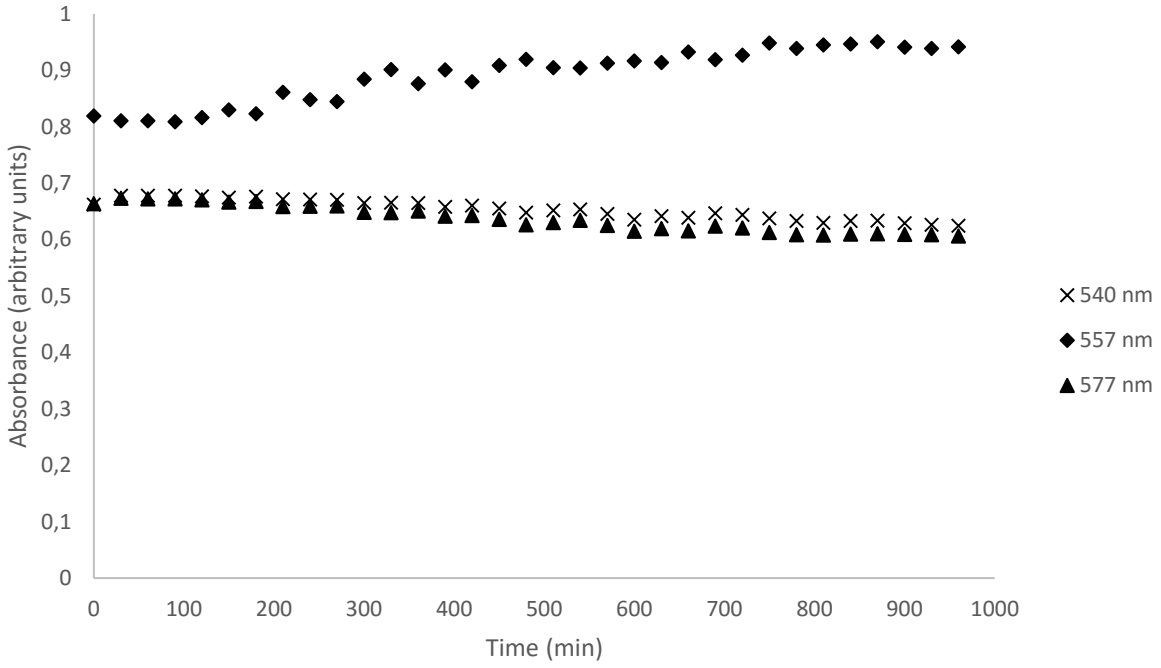

Figure 3.6: Change of absorption at selected wavelengths with increasing time in the dark (0 to 16 h) for a solution of complex **22** (10 µM) in 0.01 PBS at pH 7.4 in the presence of myoglobin (60 µM) and sodium dithionite, monitored by UV/Vis spectroscopy.

If no change is occurring in the absence of light, the absorbances at the afore-mentioned wavelengths should remain constant. No appreciable change in absorbance was observed at any of the measured wavelengths over a period of 16 hours in the dark (**Figure 3.6**). This indicates that no CO-release to myoglobin occurs in the dark over this period.

3.2.3.2 CO-release in Myoglobin Solution

For the CO-release studies of complex **22** using the myoglobin assay, an LED cluster of wavelength 365 nm was used. A solution of myoglobin in 0.01 M PBS (pH 7.4) buffer (950 µL) was degassed by bubbling with argon and reduced by addition of a microspatula of sodium dithionite, before addition of complex **22** in DMSO (50 µL). Irradiation was performed at 37 °C with stirring, in 1 – 5 minute intervals.

Photoexcitation of the myoglobin solution containing complex **22** resulted in the formation of CO-Mb, as seen by the increase in absorbance at 540 nm and 577 nm, and a decrease in absorbance at 557 nm (**Figure 3.7**).

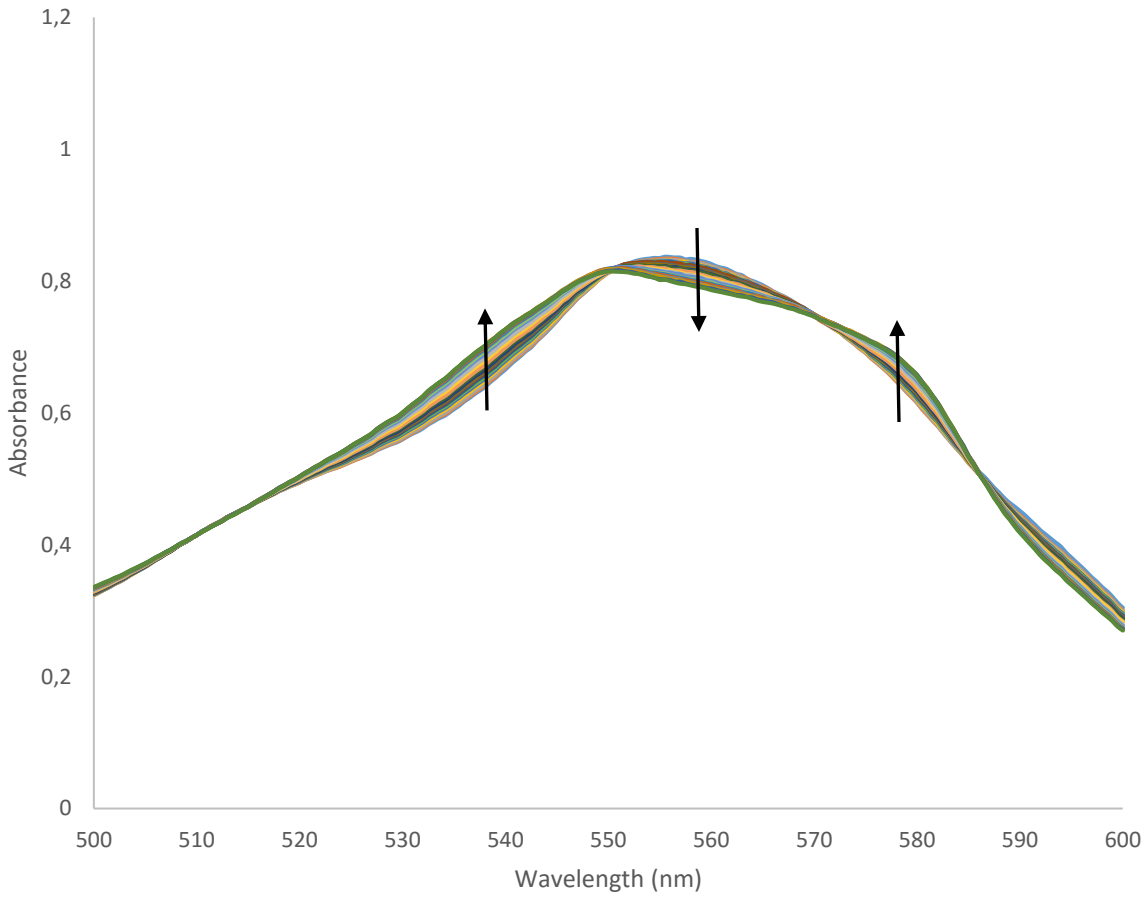

Figure 3.7: Change of UV/Vis spectrum in the Q-band region of myoglobin with increasing irradiation time at 365 nm for a solution of complex **22** (10 µM) in 0.01 PBS at pH 7.4 in the presence of myoglobin (60 µM) and sodium dithionite, monitored by UV/Vis spectroscopy.

The concentration of CO-Mb in the solution was determined at each time point, generating a plot of [CO-Mb] *vs.* time (**Figure 3.8**), using the molar extinction coefficient for CO-Mb (15.4 $mM^{-1}cm^{-1}$).[29]

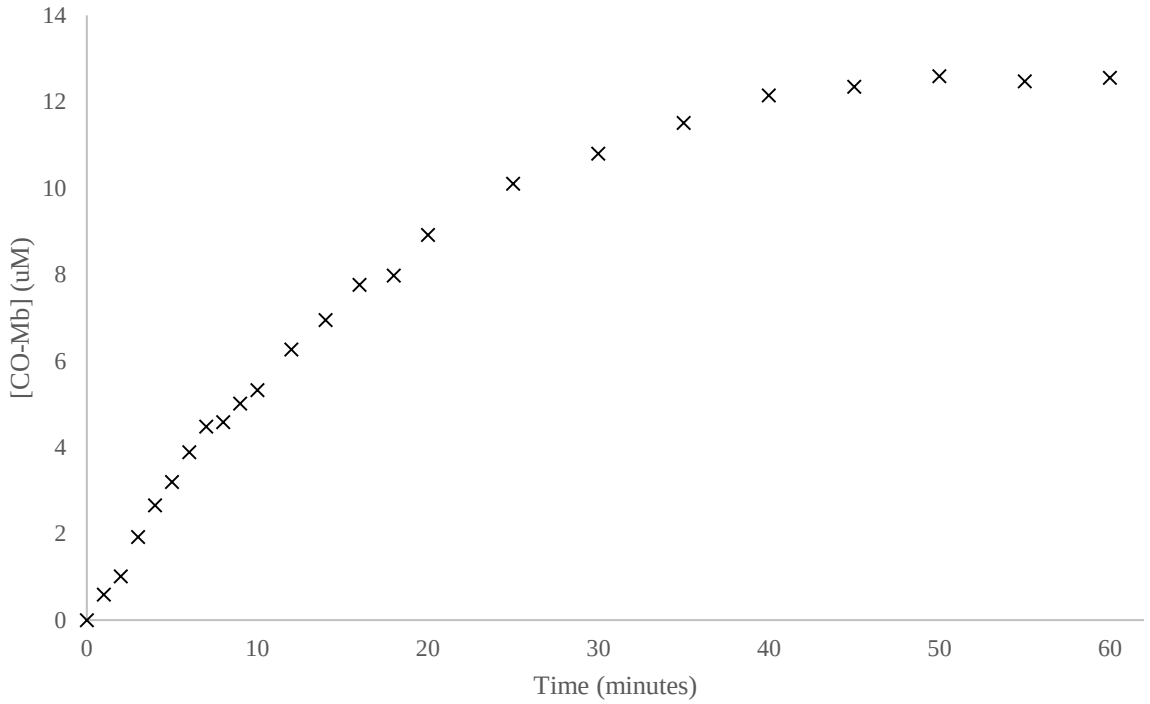

Figure 3.8: Concentration of CO-Mb (μM) formed with increasing irradiation time at 365 nm for a solution of complex **22** (10 μM) in 0.01 PBS at pH 7.4 in the presence of myoglobin (60 μM) and sodium dithionite as monitored by UV/Vis spectroscopy.

Figure 3.8 shows that the concentration of CO-Mb plateaus at *ca.* 12.5 μM for a 10 μM solution of complex **22**, indicating that, on average, approximately 1.25 molecules of CO are released per molecule of **22** (**Table 3.1**). While many Mn(I) tricarbonyl complexes release all three equivalents of CO upon exposure to light,[31, 32] some Mn(I) tricarbonyl complexes release fewer equivalents of CO, such as the complex synthesised by Smith *et al*., which releases 1.51 equivalents per tricarbonyl.[28]

Table 3.1: CO-release data for complex **22**

Compound	Conc. of CO-Mb (μM)	Eq. of CO released	Percentage of CO released (%)
22	12.55	1.26	42

The equivalents and the percentage of CO released by complex **22** is comparable to similar complexes in literature.[28] The rate of CO-release is given by a half-life ($t_{1/2}$) value, defined as the time taken for the complex to release 50 % of the total CO-ligands released. To be used as an effective therapeutic agent, the $t_{1/2}$ needs to be less than 2 hours to result in a high enough concentration of CO within the cell.[33]

The CO-release $t_{1/2}$ of complex **22** was determined by fitting a 1st order exponential growth curve to the CO-release profile of the complex (**Figure 3.8**). The data were fitted to a general equation for a 1st order exponential growth curve using data analysis and graphing software OriginPro.[34] The derivation of the $t_{1/2}$ equation is shown below.

$$y = y_0 + A_1 e^{\frac{x}{t_1}} \qquad Eqn.\ 3.1$$

$$[MbCO] = y_0 + A_1 e^{\frac{t_{1/2}}{t_1}} \qquad Eqn.\ 3.2$$

$$\frac{y_0}{2} = A_1 e^{\frac{t_{1/2}}{t_1}} + y_0 \qquad Eqn.\ 3.3$$

$$t_{1/2} = t_1 \ln\left(\frac{-y_0}{2A_1}\right) \qquad Eqn.\ 3.4$$

Equation 3.1 is the general equation for a 1st order exponential growth. Substituting the relevant values (y = [*MbCO*] and $x = t_{1/2}$) affords Equation 3.2. y_0 is the y-value at which the graph plateaus, so at $t_{1/2}$ [*MbCO*] = $y_0/2$, giving Equation 3.3. Rearrangement to make $t_{1/2}$ the subject of the equation produces Equation 3.4. Values for the variables t_1, A_1 and y_0 are given by fitting the curve in OriginPro, and are substituted into Equation 4 to reveal the $t_{1/2}$ of the complex.

The CO-release $t_{1/2}$ of complex **22** was calculated to be 12.84 minutes, which is far below the threshold of 2 hours. The $t_{1/2}$ that was obtained for complex **22** is comparable to many photo-CORMs in literature.[28, 35] It must be noted that the $t_{1/2}$ is dependent on the intensity of the light source and the compound concentration in the assay.

3.3 Antiproliferative Studies

With the established tumour-inhibiting effects exhibited by rhenium[16-19] and manganese[14, 20, 21, 36] complexes, and the current interest in metallodendrimers for biological applications, the *in vitro*

biological activity of the Re(I) complexes **16** – **18** was evaluated against epithelial carcinoma (A431), colon carcinoma (DLD-1) and ovarian carcinoma (A2780) cancer cell lines, in addition to normal fibroblast cells (BJ). The *in vitro* biological activity of Mn(I) complexes was evaluated against epithelial carcinoma (A431) and malignant melanoma (A375) cells.

The 3-(4,5-dimethylthiazol-2-yl)-2,5-diphenyltetrazolium bromide (MTT) cell proliferation assay was performed to generate a dose-response curve, from which IC_{50} values for the complexes **16** – **24** (**Figure 3.9**) were obtained. The IC_{50} value is defined as half of the maximal inhibitory concentration of a potential drug, and is a measure of the effectiveness of a substance to inhibit, in this case, the functioning of a cell. In an MTT assay, the viable cells are able to catalyse the conversion of MTT (yellow) to 3-(4,5-dimethylthiazol-2-yl)-2,5-diphenylformazan (MTT-formazan, purple) (**Scheme 3.1**) by means of NADH-dependent cellular oxidoreductase enzymes. Therefore, the lower the IC_{50} value, the more potent the compound is.

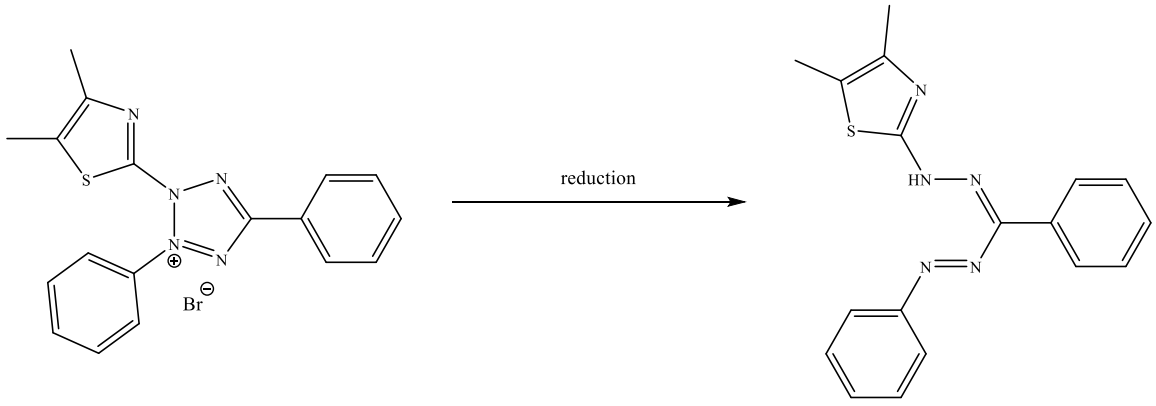

Scheme 3.1: Reduction of MTT to MTT-formazan

The change in colour is measured spectroscopically, and can be used to determine the viability of the cells in each well of the plate. From the spectroscopic measurements, a sigmoidal dose-response curve is generated, and the IC_{50} value can be interpreted. No known anti-cancer drug was used as a control in the anti-proliferative studies. The dose-response curves obtained for complex **18** against all four cell lines are shown in **Figure 3.9**. The IC_{50} results of the Re(I) complexes **16**, **17** and **18** and shown in **Table 3.2**.

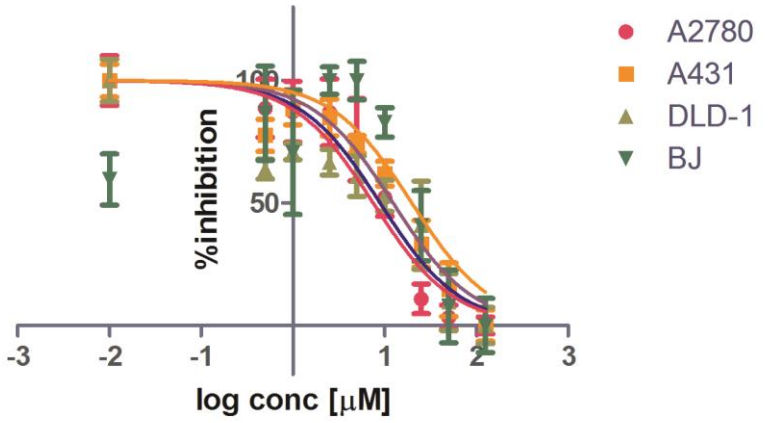

Figure 3.9: Sigmoidal dose-response curve corresponding to complex **18**.

Table 3.2: IC_{50} values of Re(I) complexes **16**, **17** and **18** against cancerous and non-tumourigenic cells

Compound	Bonding mode	n[a]	IC_{50} (μM)[b]			
			A431	DLD-1	A2780	BJ
16	[2 + 1]	1	57.84 ± 3.67	17.85 ± 1.79	26.61 ± 3.66	18.97 ± 1.76
17	[2 + 1]	3	46.64 ± 21.89	15.04 ± 2.20	36.45 ± 3.54	58.82 ± 7.65
18	[2 + 1]	4	14.09 ± 2.23	10.18 ± 0.47	6.38 ± 1.18	17.69 ± 1.50

[a] number of metal centres per molecule

[b] IC_{50} value ± standard error

The tested complexes displayed moderate to good cytotoxicity against A2780, A431 and DLD-1 tumour cells, and are toxic to some extent against the normal BJ cells. Complex **18** displays the best inhibitory effect against all of the tested cell lines. No selectivity is observed in the case of complex **16**, as the IC_{50} values are similar against the tumour and non-tumourigenic cells. Some selectivity is observed for complexes **17** and **18**, as significantly higher IC_{50} values are observed against the healthy BJ cell line, which indicates a lower toxicity towards normal human cells.

No trend is observed regarding the number of metal centres present per molecule. Complex **18** is the most cytotoxic, followed by complex **16**, while complex **17** is the least cytotoxic.

The complexes display the most potent activity against the colon carcinoma cell line (DLD-1), and the least potent activity against the epithelial carcinoma cell line (A431).

The *in vitro* cytotoxicity of Mn(I) complexes **19** – **24** was evaluated against epithelial carcinoma (A431) and malignant melanoma (A375) cell lines. The results are displayed in **Table 3.3**.

Table 3.3: IC_{50} values of Mn(I) complexes **19** – **24** against cancerous cells

Compound	Bonding mode	n[a]	IC_{50} (μM)[b]	
			A431	A375
19	[2 + 1]	1	15.57 ± 2.40	65.30 ± 7.60
20	[2 + 1]	3	14.92 ± 1.02	12.05 ± 1.72
21	[2 + 1]	4	5.26 ± 0.74	8.85 ± 0.58
22	Bidentate	1	25.16 ± 2.47	15.79 ± 1.90
23	Bidentate	3	49.65 ± 8.06	57.59 ± 4.39
24	Bidentate	4	11.23 ± 1.15	31.45 ± 3.54

[a] number of metal centres per molecule

[b] IC_{50} value ± standard error

The Mn(I) complexes displayed moderate to good cytotoxicity against the tested cell lines. [2 + 1] complex **21** displayed the most potent activity, with IC_{50} values < 10 μM. This is interesting, as complex **21** is the Mn(I) analogue of Re(I) complex **18**, which displayed the best activity of the Re(I) complexes. With the exception of complex **24** against the A375 cell line, Mn(I) complexes with a nuclearity of four (n = 4) display the best activity. A trend is observed in the [2 + 1] Mn(I) complexes where an increase in nuclearity (n) leads to an increase in activity. This is not observed for the bidentate Mn(I) complexes, where complexes **22** and **24** display the most potent cytotoxicity, followed by complex **23**.

The [2 + 1] complexes display higher *in vitro* activity than their bidentate counterparts, with an overall average IC_{50} of 20.33 μM vs 31.82 μM. The complexes display higher cytotoxicity towards the epithelial carcinoma (A431) than the malignant melanoma (A375) cell line. The cytotoxicity of the Mn(I) complexes was not evaluated against healthy cells, so the selectivity could not be assessed.

Figure 3.10 shows the IC_{50} values of complexes **16** – **24** against all the tested cell lines.

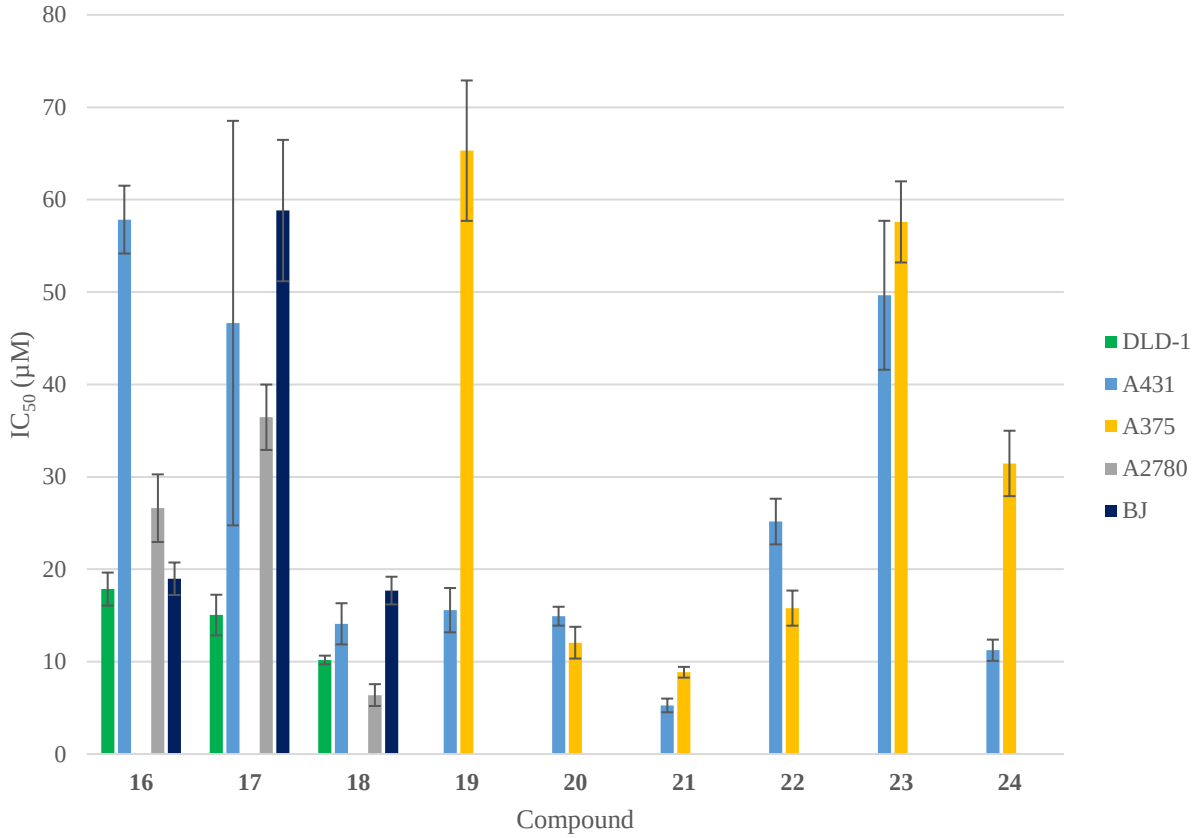

Figure 3.10: Comparison of IC_{50} values of complexes **16** – **24** against tumorous and healthy cells

The only cell line that was used to evaluate the cytotoxicity of all the complexes was the epithelial carcinoma cell line (A431). **Figure 3.11** shows a comparison of the IC_{50} values of complexes **16** – **24** against the A431 cell line.

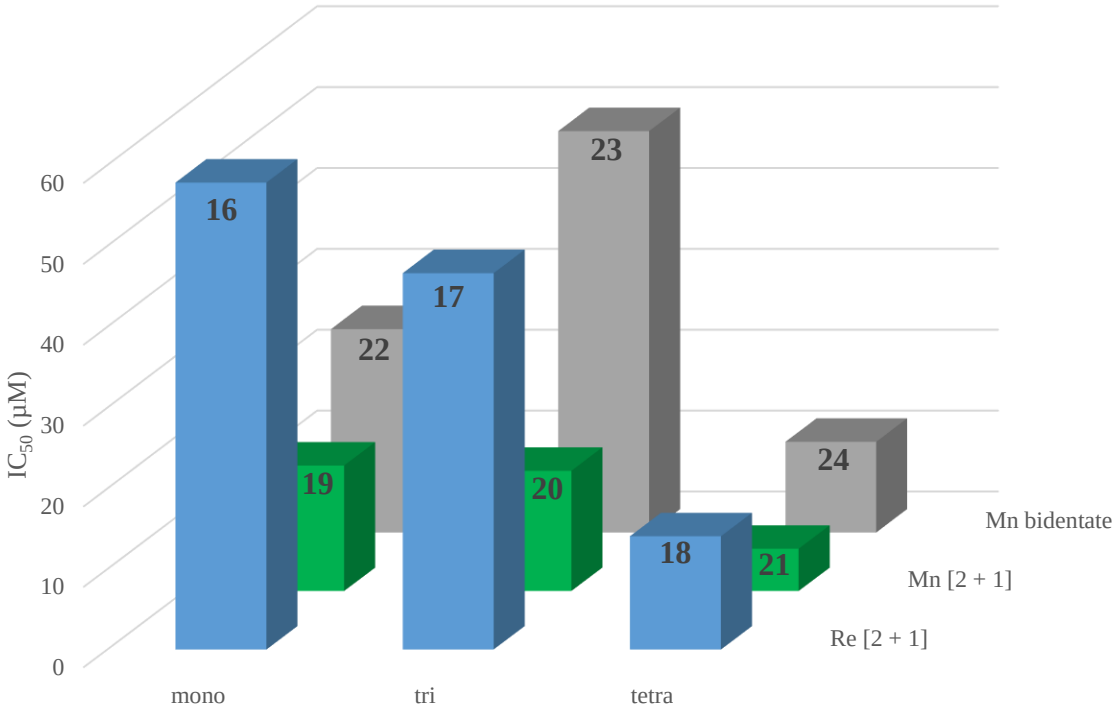

Figure 3.11: Comparison of IC_{50} values of complexes **16** – **24** against A431 epithelial carcinoma cells

While the Re(I) [2 + 1] complexes (**16** – **18**) and the Mn(I) bidentate complexes (**22** – **24)** display similar activity against the A431 cell line, the Mn(I) [2 + 1] complexes (**19** – **21**) display significantly higher activity. The Mn(I) [2 + 1] complexes display an increase of up to 3-fold compared to their counterparts in the other series. This is promising, as with the potent activity displayed by the Mn(I) [2 + 1] complexes, coupled with CO-release, could result in an extremely effective potential drug.

An Alamar Blue assay was performed on the Re(I) complexes **16** – **18** to verify the results obtained using the MTT assay. The Alamar Blue assay tests the cells ability to reduce resazurin (blue) to resorufin (fluorescent pink). The intensity of the fluorescence is proportional to the number of cells with normal metabolic activity. The fluorescence is measured spectroscopically, and is a direct indicator of the proliferating, viable cells. **Scheme 3.2** shows the reduction of resazurin to resorufin.

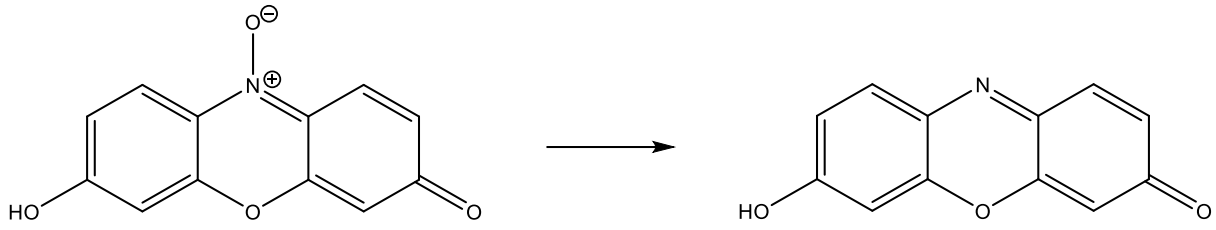

Resazurin **Resorufin**

Scheme 3.2: Reduction of resazurin to resorufin

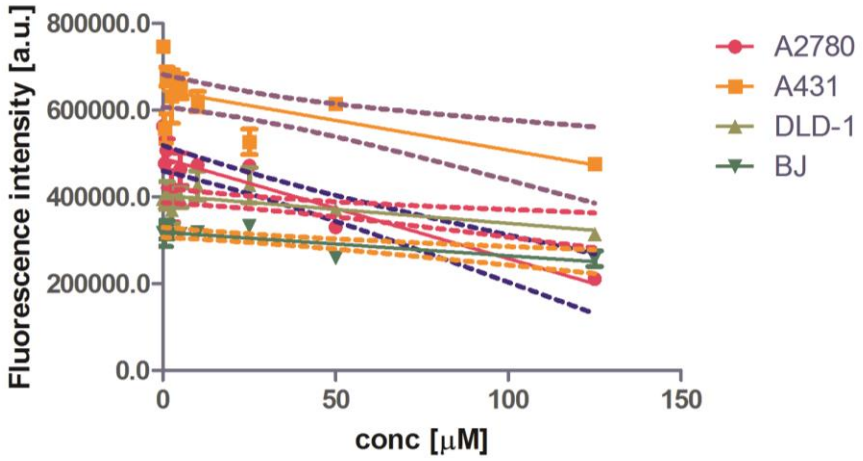

Figure 3.12: Influence of complex **18** on the cell proliferation *in vitro*.

Figure 3.12 shows the decrease in fluorescence with an increase in concentration of complex **18**. This is expected if the compound is stopping normal metabolic functioning of the cells, as less resorufin is produced, leading to a decrease in fluorescence. A deviation in the gradient of the slope from 0 negatively is an indication of the dose-dependency antiproliferative effect of the tested sample. **Figure 3.12** shows that a negative slope is observed for all cell lines treated with compound **18**. The same was observed for compound **16** against all cell lines. Compound **17** displayed a negative slope against cell lines A2780 and DLD-1, but did not display a significant (95 % confidence interval) change in fluorescent intensity with an increase in concentration against A431 and BJ cell lines.

3.4 Antiplasmodial Studies

Due to the lack of research into the antiplasmodial effects of Re(I) and Mn(I) tricarbonyl complexes, it was deemed worthwhile to evaluate the antiplasmodial activity of the synthesised compounds. Hence, complexes **16** – **24** were evaluated as potential antiplasmodial agents *in vitro* against both chloroquine-sensitive (NF54) and chloroquine-resistant (K1) strains of *Plasmodium falciparum*. The *in vitro* antiplasmodial assay was performed using a modified method described by Makler *et al.*, using the parasite lactate dehydrogenase (pLDH) assay.[37] Similarly to the MTT assay, the pLDH assay relies on the healthy parasite's ability to reduce nitro blue tetrazolium (NBT) chloride to a formazan (NBT-formazan), resulting in a colour change (**Scheme 3.3**).

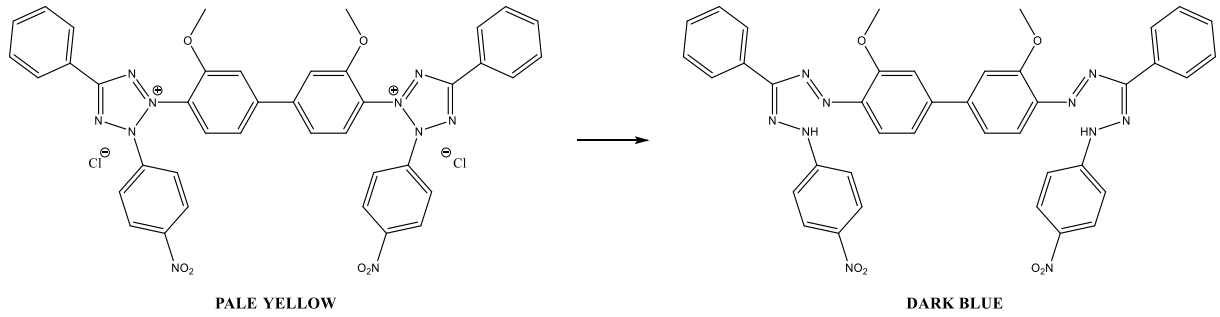

Scheme 3.3: Reduction of NBT chloride to NBT-formazan

The efficacy of the compounds was tested using the standard pLDH assay against both a chloroquine-sensitive strain and a chloroquine-resistant strain of *P. falciparum* (**Section 3.4.1**), and selected Mn(I) tricarbonyl complexes, known to release CO, were evaluated against a chloroquine-resistant strain of *P. falciparum* with irradiation using an LED array of 365 nm (**Section 3.4.2**).

3.4.1 Antiplasmodial Evaluation

The samples were tested on one occasion in triplicate, and the data obtained from the *in vitro* antiplasmodial evaluation are shown in **Table 3.4**.

Table 3.4: IC_{50} values of Re(I) and Mn(I) complexes **1**6 – **24** against CQ-sensitive (NF54) and CQ-resistant (K1) strains of *P. falciparum*.

Compound	Metal	Bonding mode	n[a]	IC_{50} (µM)[b]		RI[c]
				NF54	K1	
16	Re	[2 + 1]	1	3.29 ± 0.37	1.42 ± 0.08	0.432
16b	Re	[2 + 1]	1	3.59 ± 0.45	2.49 ± 0.12	0.694
17	Re	[2 + 1]	3	3.45 ± 0.07	2.66 ± 0.12	0.771
18	Re	[2 + 1]	4	2.20 ± 0.13	1.37 ± 0.048	0.623
19	Mn	[2 + 1]	1	8.31 ± 1.25	2.22 ± 0.093	0.267
20	Mn	[2 + 1]	3	2.81 ± 0.74	1.02 ± 0.097	0.363
21	Mn	[2 + 1]	4	3.76 ± 0.40	0.99 ± 0.02	0.263
22	Mn	Bidentate	1	2.08 ± 0.12	1.98 ± 0.14	0.952
23	Mn	Bidentate	3	4.28 ± 0.51	1.68 ± 0.25	0.393
24	Mn	Bidentate	4	4.05 ± 0.054	1.59 ± 0.13	0.393
CQ	/	/	/	0.031 ± 0.010	0.30 ± 0.032	9.67

[a] Number of metal centres per molecule

[b] IC_{50} value ± standard error

[c] Resistance index (IC_{50}[CQ-resistant]/IC_{50}[CQ-sensitive])

The complexes **16** – **24** display good activity against the NF54 and K1 strains of *P. falciparum*. The activities observed for these compounds are lower than that of chloroquine for both the CQ-sensitive and the CQ-resistant strains. All of the IC_{50} values for the metal complexes are in the low micromolar range, although chloroquine is substantially more potent than any of the metal

complexes against both the NF54 and K1 strains of *P. falciparum*. The monomeric [2 + 1] Mn(I) complex **19** displayed the lowest activity in the NF54 strain, with an IC_{50} value of 8.31 µM. All of the other complexes displayed values in the range of 2 – 4.5 µM. The complexes all displayed similar IC_{50} values against the CQ-resistant strain of *P. falciparum*, in the range of 1 – 3 µM. This may mean that the complexes follow the same mechanism of action.

Every complex displayed better activity in the CQ-resistant strain of *P. falciparum*, resulting in resistance indices of < 1. The compound with the best resistance index (RI) was complex **21**, which displayed a resistance index of 0.263. This indicates that the compound is almost four times more efficacious against the CQ-resistant strain than the CQ-sensitive strain of *P. falciparum*. The bidentate Mn(I) tricarbonyl complex **22** displayed an RI of 0.952, indicating that the activity is almost equal in both of the strains. As expected, chloroquine displays a high RI of 9.67, indicating that it is much for efficacious against the CQ-sensitive strain than the CQ-resistant, suggesting resistance towards the drug. Since the complexes exhibit similar or higher activity in the K1 strain compared to the NF54 strain, this indicates that the complexes possibly act by a different mechanism of action to CQ, and overcome the resistance mechanism experienced by CQ.

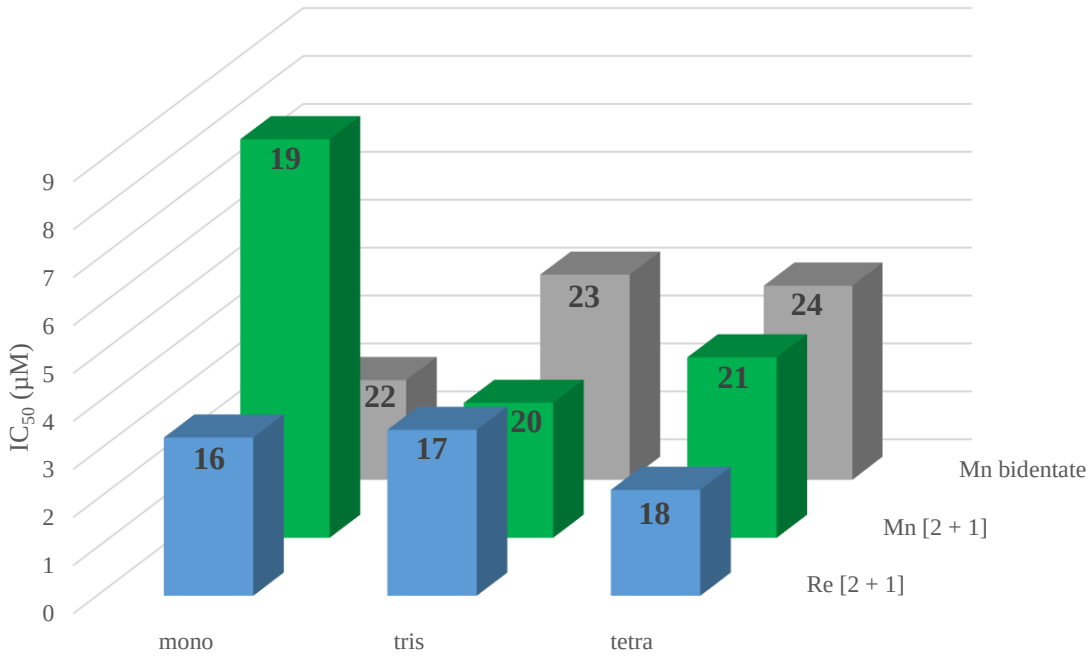

Figure 3.13: Comparison of IC_{50} values of complexes **16 – 24** against the NF54 strain of *P. falciparum*.

A general trend is observed with the Re(I) and Mn(I) [2 + 1] complexes, in which an increase in nuclearity (n) leads to an increase in efficacy in the NF54 strain of *P. falciparum* (**Figure 3.13**). This trend seems to reverse in the Mn(I) bidentate complexes, where the most active complex is the monomeric one (**22**). This trend is evident only against the NF54 strain, and is not observed against the K1 strain (**Figure 3.14**). No clear trend is observed for the efficacy of the complexes in the K1 strain. The Mn(I) bidentate complexes (**22**, **23**, **24**) all display similar activity in the K1 strain, the Mn(I) [2 + 1] complexes (**19**, **20**, **21**) show an increase in activity with an increase in nuclearity, and the tris Re(I) complex (**16**) and the protonated monomeric complex (**16b**) have lower activities than both the monomeric and tetrameric analogues (**17**, **18**). The complex displaying the best activity against the K1 strain is the tetrameric [2 + 1] Mn(I) complex **21**.

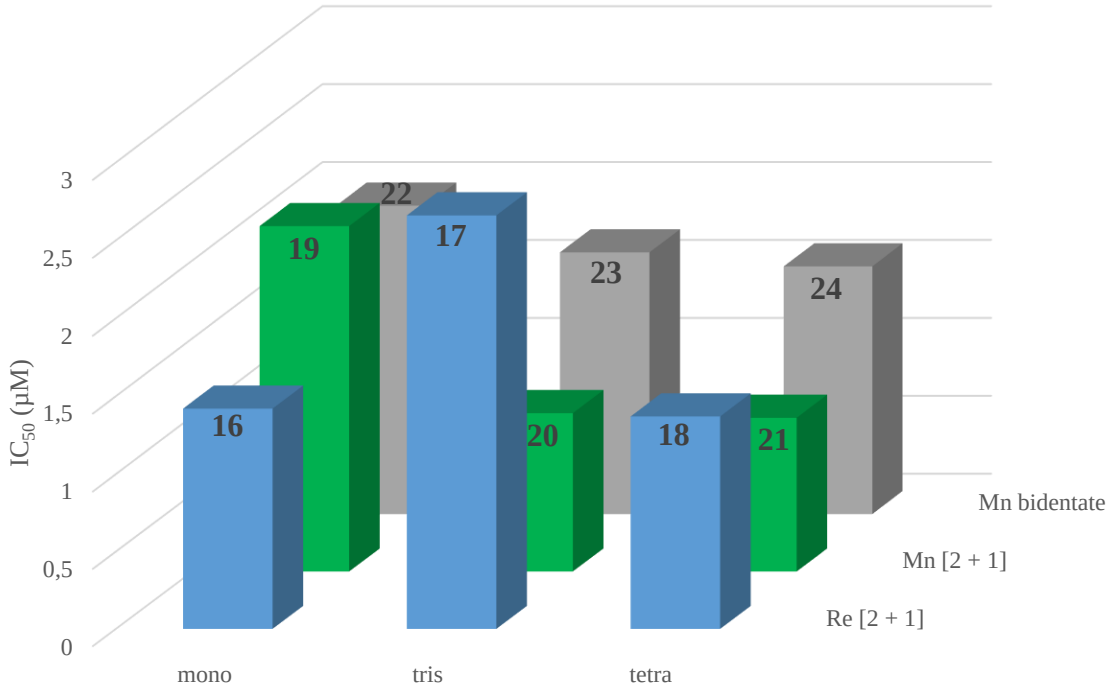

Figure 3.14: Comparison of IC_{50} values of complexes **16 – 24** against the K1 strain of *P. falciparum*.

It is clear that the Mn(I) [2 + 1] series displays the highest efficacy against the K1 strain of *P. falciparum*, but the same cannot be said for the NF54 strain, against which the Re(I) series displays the highest efficacy.

With the exception of complex **19**, the Re(I) and Mn(I) [2 + 1] complexes display similar activities against the NF54 strain of *P. falciparum*. The Mn(I) [2 + 1] complexes display better activity than the Re(I) analogues against the K1 strain.

When comparing the [2 + 1] approach and the bidentate bonding modes of the Mn(I) complexes (**19** – **21** *vs*. **22** – **24**), it can be deduced that the [2 + 1] bonding mode shows slightly higher efficacy than the bidentate bonding mode against both NF54 and K1 strains.

3.4.2 Antiplasmodial Evaluation with UV Irradiation

To perform the *in vitro* antiplasmodial evaluation of Mn(I) complexes **19**, **21**, **22** and **24**, two plates were set up simultaneously, a control plate (not irradiated) and an experiment plate (irradiated). The data for the experiment are shown in **Table 3.5**.

Table 3.5: IC_{50} values of select Mn(I) complexes against CQ-resistant (K1) strain of *P. falciparum* with and without irradiation with 365 nm LED array

Compound	**IC_{50} (µM)[b]**	
	Dark	**Irradiated[a]**
19	6.04 ± 0.95	3.76 ± 0.69
21	2.47 ± 0.11	1.46 ± 0.15
22	2.22 ± 0.14	3.41 ± 0.40
24	1.60 ± 0.29	3.132 ± 0.17
CQ	0.13 ± 0.022	0.12 ± 0.012

[a] Irradiated with 365 nm LED array for 15 minutes

[b] IC_{50} value ± standard error

The Mn(I) [2 + 1] complexes **19** and **21** show a distinct increase in efficacy against the K1 strain of *P. falciparum* upon irradiation, while the Mn(I) bidentate complexes **22** and **24** display a decrease in efficacy upon irradiation. The decrease in efficacy of complexes **22** and **24** upon irradiation is unexpected, as release of CO into the culture should decrease the viability of the parasites.[38] This change in efficacy upon irradiation is displayed in **Table 3.6** and **Figure 3.15**.

In **Table 3.6**, an IC_{50} ratio of 1 suggests that no change in efficacy occurs upon irradiation with the 365 nm LED cluster, a value of < 1 suggests an increase in activity upon irradiation, and a value of > 1 suggests that the efficacy of the compound decreases upon irradiation. Similar IC_{50} ratios for complexes **19** and **21** of *ca*. 0.60 suggest that the activity of the complexes increases by almost a factor of 2 when irradiated. On the other hand, IC_{50} ratios of 1.54 and 1.96 for complexes **22** and **24**, respectively, suggest a notable decrease in efficacy upon irradiation. As expected, the IC_{50} ratio is close to 1 for chloroquine, as irradiation should have no effect on the efficacy of the drug. It is likely that the coordination mode of the complexes influences the rate and amount of CO released from the complexes.

Table 3.6: Ratio of activity between dark and irradiated plates for complexes **19**, **21**, **22** and **24** against K1 CQ-resistant *P. falciparum*.

Compound	**IC_{50} ratio**[a]
19	0.62
21	0.59
22	1.54
24	1.96
CQ	0.92

[a] IC_{50}(dark)/IC_{50}(irradiated)

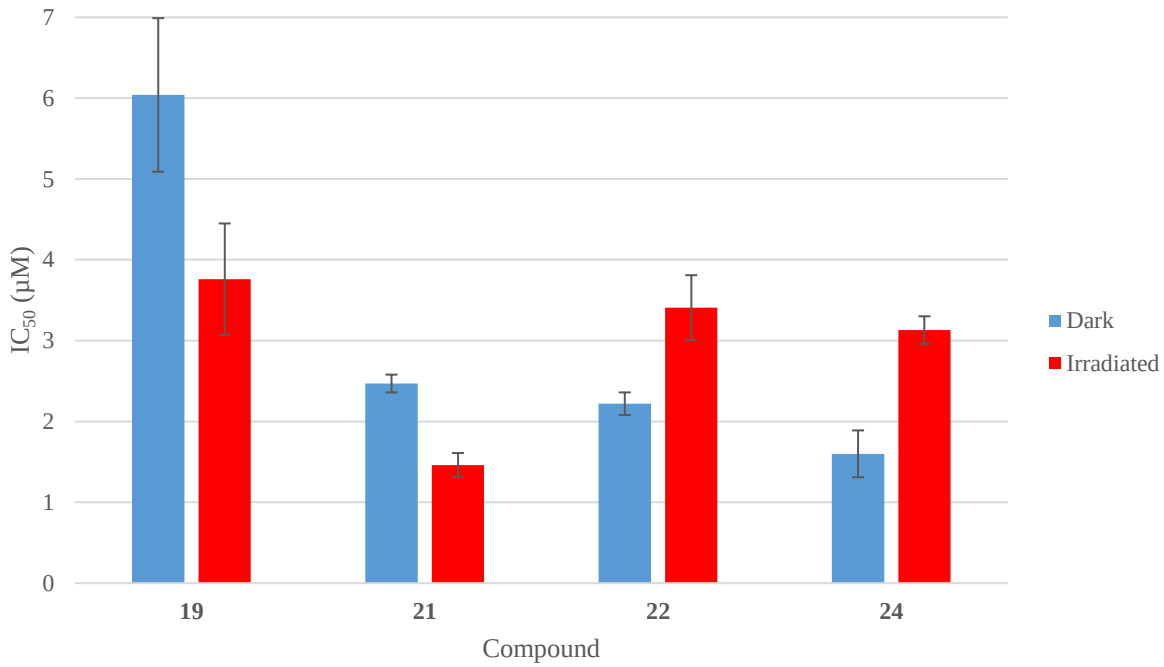

Figure 3.15: Comparison of IC_{50} values showing changes in efficacy upon irradiation

The standard antiplasmodial assay and the antiplasmodial assay with UV irradiation were performed on separate occasions, and a difference can be seen in the IC_{50} values of the tested compounds in the 'K1' column of **Table 3.4** and the 'Dark' column of **Table 3.5**. Nonetheless, the results obtained are within the same range.

The irradiation experiment could be improved upon significantly before confirming these preliminary results. Firstly, the LED array used for irradiation of the plates was not custom-made for 96-well plates, but was modified in-house from the original array used for the CO-release studies. It is therefore possible that there was uneven spread of irradiation, which may have affected the results that were obtained.

A drastic improvement in activity against the K1 strain of *P. falciparum* is observed upon irradiation of complexes **19** and **21**. This shows that CO-release using Mn(I) tricarbonyl complexes, in particular complexes with the [2 + 1] coordination mode, is a worthwhile avenue to pursue new drug candidates to combat the rise in drug resistance of *P. falciparum*.

3.5 Preliminary Radiolabelling Studies

Technetium-99m, a metastable, radioactive isotope of technetium, is a gamma-emitting radionuclide.[39] It is the most widely used radionuclide, due to its suitable half-life of 6.02 hours, and gamma-energy of 140 keV.[39, 40] The use of ^{99m}Tc allows for the real-time monitoring of organ function, diagnosis of medical conditions and follow-up disease progression using SPECT scans.[41]

In this study, the radiolabelling of ligand **10** with ^{99m}Tc, to form an analogue of complex **16**, is reported as a preliminary study into the radiolabelling of such [2 + 1] complexes.

3.5.1 Formation of ^{99m}Tc(bpy)(CO)$_3$ Species

The formation of the ^{99m}Tc(bpy)(CO)$_3$ species is achieved by heating a solution of pertechnetate ($^{99m}TcO_4^-$) with various salts packaged as a pre-purchased kit (Isolink) to afford the tricarbonyl tri-aqua ^{99m}Tc species, before the addition of excess 2,2'-bipyridyl and subsequent heating (**Scheme 3.4**). The formation was monitored by HPLC coupled to a radiodetector.

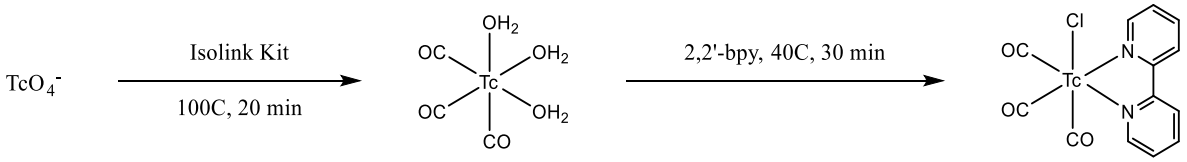

Scheme 3.4: Formation of Tc-bpy species

Figure 3.16 shows the radiotrace of the tricarbonyl tri-aqua ^{99m}Tc species. The ^{99m}Tc-tricarbonyl aqua species displays a retention time of 1.59 minutes. The peak in the radiotrace at 2.50 minutes is residual pertechnetate.

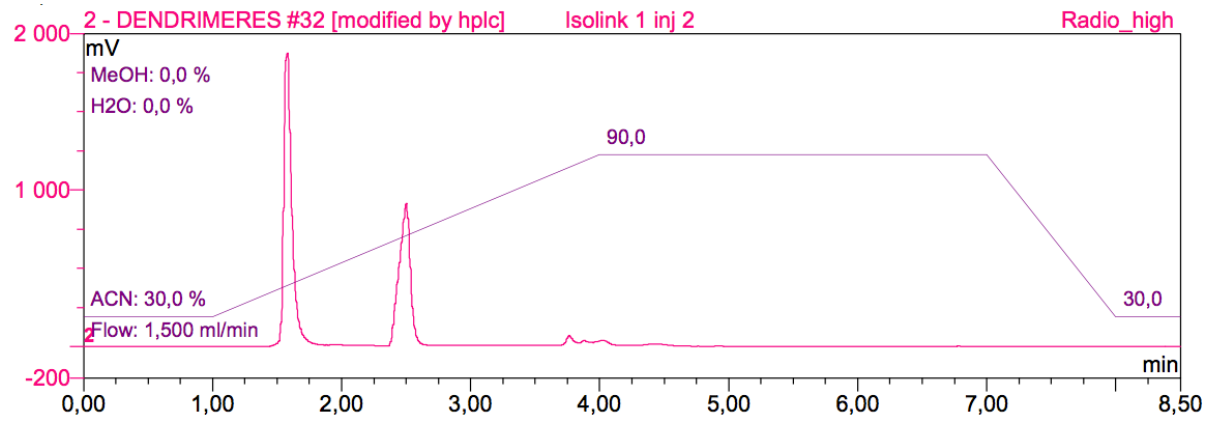

Figure 3.16: HPLC radiotrace of ^{99m}Tc-tricarbonyl species

The subsequent formation of the ^{99m}Tc(bpy)(CO)$_3$ species is shown in **Figure 3.17**. The radiotrace peak attributed to the desired species has a retention time of 4.90 minutes. The other peaks which form during this transformation could not be identified.

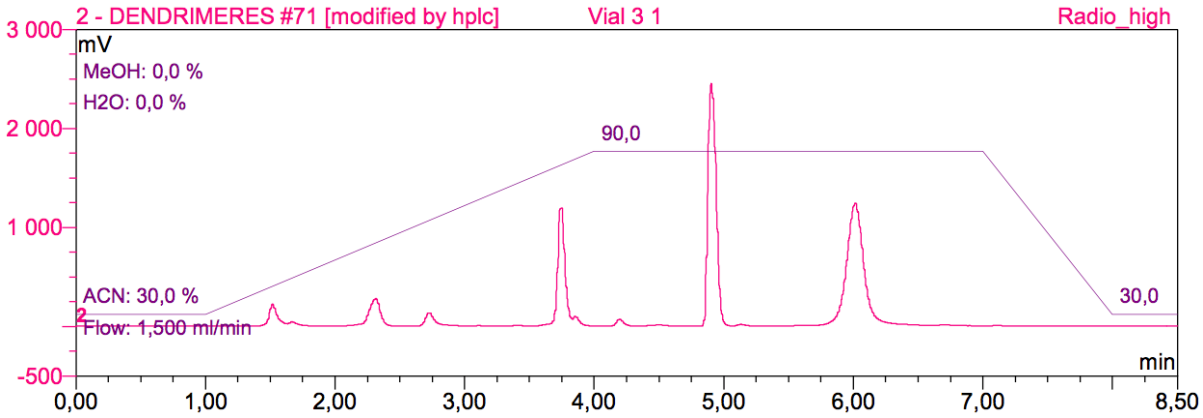

Figure 3.17: HPLC radiotrace of ^{99m}Tc(bpy)(CO)$_3$ species

With the formation of the ^{99m}Tc(bpy)(CO)$_3$ species comes many peaks in the radio spectrum that cannot be identified. The peak that belongs to the desired species is believed to be the peak with the retention time of 4.90 min. The unidentified peaks could arise from substitution of the chloride ligand with H_2O or CH_3CN, which would change the retention time of the complex.

3.5.2 Radiolabelling of Ligand 10

The desired transformation was achieved by adding the $^{99m}Tc(bpy)(CO)_3$ to a large excess of the monomeric ligand **10**. The vial was then incubated at 40 °C for 20 minutes. A radiotrace of the crude product is shown in **Figure 3.18**. The peak with the retention time of 6.98 minutes is attributed to the desired radiolabelled product.

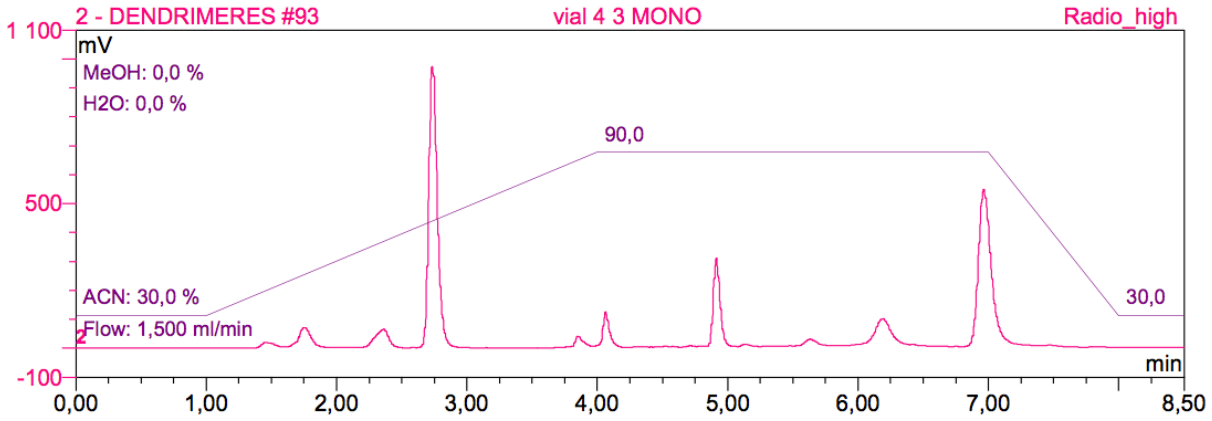

Figure 3.18: HPLC trace of crude mixture after radiolabelling ligand **10**

The isolation of the radiolabelled ligand **10** was achieved by preparative HPLC, and the radiotrace is displayed in **Figure 3.19**. Unfortunately, the Re(I) 'cold complex,' **16** (retention time = 6.00 min) did not match the retention time of the radiolabelled product (retention time = 6.98 min). The difference in retention time is likely due to the different counterions. The radiolabelled ligand **10** has a chloride counterion due to the reaction being performed in a sodium chloride solution, whereas anion exchange was performed on the Re(I) analogue, complex **16**, to form the PF_6 adduct. A similar anion exchange was attempted by adding ammonium hexafluorophosphate to the NaCl solution, but the retention time of the radiolabelled product remained unchanged. This variance in retention time due to different counterions is a known phenomenon, as was shown by Hodges and co-workers in their work with synthetic peptides.[42] The difference in retention times could also be due in part to the lag time between the radiodetector and the UV detector.

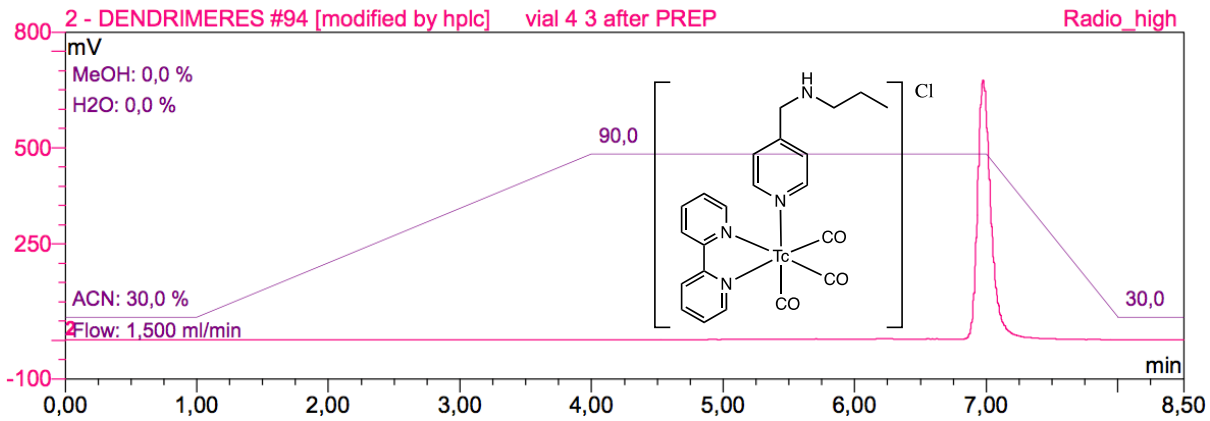

Figure 3.19: HPLC radiotrace of the radiolabelled ligand 10

Radiolabelling of multimeric 4-picolylamine ligands was attempted, but were unsuccessful due to the large excess of ligand (> 300 times for monomeric ligand **10**). This large excess of ligand resulted in a mixture of mono-, di-, tri- and tetra-substituted radiolabelled ligands, and it was not deemed worthwhile to isolate the products.

3.6 Overall Summary

The Mn(I) tricarbonyl complexes (**19** – **24**) are stable in the absence of light for an extended period of time, however, exposure to natural daylight or upon photoactivation at 365 nm using an LED array, CO-release from the complexes occurs. This was shown using electronic absorption spectra of complexes **19** – **24**, with the decrease in the MLCT absorption band indicating CO-release. Using complex **22** as a model, CO-release was confirmed using the standard myoglobin assay, monitored by UV/Vis absorption spectroscopy. Complex **22** was found to release 1.26 equivalents of CO per molecule of complex **22**, with a half-life of 12.84 minutes.

The *in vitro* anticancer activity of complexes **16** – **24** was studied using the MTT assay. Re(I) complexes **16** – **18** were evaluated against three cancerous cell lines (A431, DLD-1 and A2780) and one healthy cell line (BJ). Tetranuclear complex **18** displayed the most potent cytotoxicity, with IC_{50} values < 15 µM against all of the tested cancerous cell lines. Complexes **17** and **18** displayed some selectivity towards the cancerous cell lines over the healthy cell line. An Alamar Blue assay was performed on the Re(I) complexes to verify the results obtained using the MTT

assay. Mn(I) complexes **19** – **24** were evaluated against two cancerous lines (A431 and A375). The complexes displayed moderate to good activity. Tetranuclear complex **21** displayed the best activity against both cell lines. The [2 + 1] Mn(I) complexes displayed increased activity compared to their bidentate counterparts.

The *in vitro* antiplasmodial activity of complexes **16** – **24** was investigated using the pLDH assay against two strains of *P. falciparum*, a CQ-sensitive (NF54) and a CQ-resistant (K1) strain. The complexes displayed moderate to good efficacy against both strains, with IC_{50} values in the low micromolar range. All of the complexes displayed better activity against the CQ-resistant strain than the CQ-sensitive strain. Tetrameric complex **21** displayed the best activity against the CQ-resistant strain, as well as the best selectivity towards the CQ-resistant strain over the CQ-sensitive strain, with an IC_{50} value of 0.99 µM and a resistance index of 0.263.

The *in vitro* antiplasmodial activity of complexes **19**, **21**, **22** and **24** was investigated with irradiation with 365 nm light against the CQ-resistant strain of *P. falciparum*. Complexes **19** and **21** displayed an almost two-fold increase in activity, while complexes **22** and **24** displayed a significant decrease in activity upon irradiation, suggesting that the [2 + 1] complexes are promising candidates and should be further investigated.

Radiolabelling of ligand **10** with ^{99m}Tc was achieved to form a [2 + 1] complex by reacting ligand **10** with $^{99m}Tc(bpy)(CO)_3$ to afford the desired product. The complex was isolated using preparative HPLC. Radiolabelling of ligands **11** and **12** were unsuccessful.

References

1. L. E. Otterbein, F. H. Bach, J. Alam, M. Soares, H. T. Lu, M. Wysk, R. J. Davis, R. A. Flavell and A. M. K. Choi, *Nat. Med.*, 2000, **6**, 422-428.
2. H. O. Pae, B. M. Choi, G. S. Oh, M. S. Lee, D. G. Ryu, H. Y. Rhew, Y. M. Kim and H. T. Chung, *Mol. Pharmacol.*, 2004, **66**, 122-128.
3. B. E. Mann, in *Top. Organometal. Chem.*, 2010, vol. 32, pp. 247-285.
4. S. Brouard, L. E. Otterbein, J. Anrather, E. Tobiasch, F. H. Bach, A. M. K. Choi and M. P. Soares, *J. Exp. Med.*, 2000, **192**, 1015-1025.

5. A. Pamplona, A. Ferreira, J. Balla, V. Jeney, G. Balla, S. Epiphanio, A. Chora, C. D. Rodrigues, I. P. Gregoire, M. Cunha-Rodrigues, S. Portugal, M. P. Soares and M. M. Mota, *Nat. Med. (N. Y., NY, U. S.)*, 2007, **13**, 703-710.
6. A. Ferreira, J. Balla, V. Jeney, G. Balla and M. P. Soares, *J. Mol. Med.*, 2008, **86**, 1097-1111.
7. A. Ferreira, I. Marguti, I. Bechmann, V. Jeney, A. Chora, N. R. Palha, S. Rebelo, A. Henri, Y. Beuzard and M. P. Soares, *Cell*, 2011, **145**, 398-409.
8. G. Silva, V. Jeney, A. Chora, R. Larsen, J. Balla and M. P. Soares, *J. Biol. Chem.*, 2009, **284**, 29582-29595.
9. R. T. Figueiredo, P. L. Fernandez, D. S. Mourao-Sa, B. N. Porto, F. F. Dutra, L. S. Alves, M. F. Oliveira, P. L. Oliveira, A. V. Graca-Souza and M. T. Bozza, *J. Biol. Chem.*, 2007, **282**, 20221-20229.
10. E. Seixas, R. Gozzelino, A. Chora, A. Ferreira, G. Silva, R. Larsen, S. Rebelo, C. Penido, N. R. Smith, A. Coutinho and M. P. Soares, *Proc. Natl. Acad. Sci. U. S. A.*, 2009, **106**, 15837-15842.
11. R. Gozzelino, V. Jeney and M. P. Soares, *Annu. Rev. Pharmacool. Toxicol.*, 2010, **50**, 323-354.
12. S. Garcia-Gallego and G. J. Bernardes, *Angew. Chem. Int. Ed.*, 2014, **53**, 9712-9721.
13. R. Motterlini, J. E. Clark, R. Foresti, P. Sarathchandra, B. E. Mann and C. J. Green, *Circ. Res.*, 2002, **90**, E17-24.
14. Q.-Y. Chen, D.-F. Zhou, J. Huang, W.-J. Guo and J. Gao, *J. Inorg. Biochem.*, 2010, **104**, 1141-1147.
15. C. L. Chen, X. F. Zhu, M. X. Li, H. M. Guo and J. Y. Niu, *Russ. J. Coord. Chem.*, 2011, **37**, 435-438.
16. C. S. Parson, V.; Krauss, C.; Banerjee, H.N.; Reilly, C.; Krause, J.A.; Wachira, J.M.; Giri, D.; Winstead, A.; Mandal, S.K., *Br. J. Pharm. Res.*, 2014, **4**, 362-367.
17. Y. K. Yan, S. E. Cho, K. A. Shaffer, J. E. Rowell, B. J. Barnes and I. H. Hall, *Pharmazie*, 2000, **55**, 307-313.
18. A. W. T. Choi, M. W. Louie, S. P. Y. Li, H. W. Liu, B. T. N. Chan, T. C. Y. Lam, A. C. C. Lin, S. H. Cheng and K. K. W. Lo, *Inorg. Chem.*, 2012, **51**, 13289-13302.

19. A. Kermagoret, G. Morgant, J. d'Angelo, A. Tomas, P. Roussel, G. Bastian, P. Collery and D. Desmaële, *Polyhedron*, 2011, **30**, 347-353.
20. M. Damercheli, D. Dayyani, M. Behzad, B. Mehravi and M. S. Ardestani, *J. Coord. Chem.*, 2015, **68**, 1500-1513.
21. T. Dallagi, M. Saidi, G. Jaouen and S. Top, *Appl. Organomet. Chem.*, 2013, **27**, 28-35.
22. K. I. Ansari, J. D. Grant, S. Kasiri, G. Woldemariam, B. Shrestha and S. S. Mandal, *J. Inorg. Biochem.*, 2009, **103**, 818-826.
23. M.-W. Louie, M. Ho-Chuen Lam and K. Kam-Wing Lo, *Eur. J. Inorg. Chem.*, 2009, **2009**, 4265-4273.
24. A. Leonidova, V. Pierroz, L. A. Adams, N. Barlow, S. Ferrari, B. Graham and G. Gasser, *ACS Med. Chem. Lett.*, 2014, **5**, 809-814.
25. S. J. Spall, T. Keane, J. Tory, D. C. Cocker, H. Adams, H. Fowler, A. J. Meijer, F. Hartl and J. A. Weinstein, *Inorg. Chem.*, 2016, **55**, 12568-12582.
26. M. J. Li, X. Liu, Y. Q. Shi, R. J. Xie, Q. H. Wei and G. N. Chen, *Dalton Trans.*, 2012, **41**, 10612-10618.
27. R. R. Andréa, W. G. J. De Lange, D. J. Stufkens and A. Oskam, *Inorg. Chim. Acta*, 1988, **149**, 77-84.
28. P. Govender, S. Pai, U. Schatzschneider and G. S. Smith, *Inorg. Chem.*, 2013, **52**, 5470-5478.
29. A. J. Atkin, J. M. Lynam, B. E. Moulton, P. Sawle, R. Motterlini, N. M. Boyle, M. T. Pryce and I. J. S. Fairlamb, *Dalton Trans.*, 2011, **40**, 5755-5761.
30. S. McLean, B. E. Mann and R. K. Poole, *Anal. Biochem.*, 2012, **427**, 36-40.
31. H. M. Berends and P. Kurz, *Inorg. Chim. Acta*, 2012, **380**, 141-147.
32. S. J. Carrington, I. Chakraborty and P. K. Mascharak, *Dalton Trans.*, 2015, **44**, 13828-13834.
33. U. Schatzschneider, *Inorg. Chim. Acta*, 2011, **374**, 19-23.
34. OriginPro Evaluation 2018 (64-bit), 2017.
35. J. Niesel, A. Pinto, H. W. P. N'Dongo, K. Merz, I. Ott, R. Gust and U. Schatzschneider, *Chem. Commun.*, 2008, **15**, 1798-1800.
36. X. Chen, L. J. Tang, Y. N. Sun, P. H. Qiu and G. Liang, *J. Inorg. Biochem.*, 2010, **104**, 379-384.

37. M. T. Makler, J. M. Ries, J. A. Williams, J. E. Bancroft, R. C. Piper, B. L. Gibbins and D. J. Hinrichs, *Am. J. Trop. Med. Hyg.*, 1993, **48**, 739-741.
38. A. Pamplona, A. Ferreira, J. Balla, V. Jeney, G. Balla, S. Epiphanio, A. Chora, C. D. Rodrigues, I. P. Gregoire, M. Cunha-Rodrigues, S. Portugal, M. P. Soares and M. M. Mota, *Nat. Med.*, 2007, **13**, 703-710.
39. P. J. Blower, *Dalton Trans.*, 2015, **44**, 4819-4844.
40. C. Ghobril, G. Lamanna, M. Kueny-Stotz, A. Garofalo, C. Billotey and D. Felder-Flesch, *New J. Chem.*, 2012, **36**, 310-323.
41. M. C. Parrott, S. R. Benhabbour, C. Saab, J. A. Lemon, S. Parker, J. F. Valliant and A. Adronov, *J. Am. Chem. Soc.*, 2009, **131**, 2906-2916.
42. D. Guo, C. T. Mant and R. S. Hodges, *J. Chromatogr. A*, 1987, **386**, 205-222.

Chapter 4 Experimental Details

4.1 General Details

All reagents were purchased from Sigma-Aldrich and were used as received unless otherwise stated. Solvents were purchased from KIMIX and were used as received. Nuclear magnetic resonance (NMR) spectra were recorded on a Bruker Topspin GmbH (^{1}H at 400.22 MHz, ^{13}C{^{1}H} at 100.65 MHz, ^{31}P{^{1}H} at 162.01 MHz) or a Varian Mercury 300 (^{1}H at 300.08 MHz) spectrometer, with a Bruker Biospin GmbH casing and sample injector at 30 °C. Tetramethylsilane was used as the internal standard for the chemical shift reports. Infrared (IR) absorption spectra were recorded using a Perkin-Elmer Spectrum One FT-IR spectrometer using attenuated total reflectance (ATR). Mass spectrometry was carried out using a JEOL GC Mate II single magnetic mass spectrometer in the positive-ion mode. High resolution mass spectrometry was carried out using a Waters Synapt G2 ESI probe. Elemental analyses were carried out using a Fission EA 110 CHNS analyser or an Elementar Vario EL Cube Analyser. Melting points were determined using a Buchi B-540 apparatus. Single-crystal X-ray diffraction data were collected on a Bruker KAPPA APEX II DUO diffractometer using graphite-monochromated Mo-Kα radiation (χ = 0.71073 Å). Data collection was carried out at 173(2) K. Temperature was controlled by an Oxford Cryostream cooling system (Oxford Cryostat). Cell refinement and data reduction were performed using the program SAINT.[1] The data were scaled and absorption correction performed using SADABS.[2] The structure was solved by direct methods using SHELXS-97[2] and refined by full-matrix least-squares methods based on F^2 using SHELXL-2014[2] and using the graphics interface program X-Seed.[3] The programs X-Seed and POV-Ray[4] were both used to prepare molecular graphic images.

4.2 Synthesis

4.2.1 Synthesis of [MnBr(CO)$_5$][5] (1)

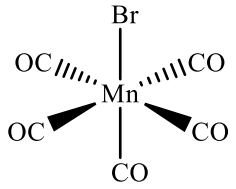

Bromine (0.262 g, 1.64 mmol) was added to a solution of dimanganese decacarbonyl (0.604 g, 1.55 mmol) in hexane under an argon atmosphere. The mixture was stirred overnight, after which the solvent was removed by rotary evaporation to afford an orange powder. The crude product was dried *in vacuo*. The powder was then sublimed at 90 °C under reduced pressure to afford the product (**1**) as an orange powder. **Yield**: 0.693 g, 81 %. **Melting point**: 152 °C (decomposition). **FTIR**: ν (cm^{-1}) = 2036 (s, CO), 1982 (s, CO). **Elemental analysis** for MnBr(CO)$_5$: Found C, 21.85 %; calcd. C, 21.85 %. **MS** (EI, *m/z*): 273.81 (100 %, [M]$^+$)

4.2.2 Synthesis of [MnBr(bpy)(CO)$_3$][6] (2)

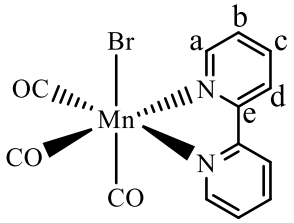

[MnBr(CO)$_5$] (0.683 g, 2.48 mmol) and 2,2'-bipyridyl (0.395 g, 2.53 mmol) were refluxed at 40 °C in Et$_2$O (50 mL) for four hours. The solution was cooled in an ice bath, and the resulting powder (**2**) was filtered using a Hirsch funnel and washed with cold Et$_2$O. **Yield**: 0.876 g, 94 %. **Melting point**: 209 °C (decomposition). **^{1}H NMR** (acetone-d_6): δ (ppm) = 9.30 (d, ^3J = 5.1 Hz, 2H, H$_a$), 8.56 (d, ^3J = 8.0 Hz, 2H, H$_d$), 8.21 (t, ^3J = 7.6 Hz, 2H, H$_c$), 7.74 (t, ^3J = 6.4 Hz, 2H, H$_b$). **^{13}C{^{1}H} NMR** (acetone-d_6): δ (ppm) = 222.01 (C$_{CO}$), 221.82 (C$_{CO}$), 220.86 (C$_{CO}$), 155.69 (C$_e$), 153.84 (C$_a$), 138.34 (C$_c$), 126.35 (C$_b$), 122.40 (C$_d$). **FTIR** ν (cm^{-1}) = 2020 (s, CO), 1939 (s, CO), 1909 (s, CO). **Elemental analysis** for MnBr(bpy)(CO)$_3$: Found C, 41.69; H, 2.10; N, 6.90 %; calcd. C, 41.63; H, 2.15; N, 7.47 %. **MS** (EI, *m/z*): 156.03 (100 %, [M-3CO-Br-Mn]$^+$), 289.87 (99.5 %, [M-3CO]$^+$), 375.85 (8.4 %, [M]$^+$).

4.2.3 Synthesis of [Re(bpy)Cl(CO)$_3$][7] (3)

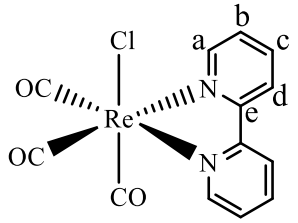

[ReCl(CO)$_5$] (0.609 g, 1.68 mmol) and 2,2'-bipyridyl (0.263 g, 1.68 mmol) were refluxed in toluene (30 mL) for two hours. The crude product precipitated as a yellow powder, which was filtered and washed with *n*-pentane to afford the desired product (**3**) as a yellow powder. **Yield**: 0.729 g, 94 %. **Melting point**: 325 – 328 °C (melt and decomposition). **^{1}H NMR** (acetone-d_6): δ (ppm) = 9.13 (ddd, ^3J = 5.5, ^4J = 1.6, ^5J = 0.8 Hz, 2H, H$_a$), 8.71 (dt, ^3J = 8.2, ^4J = 1.0 Hz, 2H, H$_d$), 8.35 (ddd, ^3J = 8.2, ^3J = 7.7, ^4J = 1.6 Hz, 2H, H$_c$), 7.81 (ddd, ^3J = 7.6, ^3J = 5.5, ^4J = 1.3 Hz, 2H, H$_b$). **^{13}C{^{1}H} NMR** (acetone-d_6): δ (ppm) = 198.11 (C$_{CO}$), 189.88 (C$_{CO}$), 189.75 (C$_{CO}$), 155.82 (C$_e$), 153.00 (C$_a$), 139.85 (C$_c$), 127.52 (C$_b$), 123.99 (C$_d$). **FTIR** ν (cm^{-1}) = 2016 (s, CO), 1867 (br, CO). **Elemental analysis** for Re(bpy)Cl(CO)$_3$: Found C, 33.77; H, 1.46; N, 5.68 %; calcd. C, 33.81; H, 1.75; N, 6.07 %. **MS** (EI, *m/z*): 377.97 (100 %, [M - 3CO]$^+$), 461.94 (44.2 %, [M]$^+$).

4.2.4 Synthesis of N-propyl-1-(pyridine-4-yl)methanimine[8] (4)

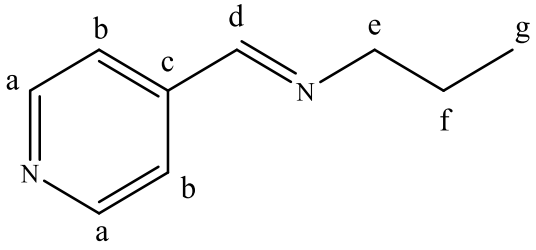

4-Pyridinecarboxaldehyde (1.05 g, 9.77 mmol) and *n*-propylamine (0.610 g, 10.3 mmol) were stirred at room temperature in DCM (50 mL) over anhydrous magnesium sulfate for 21 hours. The $MgSO_4$ was removed by gravity filtration and the solvent was removed from the filtrate, resulting in the pure product (**4**) as a red oil. **Yield**: 1.27 g, 87 %. **^{1}H NMR** (acetone-d_6): δ (ppm) = 8.66 (dd, ^3J = 4.4, ^4J = 1.6 Hz, 2H, H$_a$), 8.36 (s, 1H, H$_d$), 7.67 (dd, ^3J = 4.4, ^4J = 1.6 Hz, 2H, H$_b$), 3.61 (td, ^3J = 6.8, ^4J = 1.4 Hz, 2H, H$_e$), 1.70 (sext, ^3J = 7.2 Hz, 2H, H$_f$), 0.94 (t, J = 7.4 Hz, 3H, H$_g$). **^{13}C{^{1}H} NMR** ($CDCl_3$): δ (ppm) = 158.85 (H$_d$), 150.41 (H$_a$), 143.19 (H$_c$), 121.94 (H$_b$), 63.63 (H$_e$),

23.89 (H_f), 11.85 (H_g). **FTIR**: *v* (cm^{-1}) = 1647 (s, $C=N_{imine}$), 1598 (s, $C=N_{aromatic}$). **MS** (EI, *m/z*): 148.08 (100 %, $[M]^+$).

4.2.5 Synthesis of tris(2-((pyridine-4-ylmethylene)amino)ethyl)amine[9] (5)

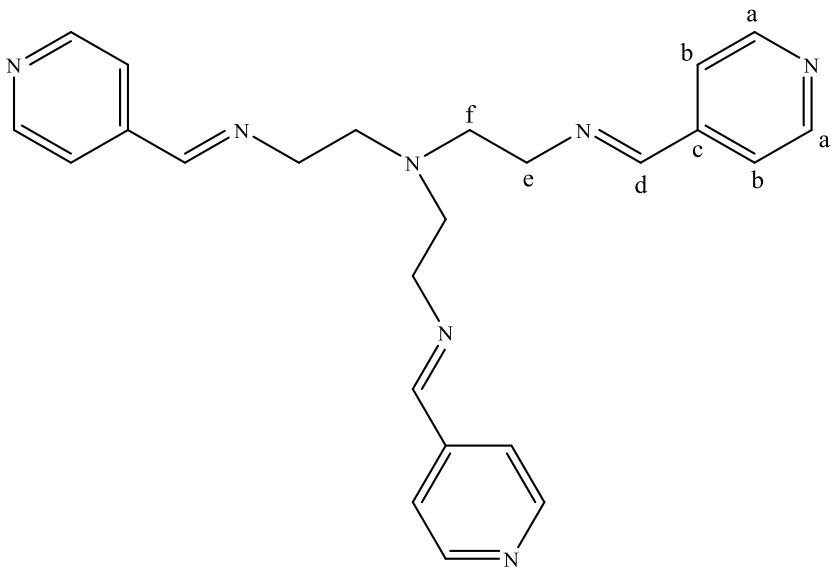

Tris-(2-aminoethyl)amine (0.111 g, 0.760 mmol) and 4-pyridinecarboxaldehyde (0.277 g, 2.58 mmol) were dissolved in DCM (20 mL). Anhydrous magnesium sulfate was added and the mixture was stirred at room temperature for 49 hours. The magnesium sulfate was removed by gravity filtration and the solvent removed from the filtrate. The resultant residue was purified by low pressure azeotropic distillation at 40 °C, with the addition of toluene in 5 mL aliquots to afford the product (**5**) as a brown residue. **Yield**: 0.294 g, 94 %. **^{1}H NMR** ($CDCl_3$): δ (ppm) = 8.63 (d, ^3J = 5.9 Hz, 2H, H_a), 8.08 (s, 1H, H_d), 7.38 (d, ^3J = 5.9 Hz, 2H, H_b), 3.71 (t, ^3J = 5.9 Hz, 2H, H_e), 2.95 (t, ^3J = 6.2 Hz, 2H, H_f). **^{13}C{^{1}H} NMR** ($CDCl_3$): δ (ppm) = 158.85 (H_d), 150.41 (H_a), 143.19 (H_c), 121.94 (H_b), 63.63 (H_e), 23.89 (H_f), 11.85 (H_g). **FTIR**: *v* (cm^{-1}) = 1643 (s, $C=N_{imine}$), 1594 (s, $C=N_{aromatic}$). **MS** (EI, *m/z*): 413.24 (35.4 %, $[M]^+$).

4.2.6 Synthesis of N^1,N^1,N^4,N^4-tetrakis(3-((pyridine-4-ylmethylene)amino)propyl)butane-1,4-diamine[10] (6)

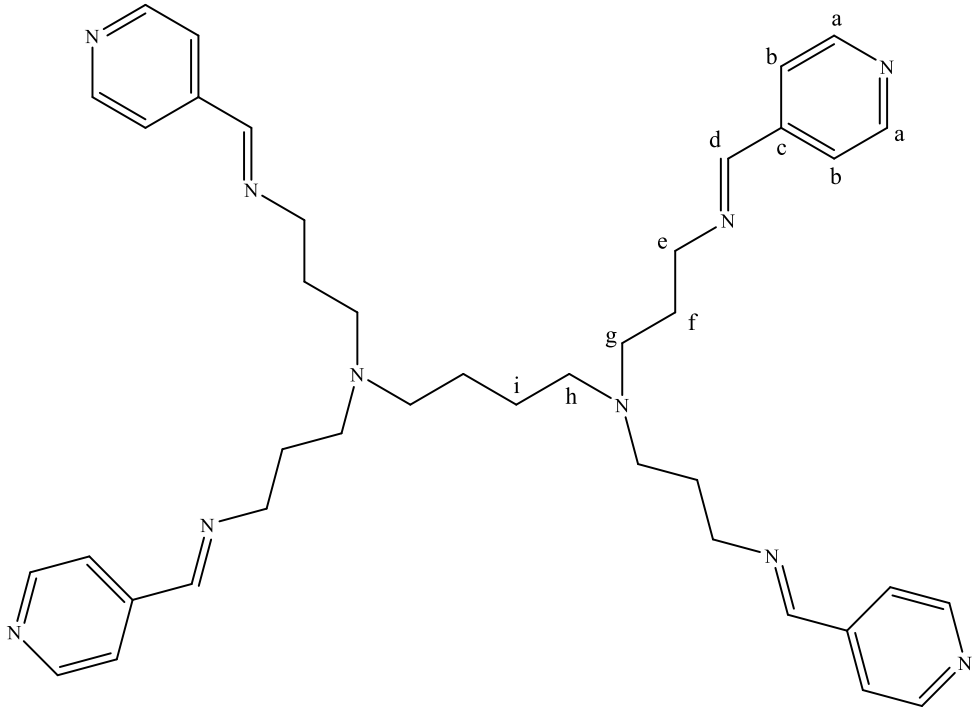

DAB-G1 dendrimer (0.0853 g, 0.269 mmol) and 4-pyridinecarboxaldehyde (0.119 g, 1.11 mmol) were dissolved in toluene (30 mL) and stirred over anhydrous magnesium sulfate for 24 hours at room temperature. The magnesium sulfate was removed by gravity filtration and the solvent removed from the filtrate. The resultant residue was taken up in DCM (20 mL) and washed with distilled water (10 × 20 mL). The organic layer was dried with anhydrous magnesium sulfate, which was subsequently removed by gravity filtration. The solvent was removed from the filtrate to afford the product (**6**) as a light brown oil. **Yield**: 0.108 g, 59 %. **^{1}H NMR** ($CDCl_3$): δ (ppm) = 8.60 (dd, ^3J = 4.4, ^4J = 1.6 Hz, 8H, H_a), 8.16 (s, 4H, H_d), 7.47 (dd, ^3J = 4.5, ^4J = 1.6 Hz, 8H, H_b), 3.59 (t, ^3J = 6.9 Hz, 8H, H_e), 2.44 (m, 8H, H_g), 2.34 (s, 4H, H_h), 1.76 (m, 8H, H_f), 1.35 (m, 4H, H_i). **^{13}C{^{1}H} NMR** ($CDCl_3$): δ (ppm) = 158.94 (C_d), 150.31 (C_a), 142.97 C_c), 121.76 (C_b), 59.68 (C_e), 54.05 (C_h), 51.60 (C_g), 28.25 (C_f), 25.24 (C_i). **FTIR**: ν (cm^{-1}) = 1645 (s, $C{=}N_{imine}$), 1596 (s, $C{=}N_{aromatic}$). **MS** (EI, *m/z*): 672.38 (100 %, $[M]^+$).

4.2.7 Synthesis of N-propyl-1-(pyridine-2-yl)methanimine [8] (7)

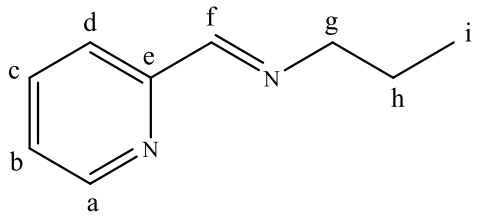

2-Pyridinecarboxaldehyde (1.04 g, 9.76 mmol) and *n*-propylamine (0.606 g, 10.3 mmol) were stirred at room temperature in DCM (50 mL) over anhydrous magnesium sulfate for 21 hours. The $MgSO_4$ was removed by gravity filtration and the solvent was removed from the filtrate, resulting in the pure product (**7**) as a dark brown oil. **Yield**: 1.02 g, 70 %. **^{1}H NMR** (acetone-d_6): δ (ppm) = 8.63 (ddd, ^3J = 4.8, ^4J = 1.7, ^5J = 1.0 Hz, 1H, H_a), 8.35 (d, ^4J = 0.5 Hz, 1H, H_f), 8.04 (dt, ^3J = 7.9, ^4J = 1.1 Hz, 1H, H_d), 7.84 (dddd, ^3J = 8.0, ^3J = 7.5, ^4J = 1.8, ^5J = 0.7 Hz, 1H, H_c), 7.41 (ddd, ^3J = 7.5, ^3J = 4.8, ^4J = 1.3 Hz, 1H, H_b), 3.63 (td, ^3J = 6.8, ^4J = 1.4 Hz, 2H, H_g), 1.81 – 1.63 (m, 2H, H_h), 0.97 (t, ^3J = 7.4 Hz, 3H, H_i). **^{13}C{^{1}H} NMR** (acetone-d_6): δ (ppm) = 161.65 (C_f), 155.09 (C_e), 149.30 (C_a), 136.32 (C_c), 124.60 (C_b), 120.28 (C_d), 62.66 (C_g), 23.76 (C_h), 11.16 (C_i). **FTIR** *v* (cm^{-1}) = 1649 (s, $C{=}N_{imine}$), 1588 (s, $C{=}N_{aromatic}$). **MS** (EI, *m/z*): 148.07 (16.0 %, $[M]^+$).

4.2.8 Synthesis of tris(2-((pyridine-2-ylmethylene)amino)ethyl)amine[9] (8)

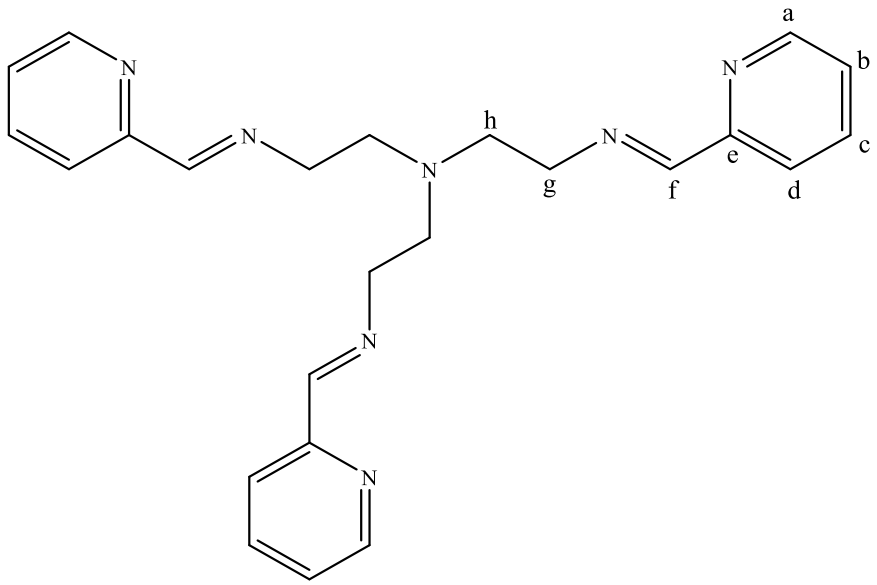

2-Pyridinecarboxaldehyde (0.955 g, 8.92 mmol) and tris(2-aminoethyl)amine (0.435 g, 2.97 mmol) were dissolved in DCM (50 mL) and stirred over anhydrous magnesium sulfate for 24 hours. The $MgSO_4$ was removed by gravity filtration and the solvent removed from the filtrate to afford the crude product as a dark red residue. The residue was distilled under reduced pressure at 60 °C, with the occasional addition of acetone (*ca.* 3 – 5 mL) to aid in removal of the excess aldehyde, to afford the product (**8**) as a dark brown oil. **Yield**: 1.09 g, 89 %. **^{1}H NMR** (acetone-d_6): δ (ppm) = 8.61 (ddd, ^3J = 4.8, ^4J = 1.7, ^5J = 1.0 Hz, 3H, H_a), 8.35 (d, ^4J = 0.5 Hz, 3H, H_f), 8.01 (dt, ^3J = 7.9, ^4J = 1.0 Hz, 3H, H_d), 7.85 – 7.73 (m, 3H, H_c), 7.38 (ddd, ^3J = 7.5, ^3J = 4.8, ^4J = 1.2 Hz, 3H, H_b), 3.80 (td, ^3J = 6.5, ^4J = 1.3 Hz, 6H, H_g), 3.02 (t, ^3J = 6.5 Hz, 6H, H_h). **^{13}C{^{1}H} NMR** (acetone-d_6): δ (ppm) = 162.55 (H_f), 155.04 (H_e), 149.26 (H_a), 136.33 (H_c), 124.57 (H_b), 120.41 (H_d), 59.84 (H_g), 55.39 (H_h). **FTIR** ν (cm^{-1}) = 1647 (s, C=N_{imine}), 1588 (s, C=$N_{aromatic}$).

4.2.9 Synthesis of N^1,N^1,N^4,N^4-tetrakis(3-((pyridine-2-ylmethylene)amino)propyl)butane-1,4-diamine[11] (9)

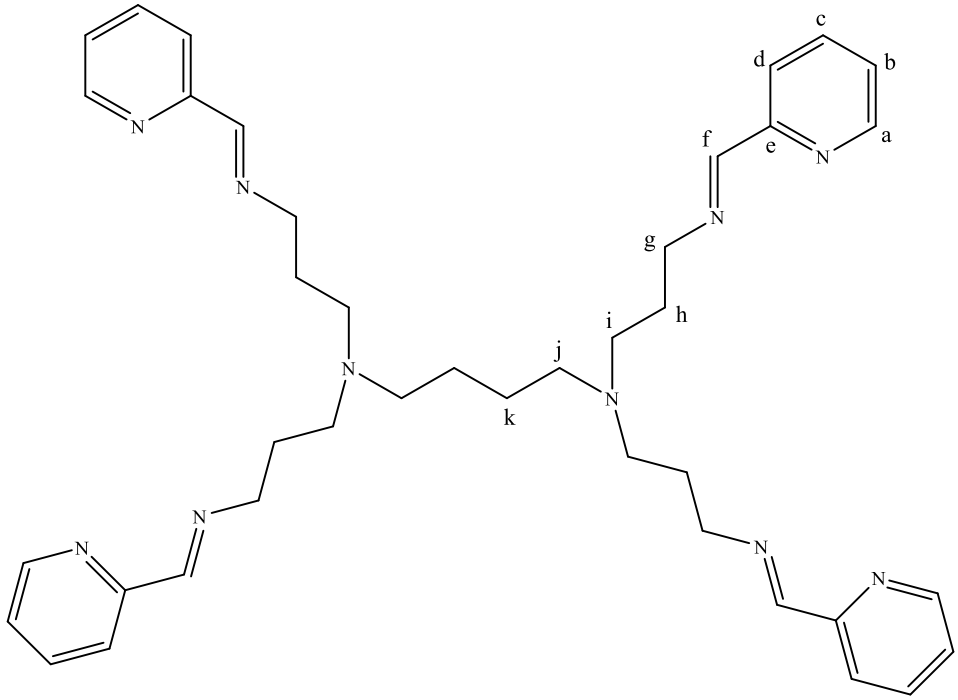

2-Pyridinecarboxaldehyde (0.693 g, 6.45 mmol) and DAB-G1 dendrimer (0.508 g, 1.60 mmol) were dissolved in dry DCM (30 mL) and stirred at room temperature over anhydrous magnesium sulfate for 24 hours. The $MgSO_4$ was removed by gravity filtration and the solvent removed from the filtrate to afford the crude product as an orange residue. The residue was taken up in DCM (20 mL) and washed with distilled water (8 × 20 mL). The organic layer was dried with anhydrous magnesium sulfate, which was subsequently removed by gravity filtration. The solvent was removed to afford the desired product (**9**) as an orange oil. **Yield**: 0.935 g, 87 %. **^{1}H NMR** ($CDCl_3$): δ (ppm) = 8.61 (ddd, ^3J = 4.9, ^4J = 1.7, ^5J = 1.0 Hz, 4H, H_a), 8.37 (d, ^4J = 0.4 Hz, 4H, H_f), 7.95 (dt, ^3J = 7.9, ^4J = 1.1 Hz, 4H, H_d), 7.74 – 7.65 (m, 4H, H_c), 7.27 (ddd, ^3J = 7.5, ^3J = 4.8, ^4J = 1.2 Hz, 4H, H_b), 3.68 (td, ^3J = 6.9, ^4J = 1.2 Hz, 8H, H_g), 2.58 – 2.49 (m, 8H, H_i), 2.47 – 2.37 (bm, J = 16.6 Hz, 4H, H_j), 1.85 (quint, ^3J = 7.1 Hz 8H, H_h), 1.47 – 1.37 (bm, 4H, H_k). **^{13}C{^{1}H} NMR** ($CDCl_3$): δ (ppm) = 162.02 (C_f), 154.71 (C_e), 149.52 (C_a), 136.60 (C_c), 124.67 (C_b), 121.33 (C_d), 59.69 (C_g), 54.11 (C_j), 51.90 (C_i), 28.46 (C_h), 25.35 (C_k). **FTIR** ν (cm^{-1}) = 1647 (s, $C{=}N_{imine}$), 1586 (s, $C{=}N_{aromatic}$).

4.2.10 Synthesis of N-(pyridin-4-ylmethyl)propan-1-amine (10)

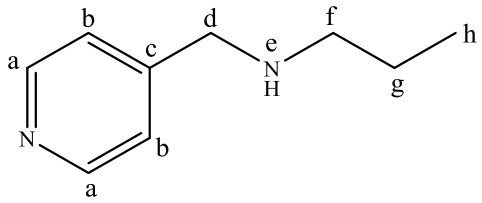

Ligand precursor **4** (1.02 g, 6.88 mmol) was stirred under argon in methanol (40 mL) in an ice bath in the presence of 3 Å molecular sieves. $NaBH_4$ (1.05 g, 27.8 mmol) was added under argon and the ice removed. The mixture was stirred at room temperature for 22 hours. The reaction was quenched with cold distilled water (40 mL), and the solvent volume reduced to 30 mL. The product was extracted with DCM (40 mL), and the organic layer was washed with distilled water (2 × 20 mL). The organic layer was then dried with $MgSO_4$, which was removed by gravity filtration before removal of the solvent to afford the product (**10**) as a yellow oil. **Yield**: 0.781 g, 76 %. **^{1}H NMR** (acetone-d_6): δ (ppm) = 8.49 (d, ^3J = 5.5 Hz, 2H, H_a), 7.35 (d, ^3J = 5.9 Hz, 2H, H_b), 3.80 (s, 2H, H_d), 2.56 (t, ^3J = 7.0 Hz, 2H, H_f), 1.52 (sext, ^3J = 7.3 Hz, 2H, H_g), 0.93 (t, ^3J = 7.4 Hz, 3H, H_h). **^{13}C{^{1}H} NMR** (acetone-d_6): δ (ppm) = 150.34 (C_c), 149.51 (C_a), 122.83 (C_b), 52.13 (C_d), 51.03 (C_f), 22.94 (C_g), 11.15 (C_h). **FTIR** ν (cm^{-1}) = 3274 (br, NH), 1600 (s, $C{=}N_{aromatic}$). **MS** (EI, *m/z*): 121.03 (100 %, $[M\text{-}C_2H_5]^+$), 149.07 (45.3 %, $[M\text{-}H]^+$).

4.2.11 Synthesis of tris(2-((pyridine-4-ylmethylene)imino)ethyl)amine (11)

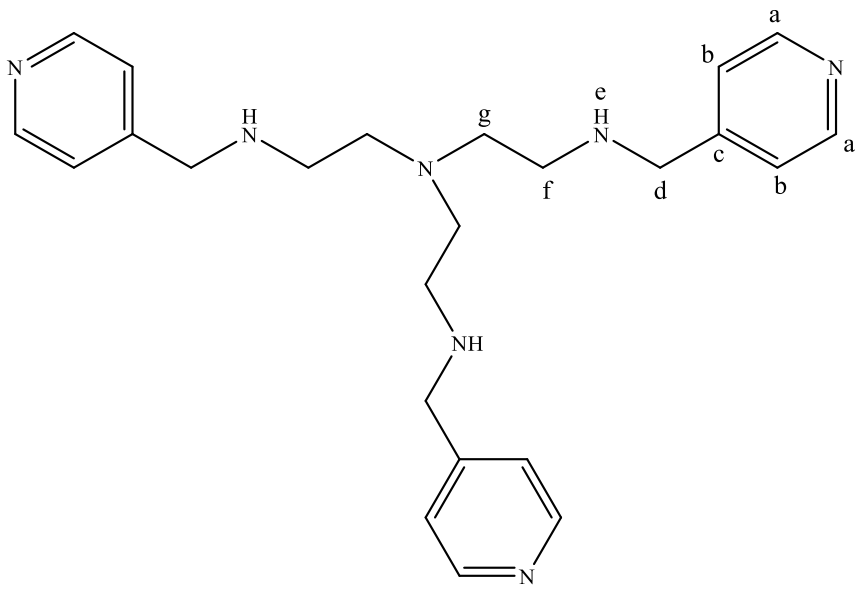

Ligand precursor **5** (1.06 g, 2.57 mmol) was stirred in methanol (30 mL) in an ice bath, under argon for ten minutes. $NaBH_4$ (1.17 g, 30.8 mmol) was added and the ice bath removed. The mixture was stirred at room temperature for 24 hours. The reaction was quenched with cold distilled water (40 mL), and the solvent volume reduced to 30 mL. The product was extracted with DCM (40 mL), and the organic layer was washed with distilled water (2 × 20 mL). The organic layer was then dried with $MgSO_4$, which was removed by gravity filtration before removal of the solvent to afford the product (**11**) as a brown oil. **Yield**: 0.932 g, 86 %. **^{1}H NMR** (acetone-d_6): δ (ppm) = 8.45 (dd, ^{3}J = 4.4, ^4J = 1.6 Hz, 6H, H_a), 7.30 (dd, ^3J = 5.3, ^5J = 0.7 Hz, 6H, H_b), 3.79 (s, 6H, H_d), 2.72 – 2.67 (m, 6H, H_f), 2.67 – 2.62 (m, 6H, H_g). **^{13}C{^{1}H} NMR** (acetone-d_6): δ (ppm) =149.57 (C_a), 123.58 (C_c) 122.93 (C_b), 54.00 (C_g), 51.93 (C_d), 46.96 (C_f). **FTIR** ν (cm^{-1}) = 3270 (br, NH), 1600 (s, C=$N_{aromatic}$). **MS** (EI, *m/z*): 298.16 (100 %, [M-$C_7H_9N_2$]$^+$), 419.26 (18.8 %, [M]$^+$).

4.2.12 Synthesis of N^1,N^1,N^4,N^4-tetrakis(3-((pyridine-4-ylmethylene)amino)propyl)butane-1,4-diamine (12)

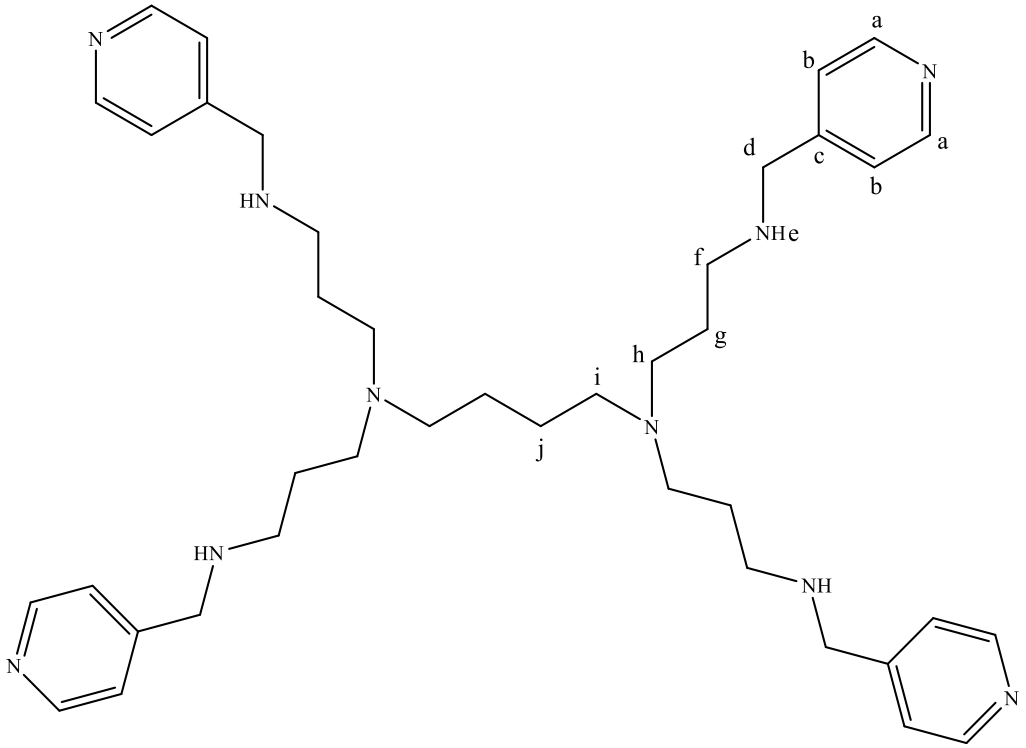

Ligand precursor **6** (0.063 g, 0.093 mmol) was stirred in methanol (30 mL) in an ice bath, under argon for ten minutes. $NaBH_4$ (0.057 g, 1.51 mmol) was added and the ice bath removed. The mixture was stirred at room temperature for 22 hours. The reaction was quenched with cold distilled water (40 mL), and the solvent volume reduced to 30 mL. The product was extracted with DCM (40 mL), and the organic layer was washed with distilled water (2 × 20 mL). The organic layer was then dried with $MgSO_4$, which was removed by gravity filtration before removal of the solvent to afford the product (**12**) as a brown oil. **Yield**: 0.0464 g, 72 %. **^{1}H NMR** (acetone-d_6): δ (ppm) = 8.48 (dd, ^3J = 4.4, ^4J = 1.5 Hz, 8H, H_a), 7.33 (d, ^3J = 5.9 Hz, 8H, H_b), 3.77 (s, 8H, H_d), 2.63 (t, ^3J = 6.7 Hz, 8H, H_f), 2.47 (t, ^3J = 6.9 Hz, 8H, H_h), 2.38 (t, ^3J = 5.7 Hz, 4H, H_i), 1.63 (p, ^3J = 6.8 Hz, 8H, H_g), 1.50 – 1.39 (m, 4H, H_j). **^{13}C{^{1}H} NMR** (acetone-d_6): δ (ppm) = 150.35 (C_c), 149.51 (C_a), 122.90 (C_b), 54.05 (C_i), 52.37 ($C_{d/h}$), 47.81 (C_f), 27.57 (C_g), 25.14 (C_j). **FTIR** ν (cm^{-1}) = 3270 (br, NH), 1602 (s, C=$N_{aromatic}$). **Elemental analysis** for $C_{40}H_{60}N_{10}\cdot 5H_2O$: Found C, 61.87 %, H, 8.90 %, N, 18.23 %; calcd. C, 62.31 %, H, 9.15 %, N, 18.17 %. **MS** (EI, *m/z*): 121.07 (100 %, $[M\text{-}C_{33}H_{51}N_8]^+$), 149.05 (78.0 %, $[M\text{-}C_{31}H_{47}N_8]^+$).

4.2.13 Synthesis of N-(pyridin-2-ylmethyl)propan-1-amine (13)

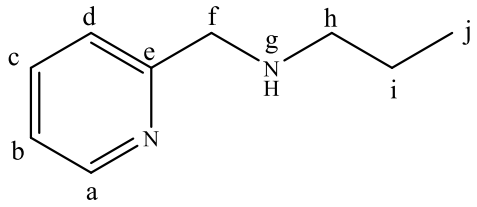

Ligand precursor **7** (0.220 g, 1.49 mmol) was stirred under argon in methanol (10 mL) in an ice bath in the presence of 3 Å molecular sieves. $NaBH_4$ (0.229 g, 6.05 mmol) was added under argon and the ice removed. The mixture was stirred at room temperature for 5 hours before gravity filtration and removal of the solvent. The resulting residue was taken up in DCM (20 mL) and washed with a saturated aqueous Na_2CO_3 solution (4 × 20 mL). The organic layer was dried with anhydrous sodium carbonate, which was subsequently removed by gravity filtration. The solvent was removed to afford the desired product (**13**) as a light brown oil. **Yield**: 0.0991 g, 44 %. **^{1}H NMR** (acetone-d_6): δ (ppm) =8.50 (ddd, ^3J = 4.8, ^4J = 1.7, ^5J = 0.9 Hz, 1H, H_a), 7.71 (qd, ^3J = 7.6, ^4J = 1.8 Hz, 1H, H_d), 7.43 (dddd, ^3J = 7.8, ^4J = 1.6, ^4J = 1.2, ^5J = 0.6 Hz, 1H, H_c), 7.22 – 7.14 (m, 1H, H_b), 3.84 (s, 2H, H_f), 2.60 – 2.55 (m, 2H, H_h), 1.59 – 1.42 (m, 2H, H_i), 0.93 (t, ^3J = 7.4 Hz, 3H, H_j). **^{13}C{^{1}H} NMR** (acetone-d_6): δ (ppm) = 161.05 (C_e), 148.90 (C_a), 136.01 (C_c), 121.65 (C_d), 121.50 (C_b), 54.99 (C_f), 51.21 (C_h), 23.06 (C_i), 11.19 (C_j). **FTIR** ν (cm^{-1}) = 3290 (br, NH), 1592 (s, $C{=}N_{aromatic}$). **MS** (EI, *m/z*): 121.07 (100 %, $[M\text{-}C_2H_5]^+$), 150.09 (28 %, $[M]^+$).

4.2.14 Synthesis of tris(2-((pyridine-2-ylmethylene)imino)ethyl)amine (14)

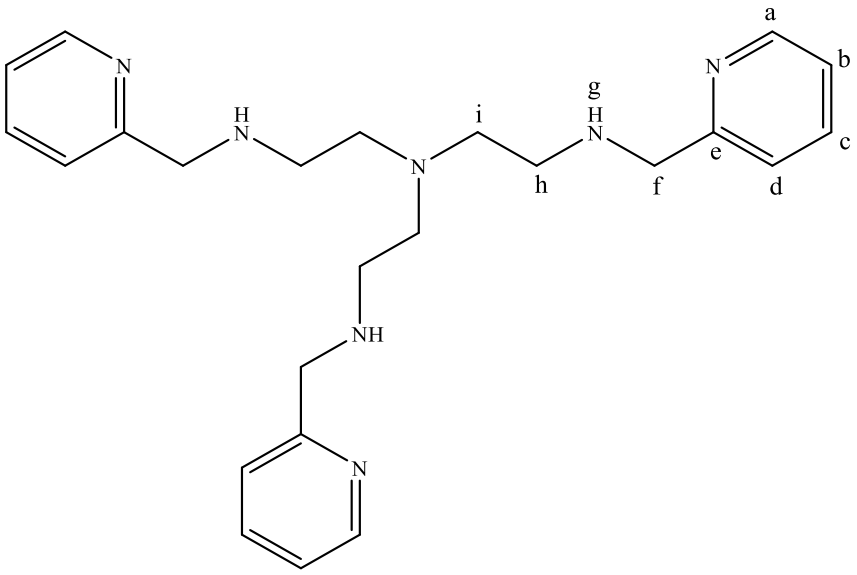

Ligand precursor **8** (1.09 g, 2.64 mmol) was stirred in methanol (30 mL) in an ice bath, under argon for ten minutes. $NaBH_4$ (1.35 g, 35.7 mmol) was added and the ice bath removed. The mixture was stirred at room temperature for 24 hours. The reaction was quenched with cold distilled water (40 mL), and the solvent volume reduced to 30 mL. The product was extracted with DCM (40 mL), and the organic layer was washed with distilled water (2 × 20 mL). The organic layer was then dried with $MgSO_4$, which was removed by gravity filtration before removal of the solvent to afford the product (**14**) as a brown oil. **Yield**: 0.775 g, 70 % **^{1}H NMR** (acetone-d_6): δ (ppm) = 8.44 (d, ^3J = 4.7 Hz, 3H, H_a), 7.65 (td, ^3J = 7.6, ^4J = 1.8 Hz, 3H, H_d), 7.42 (d, ^3J = 7.8 Hz, 3H, H_c), 7.20 – 7.12 (m, 3H, H_b), 3.86 (s, 6H, H_f), 2.83 – 2.52 (m, 12H, $H_{h/i}$). **^{13}C{^{1}H} NMR** (acetone-d_6): δ (ppm) = 160.63 (C_e), 148.89 (C_a), 136.06 (C_c), 121.76 (C_d), 121.52 (C_b), 54.78 (C_f), 54.42 (C_h), 47.27 (C_i). **FTIR** ν (cm^{-1}) = 3292 (br, NH), 1591 (s, C=$N_{aromatic}$). **MS** (EI, *m/z*): 419.90 (100 %, $[M]^+$).

4.2.15 Synthesis of N^1,N^1,N^4,N^4-tetrakis(3-((pyridine-2-ylmethylene)amino)propyl)butane-1,4-diamine (15)

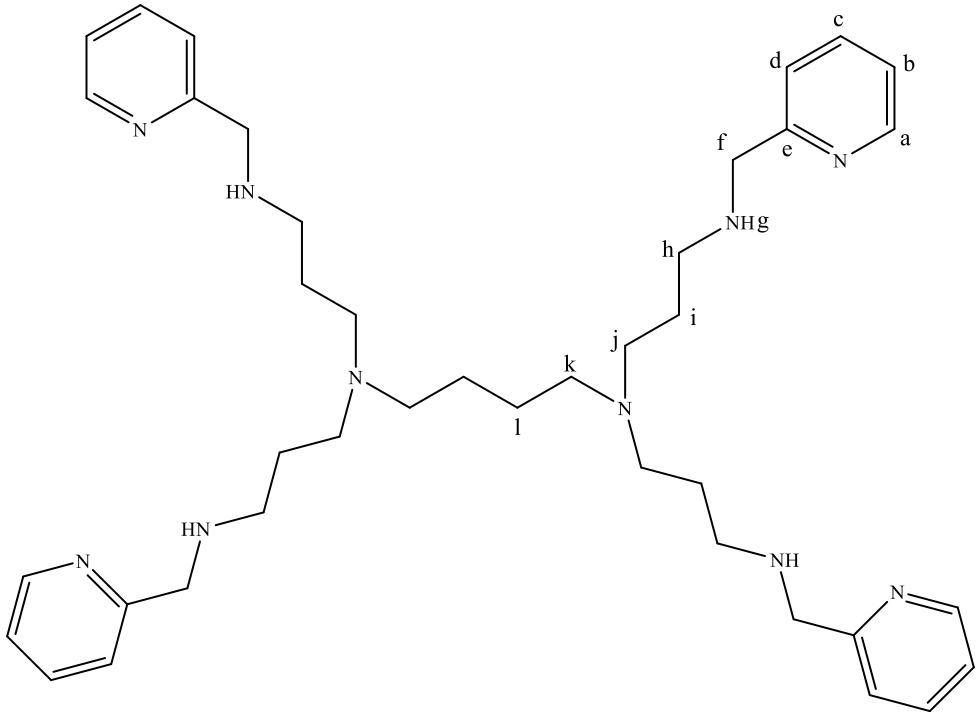

Ligand precursor **9** (0.935 g, 1.39 mmol) was stirred in methanol (30 mL) in an ice bath, under argon for ten minutes. $NaBH_4$ (0.856 g, 22.6 mmol) was added and the ice bath removed. The mixture was stirred at room temperature for 22 hours. The reaction was quenched with cold distilled water (40 mL), and the solvent volume reduced to 30 mL. The product was extracted with DCM (40 mL), and the organic layer was washed with distilled water (2 × 20 mL). The organic layer was then dried with $MgSO_4$, which was removed by gravity filtration before removal of the solvent to yield compound **15** as a dark brown, viscous oil. **Yield**: 0.662 g, 70 %. **^{1}H NMR** (acetone-d_6): δ (ppm) = 8.50 (dd, ^3J = 4.0, ^4J = 0.7 Hz, 4H, H_a), 7.70 (td, ^3J = 7.7, ^4J = 1.8 Hz, 4H, H_d), 7.42 (d, ^3J = 7.8 Hz, 4H, H_c), 7.18 (dd, ^3J = 6.9, ^4J = 5.4 Hz, 4H, H_b), 3.84 (s, 8H, H_d), 2.66 (t, ^3J = 6.7 Hz, 8H, H_h), 2.48 (t, ^3J = 6.9 Hz, 8H, H_j), 2.42 – 2.33 (m, 4H, H_k), 1.72 – 1.58 (m, 8H, H_i), 1.45 (s, 4H, H_l). **^{13}C{^{1}H} NMR** (acetone-d_6): δ (ppm) = 161.00 (C_e), 148.89 (C_a), 136.05 (C_c), 121.74 (C_d), 121.51 (C_b), 55.13 (C_f), 54.10 (C_k), 52.36 (C_h), 47.79 (C_j), 27.75 (C_i), 25.13 (C_l). **FTIR** ν (cm^{-1}) = 3288 (br, NH), 1591 (s, C=$N_{aromatic}$). **MS** (EI, *m/z*): 679.45. (100 %, $[M\text{-}H]^+$).

4.2.16 Synthesis of [Re(bpy)(CO)$_3$(10)]PF$_6$ (16)

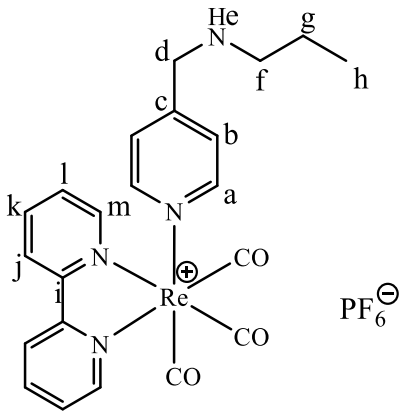

[Re(bpy)Cl(CO)$_3$] (0.105 g, 0.228 mmol) and silver triflate (0.075 g, 0.291 mmol) were stirred in DCM (30 mL) for 3 hours. The resulting precipitate (AgCl) was removed by gravity filtration. Ligand **10** was dissolved in DCM (5 mL) and added to the solution. The mixture was stirred at room temperature for 20 hours. Excess NH_4PF_6 was added to the solution, after which the solution was stirred for a further hour. Gravity filtration was employed to remove insoluble particles, and the solution was washed with distilled water (2×20 mL). The organic layer was dried with $MgSO_4$, which was subsequently removed by gravity filtration, and the solvent removed. The remaining residue was dissolved in acetone (5 mL) and distilled water (10 mL) added to the solution. The solvent was reduced until it became cloudy, and placed in the fridge for 3 hours. The resulting precipitate was removed by gravity filtration and the product extracted from the aqueous solution with DCM (2×20 mL). The organic layer was dried with $MgSO_4$, which was subsequently removed by gravity filtration. The solvent was removed, and the product dried *in vacuo* as an oily residue. **Yield**: 0.031 g, 19 %. **Melting point**: 104 – 107 °C. **^{1}H NMR** (acetone-d_6): δ (ppm) = 9.49 (ddd, ^3J = 5.5, ^4J = 1.4, ^5J = 0.7 Hz, 2H, H_m), 8.77 (d, ^3J = 8.2 Hz, 2H, H_j), 8.52 – 8.45 (m, 2H, H_k), 8.44 (dd, ^3J = 5.2, ^4J = 1.4 Hz, 2H, H_a), 8.08 – 7.97 (m, 2H, H_l), 7.46 (d, ^3J = 6.6 Hz, 2H, H_b), 3.80 (s, 2H, H_d), 2.47 (t, ^3J = 7.0 Hz, 2H, H_f), 1.51 – 1.36 (m, 2H, H_g), 0.86 (t, ^3J = 7.4 Hz, 3H, H_h). **^{13}C{^{1}H} NMR** (acetone-d_6): δ (ppm) = 195.68 (C_{CO}), 191.71 (C_{CO}), 156.21 (C_i), 155.89 (C_c), 154.04 (C_m), 151.53 (C_a), 141.48 (C_k), 129.14 (C_l), 125.61 (C_b), 124.94 (C_j), 51.43 (C_d), 51.13 (C_f), 22.80 (C_g), 11.02 (C_h). **^{31}P{^{1}H} NMR** (acetone-d_6): δ (ppm) = -144.30 (hept, J = 708.2 Hz) **FTIR** ν (cm^{-1}) = 2025 (s, CO), 1899 (br, CO), 1619 (s, C=$N_{pyridyl}$) , 1604 (s, C=N_{bpy}). **Elemental analysis** for $C_{22}H_{22}N_4O_3Re{\cdot}PF_6$: Found C, 36.98, H, 3.02, N, 7.47 %; calcd. C, 36.62, H, 3.07, N,

7.76 %. **MS** (HR-ESI, *m/z*): 577.12 (100 %, $[M\text{-}PF_6]^+$, calcd. 577.12), 427.01 (33 %, $[M\text{-}L1\text{-}PF_6]^+$, calcd. 427.01).

4.2.17 Synthesis of $[Re(bpy)(CO)_3(10)]PF_6$ (16b)

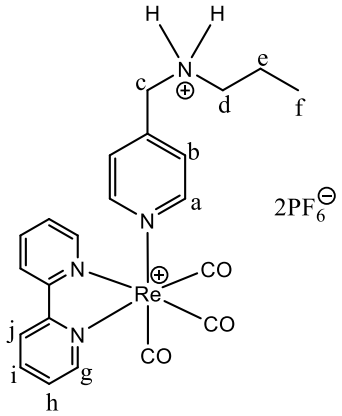

$[Re(bpy)Cl(CO)_3]$ (0.0868 g, 0.188 mmol) and silver triflate (0.0613 g, 0.238 mmol) were stirred in methanol (15 mL) for two hours. The resulting precipitate (AgCl) was removed by gravity filtration. Ligand **10** (0.0338 g, 0.225 mmol) in methanol (20 mL) was added and the solution was refluxed under argon for 21 hours. An excess of aqueous NH_4PF_6 solution was added and the solution was stirred for a further five minutes. A black precipitate formed, which was removed by gravity filtration. Deionised water (10 mL) was added, and the solvent volume was reduced until a yellow precipitate formed. The solution was cooled on ice, and the precipitate was filtered on a Hirsch funnel. **Yield**: 0.0283 g, 18 %. **^{1}H NMR** (acetone-d_6): δ = 9.55 – 9.44 (m, 2H, H_i), 8.80 – 8.65 (m, 4H, $H_{a/l}$), 8.48 (td, J = 8.0, 1.5 Hz, 2H, H_k), 8.10 – 7.92 (m, 2H, H_j), 7.70 (dd, J = 5.3, 1.4 Hz, 2H, H_b), 4.62 (s, 2H, H_d), 3.47 – 3.25 (m, 2H, H_f), 1.85 (dq, J = 15.0, 7.5 Hz, 2H, H_g), 0.99 (t, J = 7.5 Hz, 3H, H_h). **^{13}C{^{1}H} NMR** (acetone-d_6): δ = 196.49 (C_{CO}), 195.34 (C_{CO}), 191.50 (C_{CO}), 155.87 (C_l), 154.15 (C_h), 154.00 (C_c), 152.71 (C_a), 141.53 (C_j), 129.22 (C_i), 127.58 (C_b), 124.89 (C_k), 50.66 (C_e), 49.78 (C_d), 19.46 (C_f), 10.08 (C_g). **^{31}P{^{1}H} NMR** (acetone-d_6): δ = -144.30 (hept, *J* = 708.2 Hz). **FTIR** *ν* (cm^{-1}) = 2028 (s, CO), 1915 (br, CO), 1625 (s, $C{=}N_{pyridyl}$). **Elemental analysis** for $C_{22}H_{25}N_4O_4Re{\cdot}2(PF_6)H_2O$: Found C, 30.06, H, 2.60, N, 5.82 %; calcd. C, 29.87, H, 2.73, N, 6.33 %. **MS** (ES, *m/z*): 577.12 (100 %, $[M]^+$).

4.2.18 Synthesis of [(Re(bpy)(CO)$_3$)$_3$(11)](PF$_6$)$_3$ (17)

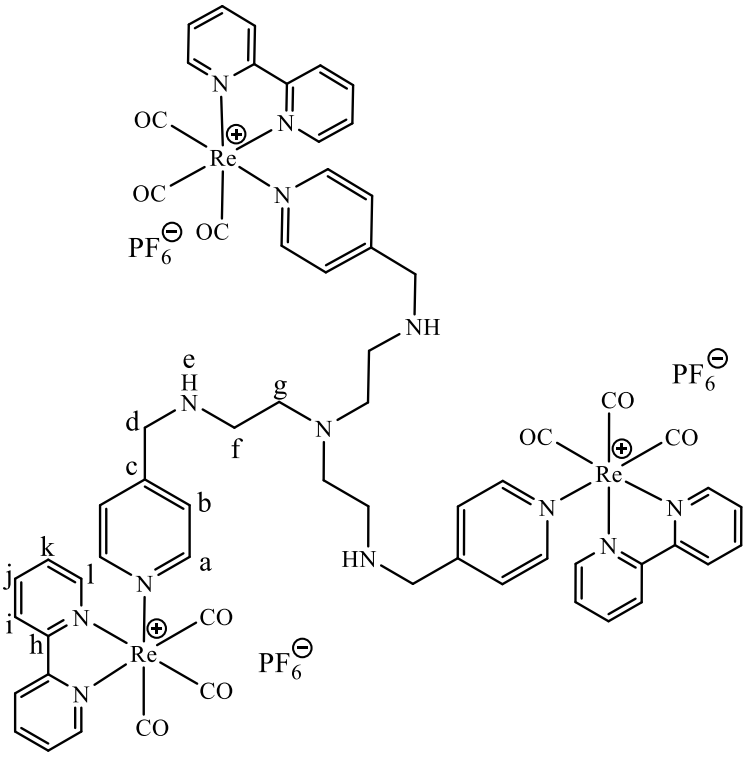

[Re(bpy)Cl(CO)$_3$] (0.131 g, 0.284 mmol) and silver triflate (0.080 g, 0.311 mmol) were stirred at room temperature in DCM for 3 hours. The resulting precipitate (AgCl) was filtered and ligand **11** (0.036 g, 0.0863 mmol) was added to the flask. The reaction mixture was stirred at room temperature for 19 hours, after which the solvent was removed and the resulting residue taken up in minimum ethanol (4 mL) and ammonium hexafluorophosphate (excess in H_2O) was added to precipitate the crude product as a yellow powder. The powder was redissolved in minimum acetone and added dropwise to isopropanol (80 mL, 75 °C). The mixture was filtered through Celite while hot, and the product removed from the Celite by washing with DCM, before removal of the solvent to afford the product as a brown powder. **Yield**: 0.073 g, 12 %. **Melting point**: 145 – 150 °C. **^{1}H NMR** (acetone-*d*$_6$): δ (ppm) = 9.44 (d, ^3J = 5.6 Hz, 6H, H$_l$), 8.78 – 8.62 (m, 6H, H$_i$), 8.51 – 8.33 (m, 12H, H$_{j/a}$), 8.07 – 7.91 (m, 6H, H$_k$), 7.41 (d, ^3J = 6.5 Hz, 6H, H$_b$), 3.79 – 3.70 (m, 6H, H$_d$), 3.33 – 3.23 (m, 6H, H$_f$), 2.94 – 2.79 (m, 6H, H$_g$). **^{13}C{^{1}H} NMR** (acetone-*d*$_6$): δ (ppm) = 195.52 (C$_{CO}$), 191.52 (C$_{CO}$), 155.82 (C$_h$), 155.36 (C$_c$), 154.01 (C$_l$), 151.73 (C$_a$), 141.43 (C$_j$), 129.12 (C$_k$), 125.90 (C$_b$), 124.84 (C$_i$), 53.06 (C$_f$), 50.37 (C$_d$), 42.17 (C$_g$). **^{31}P{^{1}H} NMR** (acetone-*d*$_6$): δ (ppm) = -144.26 (hept, *J* = 708.7 Hz). **FTIR** *v* (cm^{-1}) = 2032 (s, CO), 1907 (s, CO), 1619 (s, C=N$_{pyridyl}$) , 1605 (s, C=N$_{bpy}$). **MS** (HR-ESI, *m/z*): 566.07 (15 %, [M-3PF$_6$]$^{3+}$, calcd. 566.10). **Elemental**

analysis for $C_{63}H_{57}N_{13}O_9Re_3 \cdot 3PF_6$: Found C, 35.37, H, 2.89, N, 8.18 %; calcd. C, 35.46, H, 2.69, N, 8.35 %.

4.2.19 Synthesis of [(Re(bpy)(CO)$_3$)$_4$(12)](PF$_6$)$_4$ (18)

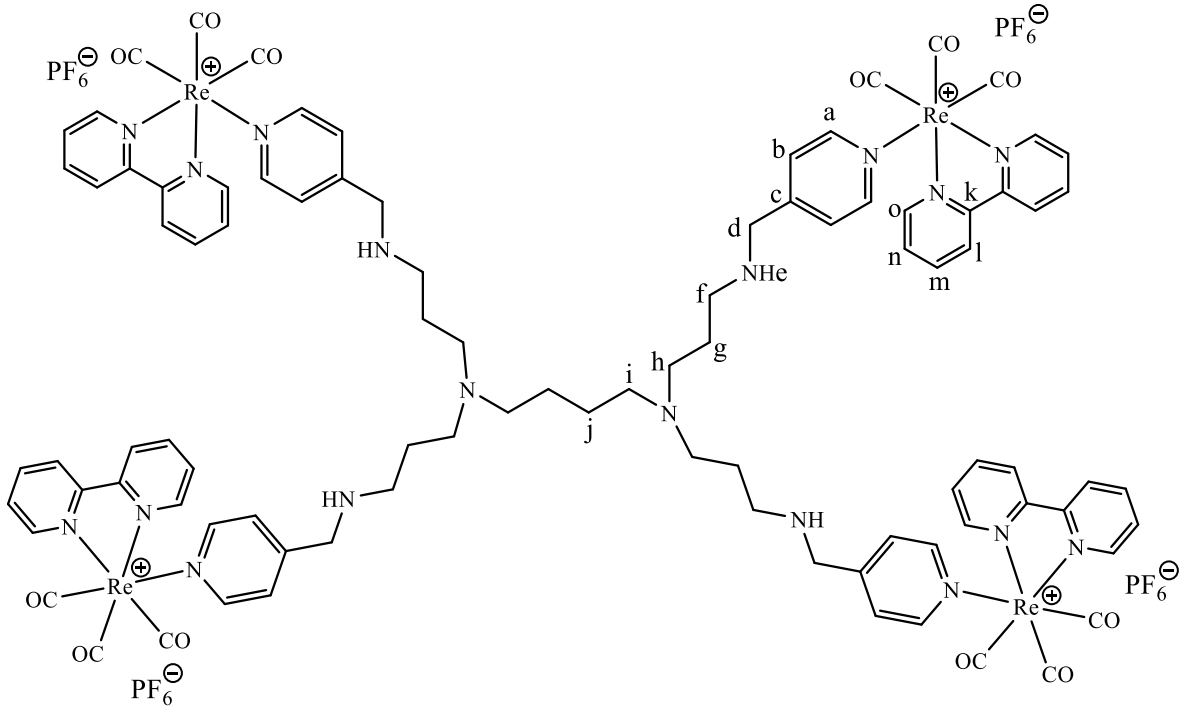

$[Re(bpy)Cl(CO)_3]$ (0.090 g, 0.194 mmol) and silver triflate (0.059 g, 0.229 mmol) were stirred in DCM (30 mL) for 3 hours. A precipitate (AgCl) was formed and removed by gravity filtration. Ligand **12** (0.033 mg, 0.0479 mmol) was dissolved in DCM (5 mL) and the solution added to the reaction mixture. The solution was stirred for 24 hours at room temperature, before the addition of NH_4PF_6 (excess) and subsequent stirring for one hour. The solvent was removed by rotary evaporation and the residue dissolved in minimum DCM. The solution was added to boiling isopropanol and stirred for five minutes. The solution was allowed to cool to room temperature, precipitating a brown powder. The powder was filtered using Celite and washed with isopropanol before being solubilised with DCM. The DCM was removed to afford the product as a brown powder. **Yield**: 0.061 g, 11 %. **Melting point**: 134 – 137 °C. **^{1}H NMR** (acetone-d_6): δ = 9.47 (ddd, ^3J = 5.4, ^4J = 1.4, ^5J = 0.7 Hz, 8H, H_o), 8.74 (d, ^3J = 8.1 Hz, 8H, H_l), 8.53 – 8.37 (m, 16H, $H_{a/m}$), 7.99 (ddd, ^3J = 7.6, ^3J = 5.5, ^4J = 1.2 Hz, 8H, H_n), 7.46 (d, ^3J = 6.6 Hz, 8H, H_b), 3.83 (s, 8H, H_d), 3.38 – 3.06 (m, 16H, $H_{f/h}$), 2.77 – 2.64 (m, 4H, H_i), 1.98 – 1.77 (m, 12H, $H_{g/j}$). **^{13}C{^{1}H} NMR**

(acetone-d_6): δ = 195.63 (C_{CO}), 191.64 (C_{CO}), 155.84 (C_k), 154.03 (C_o), 151.71 (C_a), 151.66 (C_c), 141.42 (C_m), 129.00 (C_n), 125.78 (C_b), 124.83 (C_l), 52.02 (C_f), 51.09 (C_d), 47.08 (C_h), 46.72 (C_i), 23.87 (C_g), 23.72 (C_j). **^{31}P{^{1}H} NMR** (acetone-d_6): δ = -144.26 (hept, J = 708.9 Hz). **FTIR** ν (cm^{-1}) = 2028 (s, CO), 1901 (s, CO), 1619 (s, C=$N_{pyridyl}$), 1605 (s, C=N_{bpy}). **MS** (HR-ESI, *m/z*): 590.08 (26 %, [M-CO-4PF_6]$^{4+}$), 547.05 (19 %, [M-7CO-4PF_6]$^{4+}$). **Elemental analysis** for $C_{92}H_{92}N_{18}O_{12}Re_4 \cdot 4PF_6 \cdot 5H_2O \cdot 2DCM$: Found C, 35.28, H, 3.68, N, 7.26 %; calcd. C, 34.80, H, 3.36, N, 7.77 %.

4.2.20 Synthesis of [Mn(bpy)(CO)$_3$(10)]PF$_6$ (19)

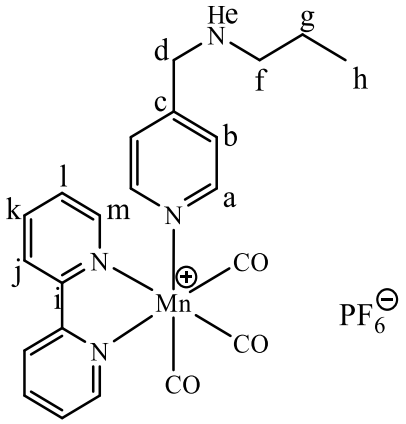

[Mn(bpy)Br(CO)$_3$] (0.162 g, 0.433 mmol) and silver triflate (0.135 g, 0.525 mmol) were stirred in DCM (30 mL) for 3 hours. The resulting precipitate (AgBr) was removed by gravity filtration. Ligand **10** (0.079 g, 0.524 mmol) was dissolved in DCM (5 mL) and added to the solution. The mixture was stirred at room temperature for 20 hours. Excess NH_4PF_6 was added to the solution, after which the solution was stirred for a further hour. Gravity filtration was employed to remove insoluble particles, and the solution was washed with distilled water (2×20 mL). The organic layer was dried with $MgSO_4$, which was subsequently removed by gravity filtration, and the solvent of the filtrate evaporated. The resulting residue was dissolved in minimum DCM and diethyl ether (ca. 8 mL) was added to form a residue. The solvent was discarded and the residue washed with diethyl ether and pentane to afford complex **19** as an oily yellow/orange residue. **Yield**: 0.169 g, 66 %. **^{1}H NMR** (acetone-d_6): δ = 9.58 (d, ^3J = 5.2 Hz, 2H, H_m), 8.62 (d, ^3J = 8.0 Hz, 2H, H_j), 8.37 (td, ^3J = 7.9, ^4J = 1.5 Hz, 2H, H_k), 8.33 (d, ^3J = 6.6 Hz, 2H, H_a), 7.99 (ddd, ^3J = 7.6, ^3J = 5.5, ^4J = 1.2 Hz, 2H, H_l), 7.40 (d, ^3J = 6.0 Hz, 2H, H_b), 3.74 (s, 2H, H_d), 2.44 (t, ^3J = 6.9 Hz, 2H, H_f), 1.50

– 1.32 (m, 2H, H_g), 0.83 (t, ^3J = 7.4 Hz, 3H, H_h). **$^{13}C\{^1H\}$ NMR** (acetone-d_6): δ = 218.72 (C_{CO}), 218.15 (C_{CO}), 155.66 (C_i), 155.30 (C_c), 154.48 (C_m), 151.90 (C_a), 140.75 (C_k), 128.54 (C_l), 125.14 (C_b), 123.95 (C_j), 51.29 (C_d), 51.07 (C_f), 22.79 (C_g), 11.06 (C_h). **$^{31}P\{^1H\}$ NMR** (acetone-d_6): -144.12 (hept, J = 708.4 Hz). **FTIR** ν (cm^{-1}) = 2025 (s, CO), 1899 (s, CO), 1619 (s, $C{=}N_{pyridyl}$), 1605 (s, $C{=}N_{bpy}$). **MS** (HR-ESI, *m/z*): 445.11 (67 %, $[M\text{-}PF_6]^+$, calcd. 445.11). **Elemental Analysis** for $C_{22}H_{22}F_6MnN_4O_3P$: Found C, 44.51, H, 4.02, N, 9.36 %; calcd. C, 44.76, H, 3.76, N, 9.49 %.

4.2.21 Synthesis of $[(Mn(bpy)(CO)_3)_3(11)](PF_6)_3$ (20)

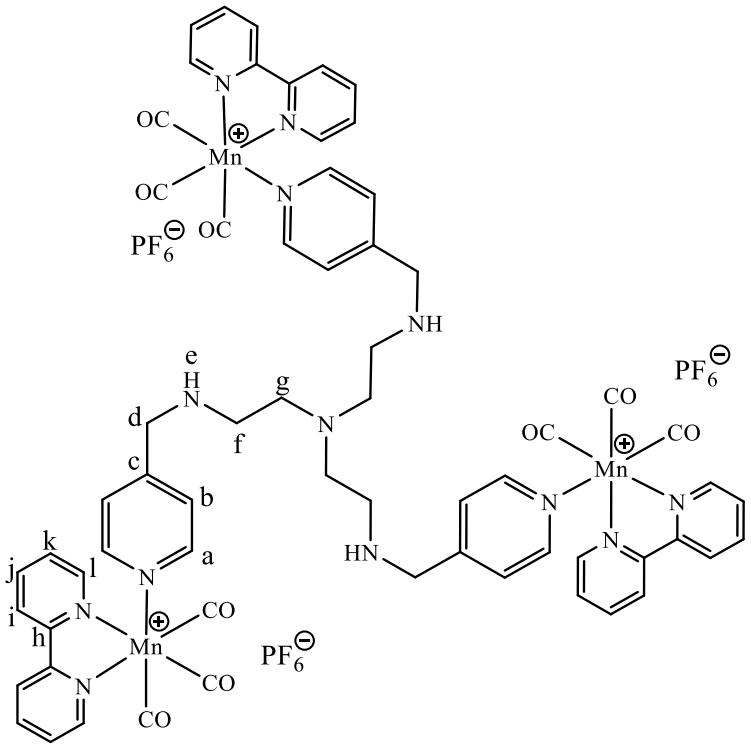

$[Mn(bpy)Br(CO)_3]$ (0.159 g, 0.425 mmol) and silver triflate (0.140 g, 0.543 mmol) were stirred at room temperature in DCM (30 mL) for 3 hours. The resulting precipitate (AgBr) was removed by filtration and ligand **11** (0.054 g, 0.129 mmol) was added to the flask. The reaction mixture was stirred at room temperature for 19 hours, after which excess NH_4PF_6 was added to the reaction flask, followed by a further hour of stirring at room temperature. The mixture was filtered and washed with H_2O (2 × 20 mL) and the organic layer was dried with $MgSO_4$, which was subsequently removed by filtration. The solvent was removed by rotary evaporation. The resultant residue was dissolved in minimum DCM, which was added to boiling isopropanol (80 mL) with

stirring. The mixture was allowed to cool, and was filtered through Celite. The product was obtained by washing the Celite with DCM and removing the solvent to afford complex **20** as a pale-yellow powder. **Yield**: 0.052 g, 31 %. **Melting point**: 156 – 160 °C (melt and decomposition). **^{1}H NMR** (acetone-d_6): δ (ppm) = 9.61 – 9.53 (m, 6H, H_l), 8.60 – 8.49 (m, 6H, H_i), 8.40 – 8.23 (m, 12H, $H_{j/a}$), 8.00 – 7.87 (m, 6H, H_k), 7.34 (t, ^3J = 6.0 Hz, 6H, H_b), 3.88 – 3.61 (m, 6H, H_d), 3.35 – 3.12 (m, 6H, H_g), 3.08 – 2.83 (m, 6H, H_f). **^{13}C{^{1}H} NMR** (acetone-d_6): δ (ppm) = 156.59 (C_c), 155.46 (C_l), 153.08 (C_j), 153.04 (C_h), 141.60 (C_a), 129.41 (C_k), 126.31 (C_b), 124.79 (C_i), 54.13 (C_g), 51.20 (C_d), 44.09 (C_f). **^{31}P{^{1}H} NMR** (acetone-d_6): δ (ppm) = -144.13 (hept, J = 708.7 Hz). **FTIR** ν (cm^{-1}) = 2031 (s, CO), 1907 (s, CO), 1619 (s, C=N$_{pyridyl}$), 1606 (s, C=N$_{bpy}$). **MS** (HR-ESI, *m/z*): 434.06 (21 %, [M-3PF$_6$]$^{3+}$calcd. 434.75). **Elemental analysis** for $C_{63}H_{57}N_{13}O_9Mn_3 \cdot 3PF_6 \cdot 3H_2O$: Found C, 42.05, H, 3.70, N, 9.79 %; calcd. C, 42.18, H, 3.54, N, 10.15 %.

4.2.22 Synthesis of [(Mn(bpy)(CO)$_3$)$_4$(11)](PF$_6$)$_4$ (21)

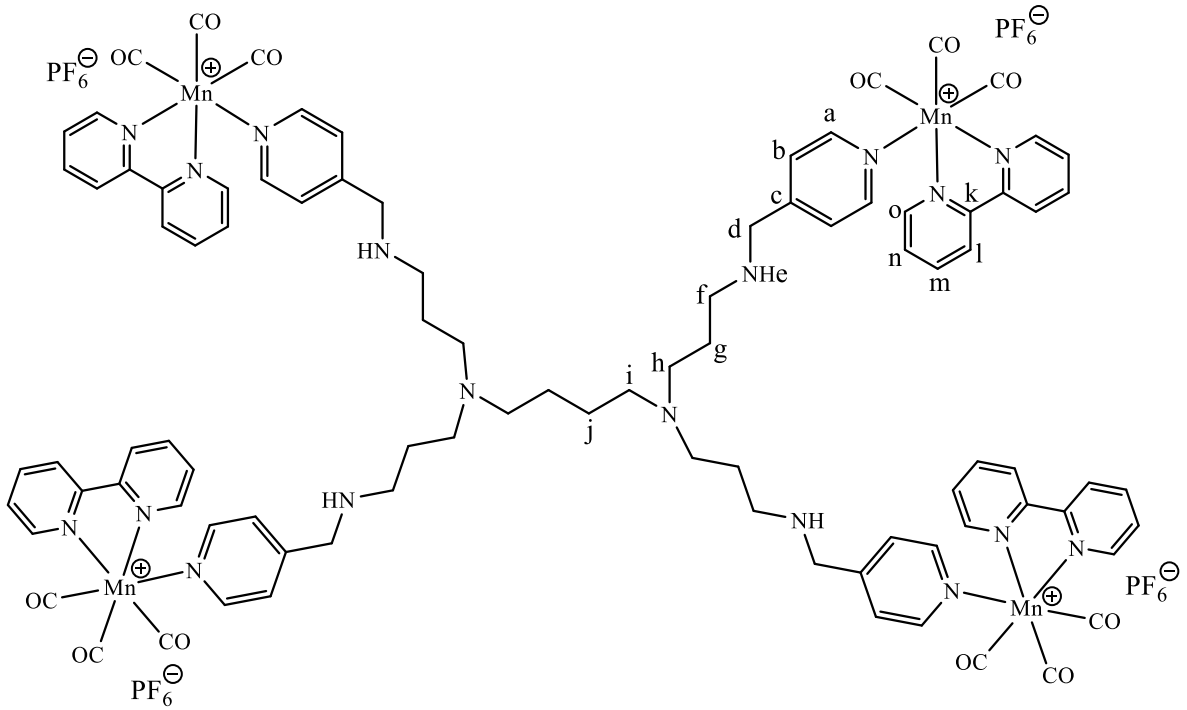

[Mn(bpy)Br(CO)$_3$] (0.107 g, 0.286 mmol) and silver triflate (0.085 g, 0.331 mmol) were stirred at room temperature in DCM (30 mL) for 3 hours. The resulting precipitate (AgBr) was filtered off

and ligand **12** (0.044 g, 0.065 mmol) was added to the flask. The reaction mixture was stirred at room temperature for 19 hours, after which excess NH_4PF_6 was added to the reaction flask, followed by a further hour of stirring at room temperature. The mixture was filtered and washed with H_2O (2 × 20 mL) and the organic layer was dried with $MgSO_4$, which was subsequently removed by rotary evaporation. The resultant residue was dissolved in minimum DCM, which was added to boiling isopropanol (80 mL) with stirring. The mixture was allowed to cool, and was filtered through Celite. The product was obtained by washing the Celite with DCM and removing the solvent to afford complex **21** as a dull yellow powder. **Yield**: 0.049 g, 40 %. **Melting point**: 156 – 159 °C (melt and decomposition). **^{1}H NMR** (acetone-d_6): δ = 9.64 – 9.50 (m, 8H, H_o), 8.65 – 8.52 (m, 8H, H_l), 8.42 – 8.28 (m, 16H, $H_{m/a}$), 7.96 (dt, ^3J = 6.4, ^4J = 4.7 Hz, 8H, H_n), 7.35 (d, ^3J = 4.6 Hz, 8H, H_b), 3.76 (d, ^4J = 3.3 Hz, 8H, H_d), 3.37 – 3.22 (m, 8H, H_f), 3.22 – 3.11 (m, 8H, H_h), 2.97 – 2.82 (s, 4H, H_i), 1.96 – 1.79 (m, 8H, H_g), 1.79 – 1.72 (m, 4H, H_j). **^{13}C{^{1}H} NMR** (acetone-d_6): δ = 219.65 (C_{CO}), 218.98 (C_{CO}), 156.60 (C_C), 155.44 (C_o), 153.06 (C_o), 153.02 (C_m), 141.62 (C_a), 129.44 (C_n), 126.22 (C_b), 124.78 (C_l), 54.19 (C_f), 53.34 (C_o), 52.97 (C_h), 51.83 (C_d), 48.30 (C_i), 24.27 (C_g), 21.89 (C_j). **^{31}P{^{1}H} NMR** (acetone-d_6): δ = -144.13 (hept, J = 708.7 Hz). **FTIR** ν (cm^{-1}) = 2028 (s, CO), 1901 (s, CO), 1619 (s, $C{=}N_{pyridyl}$), 1606 (s, $C{=}N_{bpy}$). **MS** (HR-ESI, *m/z*): 964.90 (19.3 %, $[M\text{-}8CO\text{-}2PF_6]^{2+}$, calcd. 964.22). **Elemental analysis** for $C_{92}H_{92}N_{18}O_{12}Mn_4{\cdot}4PF_6{\cdot}5H_2O{\cdot}DCM$: Found C, 42.22, H, 4.28, N, 9.70 %; calcd. C, 42.69, H, 4.01, N, 9.64 %.

4.2.23 Synthesis of [MnBr(CO)$_3$(13)] (22)

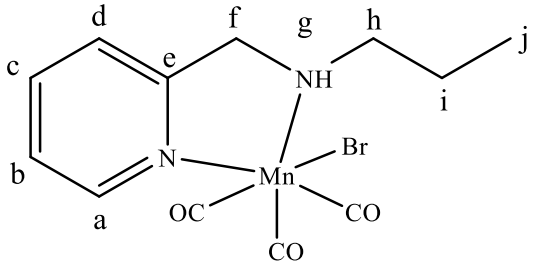

[MnBr(CO)$_5$] (0.184 g, 0.670 mmol) and ligand **13** (0.104 g, 0.695 mmol) were stirred together in DCM (10 mL) for 23 hours. The solvent was removed, and the residue dissolved in DCM (2 mL). Diethyl ether (10 mL) was added to precipitate the product. The product was filtered on a Hirsch funnel and washed with diethyl ether and *n*-pentane to yield the product (**22**) as an orange powder.

Yield: 0.188 g, 76 %. **Melting point**: 155 – 159 °C (melt and decomposition). **^{1}H NMR** (acetone-d_6): δ = 8.98 (d, ^{3}J = 5.4 Hz, 1H, H_a), 7.98 (td, ^{3}J = 7.7, ^{4}J = 1.5 Hz, 1H, H_c), 7.61 (d, ^{3}J = 7.9 Hz, 1H, H_d), 7.58 – 7.49 (m, 1H, H_b), 4.75 (dd, ^{2}J = 15.7, ^{4}J = 4.8 Hz, 1H, H_f), 4.21 (dd, ^{2}J = 15.6, ^{3}J = 10.8 Hz, 1H, H_f), 3.95 (s, 1H, H_g) 3.40 – 3.06 (m, 2H, H_h), 2.02 – 1.84 (m, 2H, H_i), 1.05 (t, ^{3}J = 7.4 Hz, 3H, H_j). **^{13}C{^{1}H} NMR** (acetone-d_6): δ = 222.50 (C_{CO}), 221.94 (C_{CO}), 221.76 (C_{CO}), 160.24 (C_e), 153.36 (C_a), 138.57 (C_d), 124.64 (C_b), 121.80 (C_c), 58.37 (C_h), 58.23 (C_f), 21.54 (C_i), 10.59 (C_j). **MS** (HR-ESI, *m/z*): 367.92 (25.3 %, $[M]^+$, calcd. 367.96), 283.96 (100 %, $[M\text{-}3CO]^+$, calcd. 283.97). **Elemental analysis** for $C_{12}H_{14}BrMnN_2O_3$: Found C, 39.16, H, 3.89, N, 7.15 %; calcd. C, 39.05, H, 3.82, N, 7.59 %.

4.2.24 Synthesis of [(MnBr(CO)$_3$)$_3$(14)] (23)

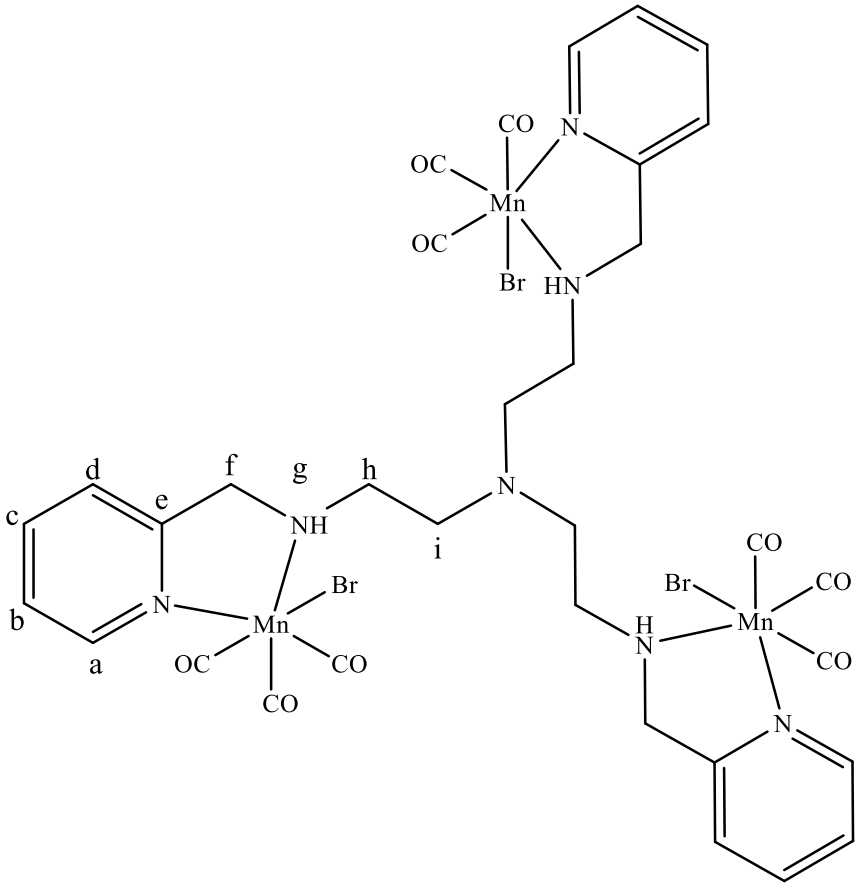

$[MnBr(CO)_5]$ (0.093 g, 0.338 mmol) and ligand **14** (0.047 g, 0.113 mmol) were dissolved in DCM (30 mL). The mixture was stirred at room temperature for 19 hours. The solvent was removed by

rotary evaporation, and the resulting residue redissolved in DCM (1 mL). Addition of diethyl ether (8 mL) caused the precipitation of the product (**23**) as an orange solid. The solid was filtered on a Hirsch funnel and washed with diethyl ether and *n*-pentane. **Yield**: 0.079 g, 65 %. **Melting point**: 216 °C (decomposition). **^{1}H NMR** (acetone-d_6): δ (ppm) = 9.00 – 8.82 (m, 3H, H_a), 8.06 – 7.78 (m, 3H, H_c), 7.68 – 7.40 (m, 6H, $H_{b/d}$), 5.06 – 4.70 (m, 3H, H_f), 4.49 – 4.01 (m, 3H, $H_{f'}$), 3.88 – 3.67 (m, 3H, H_h), 3.67 – 3.35 (m, *3*H, $H_{h'}$), 3.35 – 3.03 (m, 6H, H_i). **^{13}C{^{1}H} NMR** (acetone-d_6): δ (ppm) =222.32 (C_{CO}), 222.06 (C_{CO}), 221.93 (C_{CO}), 159.70 (C_e), 153.33 (C_a), 138.55 (C_d), 124.72 (C_c), 121.81 (C_b), 58.67 (C_f), 54.35 (C_h), 52.85 (C_i). **FTIR** ν (cm^{-1}) = 2020 (s, CO), 1895 (br, CO), 1609 (s, $C{=}N_{aromatic}$). **MS** (HR-ESI, *m/z*): 995.88 (100 %, $[M\text{-}Br]^+$, calcd. 995.88). **Elemental analysis** for $C_{33}H_{33}Br_3Mn_3N_7O_9 \cdot 0.5Et_2O$: Found C, 37.88, H, 3.68, N, 9.69 %; calcd. C, 38.34, H, 3.53, N, 8.82 %.

4.2.25 Synthesis of [(MnBr(CO)$_3$)$_4$(15)] (24)

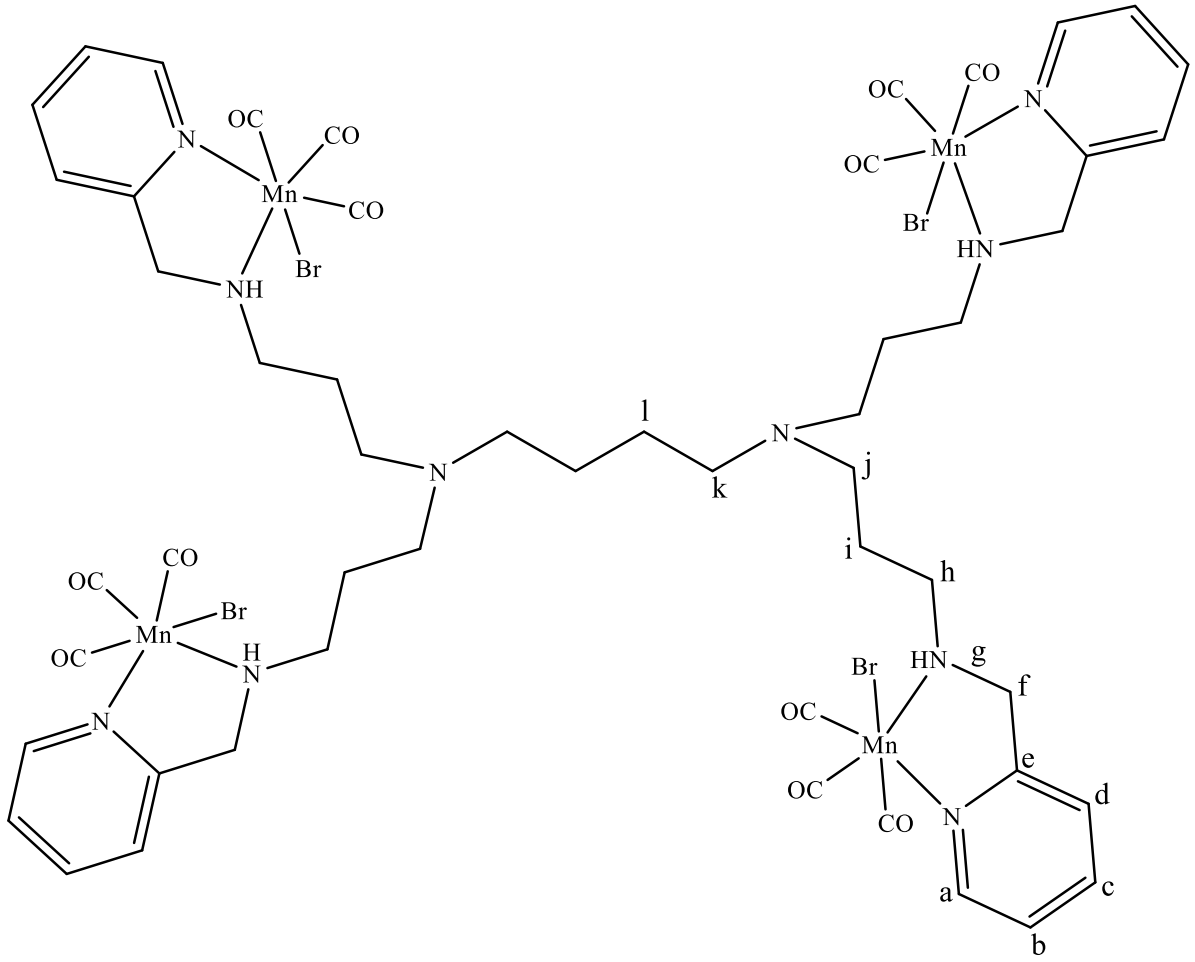

[MnBr(CO)$_5$] (0.229 g, 0.835 mmol) and ligand **15** (0.139 g, 0.204 mmol) were dissolved in DCM (30 mL). The mixture was stirred at room temperature for 19 hours. The solvent was removed by rotary evaporation, and the resulting residue redissolved in DCM (1 mL). Addition of diethyl ether (8 mL) caused the precipitation of the product (**24**) as an orange solid. The solid was filtered on a Hirsch funnel and washed with diethyl ether and *n*-pentane. **Yield**: 0.225 g, 71 %. **Melting point**: 159 °C (decomposition). **^{1}H NMR** (acetone-d_6): δ (ppm) = 9.09 – 8.87 (m, 4H, H_a), 8.08 – 7.85 (m, 4H, H_c), 7.68 – 7.33 (overlapping m, 8H, $H_{b/d}$), 4.80 (s, 4H, H_f), 4.21 (s, 4H. $H_{f'}$), 3.50 (s, 4H, H_h), 3.36 – 3.16 (m, 4H, $H_{h'}$), 2.91 – 2.46 (overlapping m, 12H, $H_{j/k}$), 2.33 – 2.14 (m, 4H, H_i), 1.62 (s, 4H, H_l). **^{13}C{^{1}H} NMR** (acetone-d_6): δ (ppm) = 222.54 (C_{CO}), 222.06 (C_{CO}), 221.93 (C_{CO}), 160.32 (C_e) 153.31 (C_a), 138.55 (C_d), 124.60 (C_b), 121.80 (C_c), 58.30 (C_f), 55.71 (C_h), 53.70 (C_k), 51.95 (C_j), 25.53 (C_i), 24.59 (C_l). **FTIR** ν (cm^{-1}) = 2020 (s, CO), 1889 (br, CO), 1609 (s, C=N$_{aromatic}$). **MS** (HR-ESI, *m/z*): 1337.03 (79 %, [M-MnBr(CO)$_3$+H]$^+$, calcd. 1337.03), 1556.87

(63 %, $[M+H]^+$, calcd. 1556.87). **Elemental analysis** for $C_{52}H_{60}Br_4Mn_4N_{10}O_{12}\cdot 0.5$*n*-pentane: Found C, 40.91, H, 4.49, N, 9.63 %; calcd. C, 40.70, H, 4.11, N, 8.79 %.

4.3 Photochemical Studies

Electronic spectra were recorded in a mixture of DMSO and 0.01 M PBS (pH 7.4) solution (5:95 % *v/v*) using a Cary 60 UV/Vis spectrometer with a fibre optic dip probe attachment. Dark stability in DMSO/PBS solution was determined by taking a reading every 30 minutes for 16 hours, before irradiating the samples with 365 nm radiation using a custom-built LED array, measuring the electronic absorption spectrum every minute for 12 minutes.

The myoglobin solution was prepared by sonicating *ca*. 30 mg of myoglobin from equine skeletal muscle (purchased from Sigma Aldrich) in 10.0 mL 0.01 M PBS solution. The concentration of the myoglobin was determined using a UV/Vis spectrum of the solution and the Beer-Lambert Law with the known extinction coefficient (13.8 $mM^{-1}cm^{-1}$ at 557 nm). A stock DMSO solution of the complex was prepared with a concentration of 2000 µM. The Fe^{3+} in myoglobin was reduced to Fe^{2+} by adding a microspatula of sodium dithionite. Complex stock solution and reduced myoglobin solution were added to the cuvette in volumes to make concentration of 10 µM complex and 60 µM myoglobin, made up to 1.0 mL with 0.01 mL PBS solution. The solution was then degassed with Ar. A t = 0 spectrum was recorded, and the cuvette was irradiated with a custom-built 365 nm LED array for an hour. Irradiation was interrupted to record the UV/Vis spectra every minute for the first 10 minutes, every 2 minutes from 10 – 20 minutes, and every 5 minutes thereafter.

4.4 Antiproliferative Studies

All of the cancerous cell lines were acquired from the European Collection of Authenticated Cell Cultures through Sigma Aldrich. The normal human fibroblast cell line (BJ) was acquired from the American Type Culture Collection. The cells were cultured under conditions recommended by the cell bank using cell culture media and supplements from Sigma Aldrich. The cells were seeded on 96-well Nunclon Delta surface assay plates in wells containing 200 µL cell suspension. The compounds were diluted in DMSO, and serial dilutions were prepared using 0.01 M PBS solution,

to obtain concentrations in the range of 10 – 2500 µM. Each well containing cells was treated with the respective compound in a proportion of 1:20 (compound:cell culture media), to obtain a final concentration range of 0.5 – 125 µM of the compound in the cell culture media. The cells were subjected to the treatment for 24 hours. Untreated cells were used as a reference, and cell culture media without cells was used as a blank. Three independent experiments were performed, each in duplicate. The MTT reagent and the Hank's media to dissolve the salt (5 mn/mL final concentration) were purchased from Sigma Aldrich. Measurements were made at 492 nm and 570 nm using a Synergy 2.0 microplate reader, and the absorbance data were implemented using GraphPad Prism 5 software to obtain the sigmoidal curves and the IC_{50} values.

The Alamar Blue dye was purchased from Thermo Fisher Scientific. The plates were loaded with cells and incubated and treated in the same way as for the MTT assay. After 24 hours of incubation, 40 µL of dye was added to each sample, and the plate was incubated for three hours. The fluorescence of each well was measured using an excitation wavelength of 540 nm and was measured at 620 nm using the Synergy 2.0 microplate reader.

4.5 Antiplasmodial Studies

The samples were evaluated in triplicate against CQ-sensitive (NF54) and CQ-resistant (K1) strains of *Plasmodium falciparum*. *In vitro* cultures of asexual erythrocyte stages of the parasite were sustained using a modified literature method.[12] The lactate dehydrogenase assay was employed to evaluate the *in vitro* antiplasmodial activity of the sample.[13] Stock solutions of 20 mg/mL were prepared in DMSO. The stock solution was stored at -20 °C, and dilutions were prepared on the day of the experiment. Chloroquine was used as a reference drug for all experiments. A starting concentration of 10 000 ng/mL was used as a starting concentration, which was serially diluted in medium until a concentration of 2 ng/mL was obtained. The IC_{50} values were obtained using a sigmoidal dose-response curve generated using GraphPad Prism 4 software.

Antiplasmodial activity with CO-release was determined by irradiating the 96-well plate for 15 minutes with a custom-built LED array at the beginning of the incubation period with the potential drug.

4.6 Radiolabelling Studies

The formation of the ^{99m}Tc-tricarbonyl species was performed using an Isolink Kit (2.9 mg sodium tetraborate decahydrate, 7.8 mg sodium carbonate, 9.0 mg potassium sodium tartrate tetrahydrate and 4.5 mg sodium boranocarbonate). 1 mL of aqueous pertechnetate solution (TcO_4^-) was added to the Isolink kit, which was subsequently heated to 100 °C for 20 min to form the ^{99m}Tc tricarbonyl aqua species. The solution is then added to excess 2,2'-bipyridyl (1 mg) and heated at 40°C for 30 min to form the $^{99m}Tc(bpy)(CO)_3$ species. The contents of the vial containing the $^{99m}Tc(bpy)(CO)_3$ species was added to excess of the ligand (*ca*. 300 mmol) and the vial incubated at 40 °C for 20 minutes.

Analytical HPLC was performed on an Agilent Series 1200 machine coupled to a diode array UV/Vis detector and a Gina Star, Raytest Gabi Gamma Detector Benzstrasse 4, D-75334 Straubenhard radiodetector. A reverse phase Phenomenex Luna C-18 column was used with a flow rate of 1.5 mL/min. For the preparative HPLC, a preparative Phenomenex Luna C-18 column was used with a flow rate of 7.0 mL/min. The HPLC method begins with an isocratic mixture of 30 % acetonitrile in 0.1 M NH_4OAc solution for 20 seconds. At 20 seconds, the % acetonitrile increases linearly to 90 % at 5.0 minutes and remains isocratic until 8 minutes, where it decreases back to 30 %. HPLC-grade solvents were used.

References

1. SAINT Version 7.60a, 2006.
2. SHELXS-97, SHELXL-2014 and SADABS version 2.05, 1997.
3. L. J. Barbour, *J. Supramol. Chem.*, 2001, 189-191.
4. *USA Pat.*, WO8304095A1, 1983.
5. S. P. Schmidt, W. C. Trogler and F. Basolo, in *Inorg. Synth.*, ed. R. J. Angelici, 1990, vol. 28, pp. 160-165.
6. I. Chakraborty, S. J. Carrington and P. K. Mascharak, *ChemMedChem*, 2014, **9**, 1266-1274.
7. E. Portenkirchner, K. Oppelt, C. Ulbricht, D. A. M. Egbe, H. Neugebauer, G. Knör and N. S. Sariciftci, *J. Organomet. Chem.*, 2012, **716**, 19-25.
8. N. Wilhelms, S. Kulchat and J. Lehn, *Helv. Chim. Acta*, 2012, **95**, 2635-2651.

9. M. Wenzel, K. Wichmann, K. Gloe, K. Gloe, H.-J. Buschmann, K. Otho, M. Schröder, A. J. Blake, C. Wilson, A. M. Mills, L. F. Lindoy and P. G. Plieger, *CrystEngComm*, 2010, **12**, 4176.
10. P. Govender, N. C. Antonels, J. Mattsson, A. K. Renfrew, P. J. Dyson, J. R. Moss, B. Therrien and G. S. Smith, *J. Organomet. Chem.*, 2009, **694**, 3470-3476.
11. G. Smith, R. Chen and S. Mapolie, *J. Organomet. Chem.*, 2003, **673**, 111-115.
12. W. Trager and J. B. Jensen, *J. Parasitol.*, 2005, **91**, 484-486.
13. M. T. Makler, J. M. Ries, J. A. Williams, J. E. Bancroft, R. C. Piper, B. L. Gibbins and D. J. Hinrichs, *Am. J. Trop. Med. Hyg.*, 1993, **48**, 739-741.

Chapter 5 Overall Summary, Conclusions and Future Outlook

5.1 Summary and Conclusions

The aim of this study was to:

- design and prepare various mono- and multimeric group 7 tricarbonyl complexes,
- evaluate them as antiproliferative and antiplasmodial agents, and
- assess their CO-releasing properties and radiolabelled properties.

Specifically, three scaffolds, a mono-, tris- and tetrameric scaffold were functionalised with 2- and 4-picolyl entities to afford two series of ligands. The 2-picolylamine ligands were functionalised with an Mn(I) tricarbonyl entity, which bonded in an (*N*,*N*)-bidentate coordination mode. The 4-picolylamine ligands were functionalised with Mn(I) and Re(I) bipyridyl tricarbonyl moieties, following the [2 + 1] approach. The complexes that are reported herein have been characterised using an array of spectroscopic and analytical techniques, and have been synthesised for the first time to the best of our knowledge.

The ligands were prepared *via* Schiff base condensation reaction between either 2- or 4-pyridinecarboxaldehyde and the appropriate dendritic amine. Characterisation of these ligands confirmed the presence of the proposed compounds in high purity. The $[M(bpy)(CO)_3X]$ (X = halide) precursors (**2** and **3**) were formed by reaction of the appropriate metal precursor with 2,2'-bipyridyl. The 4-picolylamine ligands (**10** – **12**) were reacted with $[M(bpy)(CO)_3X]$ in the presence of AgOTf as a halide abstractor to yield a series cationic of Re(I) (**16** – **18**) and Mn(I) (**19** – **21**) [2 + 1] complexes. The spectroscopic and analytical data showed that the bonding of the metal to the ligand was *via* the 4-pyridyl nitrogen, and in a [2 + 1] fashion. The shift of the C=N absorption band in the infrared spectrum to higher wavenumbers, in addition to the upfield shift of the proton peak (**H** – C – N – M) in the ^{1}H NMR spectrum, is evidence that the complexation occurred *via* the pyridyl nitrogen.

The 2-picolylamine ligands (**13** – **15**) were reacted with metal precursor [$MnBr(CO)_5$] to afford a series of neutral Mn(I) tricarbonyl complexes (**22** – **24**). Complexation and the bidentate (*N*,*N*) coordination mode was confirmed by splitting of the magnetically non-equivalent protons in ^1H NMR spectrum of the complexes, which were not present in the pure ligand.

The stability and CO-release properties of the Mn(I) tricarbonyl complexes (**19** – **24**) were evaluated using UV/Vis absorption spectroscopy. All of the complexes are stable in the absence of light for an extended period of time. CO-release is triggered by photoactivation using a 365 nm LED array, and is observed by the decrease in intensity of the MLCT absorption band in the electronic spectra of the complexes. Mononuclear complex **22** was used as a model, with which CO-release was confirmed using the standard myoglobin assay.

The *in vitro* antiproliferative activity of the Re(I) and Mn(I) tricarbonyl complexes **16** – **24** was evaluated using the MTT assay. The Re(I) complexes **16** – **18** were evaluated against three cancerous cell lines (A431, DLD-1 and A2780) and one non-tumourigenic cell line (BJ). The most effective compound against these cell lines was complex **18**, which displayed IC_{50} values of < 15 μM against all tested cancerous cell lines. Selectivity towards the cancerous cell lines over the non-tumourigenic cell line was observed for both multinuclear complexes **17** and **18**, while complex **16** displayed no selectivity. An Alamar Blue assay was performed to confirm the results obtained using the MTT assay. Mn(I) complexes **19** – **24** were evaluated against two cancerous cell lines, A431 and A375, using the MTT assay. Again, the tetranuclear complex (**21**) displayed the most potent activity against both tested cell lines. The complexes synthesised with the [2 + 1] approach (**19** – **21**) displayed increased activity over their bidentate equivalents (**22** – **24**).

The *in vitro* antiplasmodial activity of complexes **16** – **24** was evaluated against CQ-sensitive (NF54) and CQ-resistant (K1) strains of *P. falciparum* using the pLDH assay. All of the complexes displayed good efficacy against both strains, with IC_{50} values in the low micromolar region. The most potent activity against the CQ-resistant strain was observed using tetranuclear complex **21**.

The *in vitro* antiplasmodial activity of Mn(I) complexes **19**, **21**, **22** and **24** was evaluated with irradiation of the 96-well plates with 365 nm light against the CQ-resistant strain of *P. falciparum*. [2 + 1] complexes **19** and **21** displayed an increase of activity upon irradiation, while bidentate complexes **22** and **24** displayed a notable decrease in activity upon irradiation.

Radiolabelling of ligand **10** with ^{99m}Tc was accomplished by reacting ligand **10** with ^{99m}Tc(bpy)(C)O)$_3$ to afford a [2 + 1] complex. The product was isolated using preparative HPLC. Radiolabelling of ligands **11** and **12** with ^{99m}Tc were unsuccessful.

5.2 Future Outlook

The results presented herein show that group 7 metallodendrimers display great promise in the field of therapeutic and diagnostic drug design. Improvements to the compounds may be brought about in various manners, including the synthesis of higher generation dendrimers. The increase in dendrimer generation allows for the exploitation of the EPR effect, increasing the selectivity of the potential drugs, as well as a likely increase in activity due to the number of metal centres. Another modification could be the use of a modified 2,2'-bipyridyl moiety in the [2 + 1] complexes. The introduction of water-solubilising groups, or the use of a simple molecule, such as a 2,2'-bipyridyldiol, as a co-ligand, would increase the solubility in aqueous media, allowing for an increase in bioavailability of the potential drug.

In order to make a true comparison, the myoglobin assay should be used to fully characterise the CO-release properties of Mn(I) complexes. Antiproliferative activity should be determined for all of the Mn(I) complexes with 365 nm irradiation. Following in a similar vein, the antiplasmodial assays with irradiation should be repeated to confirm the results obtained.

A structure-activity relationship study should be performed to rationalise any trend found in the biological studies. Other photophysical properties should be obtained for the complexes, such as quantum yield and steady state lifetime, to determine whether there is any correlation between these properties and the complexes resultant biological activities.

Radiolabelling of the multimeric ligands should be performed using a protocol that allows for excess ^{99m}Tc, in order to fully functionalise the dendritic arms. Furthermore, the identity of the radiolabelled product form by the radiolabelling of ligand **10** should be confirmed using an HPLC trace of complex **16**, rather than complex **16b**, which was used.

Mechanistic studies should be performed for both the antiproliferative and the antiplasmodial studies. For the antiproliferative studies, the use of knockout cell lines can be used to determine

which transport protein is being utilised to gain access to the cell, as well as apoptotic studies to determine the mechanism of action of the potential drug. With regard to the antiplasmodial mechanism, β-haematin studies should be performed in order to determine a possible mode of antiplasmodial action.